

Bio-inspired design of anti-biofouling surface topographies

By: Nicholas Lin

Department of Chemical Engineering
McGill University, Montreal, Québec, Canada

December 2017

A thesis submitted to McGill University in partial fulfillment of the requirements of the degree
of Master of Engineering

© Nicholas Lin 2017

Abstract

The undesired accumulation of surface-attached biological matter, referred to as biofouling, is detrimental to human health and industrial processes, especially if the biological matter in question is pathogenic bacteria. Traditional chemical-based approaches to create anti-biofouling or antibacterial surfaces face numerous drawbacks and are becoming less and less effective as antibacterial resistance accelerates. The next-generation of anti-biofouling and antibacterial surfaces employ physical topography or a synergistic combination of topography and chemistry to achieve antibacterial activity. Insects, animals, and plants have evolved unique surface topographies designed to prevent the accumulation of biological matter and are worthy of further investigation as a source of bio-inspiration. A comprehensive and critical review of the related literature describes traditional design approaches and next-generation bio-inspired strategies respectively for anti-biofouling and antibacterial materials. A novel study of the micro- and nanoscale topographical features of the reed canary grass leaf was conducted. Near the tip of the leaf, it was found that moving droplets of water favored motion in one direction because of gradients in topography and surface energy. While the entirety of the leaf was highly hydrophobic thus indicative of anti-biofouling or accumulation of debris, the surface is not antibacterial. Finally, a preliminary study of a bio-inspired micro-reservoir topography to contain hydrophobic antibacterial ionic liquids that combines nature-inspired topography with proven antibacterial moieties is described. The ionic liquids – benzalkonium docusate and lidocaine docusate – do not evaporate and, due to their highly insoluble nature and confinement within micro-reservoirs, can potentially maintain the antibacterial properties of the surface over an extended duration.

Resumé

L'accumulation indésirable de matière biologique sur les surfaces, appelée biofouling, est néfaste pour la santé humaine et pour certains procédés industriels, en particulier si la matière biologique en question est constituée de bactéries pathogènes. Les approches chimiques traditionnelles pour créer des surfaces antibactériennes ou des anti-biofouling présentent de nombreux inconvénients et deviennent de moins en moins efficaces à mesure que les résistances bactériennes s'accroissent. La nouvelle génération de surfaces antibactériennes et d'anti-biofouling se basent sur la topographie physique, ou une combinaison de cette dernière avec des éléments chimiques, pour obtenir une activité antibactérienne. Les animaux et les plantes ont développé lors de leur évolution d'unique topographies de surfaces, conçues pour éviter l'accumulation de matière biologique, et semblent prometteuses en tant que source de bio-inspiration. Une revue de la littérature connexe décrit les approches traditionnelles et les stratégies bio-inspirées de la prochaine génération, respectivement pour les matériaux anti-biofouling et antibactériens. Une nouvelle étude des caractéristiques topographiques micro et nanométrique de la feuille de *Phalaris arundinacea*. Près du point de la feuille, les gouttelettes d'eau favorisaient le mouvement dans une direction à cause des gradients de la topographie et de l'énergie de surface. Alors que la totalité de la feuille était hautement hydrophobe, ce qui indique un anti-biofouling ou une accumulation de débris, la surface n'est pas antibactérienne. Enfin, une étude préliminaire d'une topographie micro-réservoir bio-inspirée pour contenir des liquides ioniques antibactériens qui combine la topographie inspirée de la nature avec des fragments antibactériens éprouvés est décrite. Les liquides ioniques – benzalkonium docusate et lidocaine docusate - ne s'évaporent pas et, en raison de leur nature hautement insoluble et de leur confinement dans des micro-réservoirs, ils peuvent potentiellement maintenir les propriétés antibactériennes de la surface pendant une durée prolongée.

Thesis Acknowledgements

Many individuals assisted in my Master's thesis research and I am grateful for their contributions. Specifically, I would like to thank Prof. Nathalie Tufenkji for guiding my academic career with patience ever since I first joined her laboratory as an undergraduate researcher. I look forward to working with her in the near future. I am also grateful for Dr. Robin D. Rogers, who challenged me to improve constantly and who exemplifies excellence in research. These past two years as a Master's candidate have been the most rewarding time of my life in terms of personal development primarily due to the co-supervision by Prof. Tufenkji and Dr. Rogers.

Next, I would like to thank two others who took on unofficial mentorship roles and who irrevocably improved my research through active collaborations: Postdoctoral fellow Dr. Paula Berton assisted me through the world of chemistry and the nuances of academia, while Prof. Christopher Moraes offered valuable and unique insights into scientific pursuits in general.

Lastly, I would like to thank the members of the Biocolloids and Surfaces Laboratory and the Robin D. Rogers Research Group who supported my research as well as my friends and family for their unwavering encouragements. Thanks also to my friend and colleague Emeric Mahé for his help in translating the abstract of this thesis.

The work described in this thesis was undertaken, in part, thanks to funding from the Canada Excellence Research Chairs (CERC) program, the Canada Research Chairs (CRC) program, the Natural Sciences and Engineering Research Council of Canada (NSERC) Discovery program and the Eugenie Ulmer-Lamothe (EUL) fund in the Department of Chemical Engineering at McGill University.

Preface and Contribution of Authors

This thesis was arranged in accordance with the McGill University thesis preparation guidelines in a manuscript-based format. Chapter 1 consists of a thesis introduction.

Chapter 2 presents a critical literature review that is currently under peer-review titled “Nanodarts, nanoblades, and nanospikes: Mechano-bactericidal nanostructures and where to find them.” The authors are Nicholas Lin, Paula Berton, Christopher Moraes, Robin D. Rogers, and Nathalie Tufenkji. The manuscript was researched and drafted by N. Lin and edited by P. Berton, C. Moraes, R.D. Rogers and N. Tufenkji.

Chapter 3 consists of a manuscript to be submitted for publication titled “Anisotropic and metastable hydrophobicity of the leaf canary grass leaf.” The authors will be Nicholas Lin, Victor Uong, Paula Berton, Reghan James Hill, Robin D. Rogers, and Nathalie Tufenkji. Experimental work was designed and performed by N. Lin who was assisted by V. Uong, an undergraduate research assistant. Microscopy and contact angle measurements was conducted by N. Lin. Data analysis was conducted by N. Lin, assisted by V. Uong and R.J. Hill. The manuscript was drafted by N. Lin and P. Berton while R.J. Hill, R.D. Rogers and N. Tufenkji provided guidance and supervision throughout the project and in manuscript editing.

Chapter 4 contains experimental data of an ongoing project tentatively titled “Evaluating the antibacterial properties of hydrophobic ionic liquids” N. Lin and P. Berton designed the experiments and carried out data analysis. N. Lin fabricated the micro-well device and conducted all microbiology experiments. R.D. Rogers and N. Tufenkji provided guidance and supervised the work.

Chapter 5 summarizes the thesis and offers suggestions for future work.

Table of Contents

Abstract.....	ii
Resumé.....	iii
Thesis Acknowledgements	iv
Preface and Contribution of Authors	v
Chapter 1: Introduction.....	1
1.1 Antibacterial compounds and antibacterial resistance.....	1
1.2 Biofilms and biofouling	2
1.3 Modern antibacterial approaches	4
1.4 Biomimetic strategies for anti-biofouling topographies	5
1.5 Bio-inspired strategies for antibacterial surfaces.....	6
1.6 Thesis objectives.....	7
1.7 References.....	8
Chapter 2: Nanodarts, nanoblades, and nanospikes: Mechano-bactericidal nanostructures and where to find them	10
2.1 Abstract.....	10
2.2 Introduction.....	11
2.3 Nanodarts and nanoblades as mechano-bactericidal colloids.....	14
2.4 Nanopillars, nanospikes, and other mechano-bactericidal nanotopographies	25
2.5 Future outlook.....	37
2.6 Concluding perspectives	40
2.7 Acknowledgements.....	43
2.8 Conflicts of interest.....	43
2.9 References.....	43
Chapter 3: Anisotropic and metastable hydrophobicity of the leaf canary grass leaf	52
3.1 Abstract.....	52
3.2 Introduction.....	53
3.3 Experimental.....	55
3.4 Results and discussion	57
3.5 Conclusions.....	69
3.6 Acknowledgements.....	69
3.7 Supplementary information	70
3.9 References.....	77
Chapter 4: Micro-reservoir surfaces containing hydrophobic antibacterial ionic liquids.....	79
4.1 Abstract.....	79

4.2 Introduction.....	80
4.3 Experimental.....	83
4.4 Results and discussion	85
4.5 Conclusions and future Work	94
4.6 References.....	95
Chapter 5: Conclusions and future work	96

Chapter 1: Introduction

Bacteria and biomacromolecules are ubiquitous in the environment. In many cases, the presence of bacteria poses no harm and can even provide symbiotic contributions. However, accumulation of biological matter or pathogenic bacteria that are detrimental to industrial processes or human health must be treated and eliminated to prevent significant damage.

1.1 Antibacterial compounds and antibacterial resistance

The introduction of antibacterial compounds over 70 years ago is arguably the most important medical intervention to date as it promised a means to control bacterial contamination [1]. However, traditional antibacterial treatments for common bacterial pathogens are currently failing at an alarming pace as a result of antibacterial resistance – a consequence of humanity’s overuse of antibacterial compounds. Antibacterial resistance drastically reduces the effectiveness of antibacterial treatments and can originate in various ways. In the near future, bacteria that were once easily eradicated by antibacterial treatment may proliferate unchecked as a result of resistance [2]. Thus, novel strategies to inhibit or prevent microbial contamination is currently considered one of the greatest needs of our time [3].

While the molecular basis behind resistance events is beyond the scope of this thesis, the root cause of antibacterial resistance can be summarized as follows. Some bacterial strains are intrinsically genetically resistant to certain antibacterial compounds. After the compound is deployed, these strains survive and are “selected” while strains that are susceptible are eliminated from the population. The selected resistant strains pass on their resistance genes to their daughter cells or to other bacteria that are within the vicinity [3]. Bacteria can also acquire or develop resistance, either through mechanisms such as minimizing the intracellular concentrations of the

antibacterial compound or modifying the antibacterial target or inactivating the compound by enzyme-mediated recognition and hydrolysis [4].

The very use of antibacterial compounds leads to the exacerbation of antibacterial resistance, as antibacterials select for intrinsically-resistant strains while also providing a sublethal background dose for other strains to acquire resistance [4]. Despite current knowledge of antibacterial resistance, the status quo in the design of antibacterial materials remains unchanged: to load a material with antibacterial agents and expect them to leach out over time in an effort to prevent bacterial growth. In reality, the leached compounds not only foster the development of resistance but also introduce unintentional toxicity [4, 5]. If the desired application is biomedical, for example, then cells of the host may be damaged as a result [4, 5]. Even if environmental and health aspects are overlooked, leaching strategies from a product design perspective are ineffective. The burst-release kinetics of leached compounds are short lived and thus require replenishing, not to mention the compounds often fail to reach the intended target at a sufficient concentration since the diffusion of leached compounds is uncontrolled and directionless [5]. Antibacterial strategies that rely on non-leaching methods to prevent bacterial proliferation are therefore highly sought after and represent a focal point in modern antibacterial research.

1.2 Biofilms and biofouling

While bacteria are often depicted as free-floating (planktonic) unicellular microorganisms, the majority of bacterial species prefer to form communities attached upon surfaces [6]. It is well known that a surface favorable for bacterial growth will trigger the expression of cellular appendages of a nearby bacterium to attach to the surface [7]. Fimbriae, pili, flagella and cilia are examples of bacterial appendages that play a role in attachment. In some cases, even chemically-unfavorable surfaces can be made favorable by molecules secreted from bacteria that “mask” the

original surface such that attachment proceeds anyways [8]. Next, the bacterium rapidly multiplies upon the surface through binary fission while excreting a sticky substance known as the exopolysaccharide matrix (EPS). EPS acts as a diffusion-limiting barrier against deleterious molecules in the environment while also sheltering the biomass from being swept away by fluid shear [9]. This community of bacterial cells – known as a biofilm – enhances the collective ability of the bacteria to survive in numerous ways and is thus difficult to eliminate once formed. Worse yet, some species that produce bacterial spores can remain metabolically dormant, only sporulating once the condition is favorable again. Lastly, the biofilm cycle repeats again when planktonic cells detach from a matured biofilm to colonize a surface elsewhere [10].

Biofilm formation is an example of biofouling. More specifically, biofouling occurs when biological macromolecules or microorganisms deposit or attach onto a surface [11]. Biofouling reduces the efficiency of numerous industrial processes. Marine biofouling is initiated by a combination of bacteria and algal biofilms and causes drag and increases the fuel burn of ships by up to 40% [12]. In energy pipelines, biofouling reduces fluid flow and triggers microbially-influenced corrosion of metallic piping components [13].

The presence of biofouling also greatly jeopardizes processes with direct human interactions in which sterility is of paramount importance. In food packaging and water treatment, human-pathogenic biofilms (and planktonic bacteria) lead to foodborne or waterborne outbreaks of diseases that are particularly life-threatening to individuals with weak immune systems [14]. In medical care, implant devices contaminated with bacteria pose immediate hazards to a patient's health. According to a 2010 study within the United States, more than half a million deaths per year are attributed to biofilms while the total annual cost for biofilm infections is roughly estimated to be \$94 billion [15]. Evidently, the need to prevent biofilm formation and biofouling is one that

is critical to industrial processes and human health alike. However, current antibacterial strategies are unsatisfactory in eliminating the presence of bacteria.

Herein, the definition of anti-biofouling and antibacterial materials follows those established by Hasan *et al.* [16]. Anti-biofouling describes materials that resist or prevent attachment of microorganisms but have no impact on a bacterium's health. Conversely, antibacterial agents may or may not influence bacterial attachment mechanisms but instead impart deleterious effects on bacterial growth. Within the domain of antibacterial agents, two further classifications can be made: Bacteriostatic agents halt bacteria proliferation or suppress their pathogenicity (although cells remain viable), whereas bactericidal materials actively destroy bacteria so that they are no longer viable.

1.3 Modern antibacterial approaches

Due to a biofilm's persistence, attempts to eradicate it entirely are challenging and expensive. Nowadays, it is generally agreed upon that the optimal strategy is not to attack a biofilm, but focus on preventing initial bacterial attachment instead, thereby eliminating the opportunity for biofilm formation in the first place. While this may seem obvious, designing a surface capable of eliminating all traces of initial bacterial colonizers is not a straight-forward endeavor. Many modern approaches in preventing initial attachment have been proposed yielding varying levels of success.

For example, covalently functionalized antibacterial surfaces are designed as non-leaching materials in order to mitigate the excessive release of compounds into the environment [5]. However, as mentioned above, even when a surface is chemically unfavorable, macromolecules such as proteins and polysaccharides from the local environment or secreted by bacteria can form a "conditioning film" on the surface, masking antibacterial functional groups. This renders the

covalently functionalized material ineffective thus allowing bacterial adhesion and proliferation to proceed [17, 18]. Alternatively, the use of bacteriophage (viruses that kill bacteria, known as phage therapy) immobilized to surfaces is intriguing but resistance to phage binding mechanisms has been observed, raising doubt over treatment consistency [19]. Genetically engineering phage to counter resistance could pave the way for immense opportunities but the disposal of genetically engineered phage brings about concerns regarding their fate post-treatment [20].

Clearly, strategies differing from those already proposed are needed to address the inadequacies of current antibacterial materials. Thus, a subset of modern antibacterial research has turned to biology for inspiration in attempts to mimic or build upon time-tested designs found in nature.

1.4 Biomimetic strategies for anti-biofouling topographies

Anti-biofouling surfaces can be achieved through chemical-based or physical-based approaches. Both are employed in nature and both are explored in this thesis. Microbial pathogens have lived alongside plants, animals, and insects for hundreds of millions of years. Over time, bacteria have evolved mechanisms to colonize biotic and abiotic surfaces to improve their chances of survival. Concurrently, flora and fauna have also optimized unique protective strategies through evolution to combat the presence of bacteria [16]. Biomimicry in antibacterial research aims to duplicate these proven mechanisms of nature and transfer them onto artificial surfaces to achieve the same functionality.

Chemical-based antibacterial strategies are abundant in nature. Plants excrete toxins or contain essential oils that are biologically active. The exterior peel of the North American cranberry fruit (*Vaccinium macrocarpon*), for example, contains high concentrations of natural phenolic compounds such as proanthocyanidins that suppress the expression of bacterial

appendages of colonizing bacteria [21]. Some herbs and spices are also well known for high concentrations of antibacterial compounds. Berberine and magnocurarine are some antibacterial compounds found in many plants [22]. These compounds fall into the broad group of chemicals known as quaternary ammonium compounds (QACs), which are often used as disinfecting agents as they damage and disrupt the bacterial cell membrane [23].

Physical-based anti-biofouling strategies, on the other hand, rely on microscopic surface topography. Arguably the most well-studied plant surface, the lotus leaf consists of waxy crystalloid nanobumps superimposed on microscale convex cells [24]. The wax itself is already hydrophobic but the addition of the nanobumps enhances the leaf's water-repellency properties more than what surface chemistry alone can provide. The topographical arrangement provides microscopic cavities that trap air pockets on the leaf surface. Consequentially, droplets of water that land on a lotus leaf are suspended upon air, unable to wet the superhydrophobic surface in what is referred to as the Cassie-Baxter state of wettability [25]. When the leaf is tilted ever so slightly, droplets of water slide off with little resistance, collecting with them contaminants – biological or otherwise – as they roll off the leaf surface. The result is a lotus leaf surface that appears to stay clean at all times (so that photosynthesis can proceed uninhibited), a phenomenon described as self-cleaning [24]. Structural hierarchy, that is, combining micro- and nanostructures onto a single topography, is one of the most popular and effective ways to generate a self-cleaning surface [26]. The lotus's self-cleaning function has translated into biomimetic products such as anti-adhesive windows and roof tiles and other construction materials [27].

1.5 Bio-inspired strategies for antibacterial surfaces

A self-cleaning surface such as the lotus leaf can be considered anti-biofouling as droplets carrying microorganisms may roll off before cellular appendages can initiate attachment.

However, they are not antibacterial as they are incapable of directly affecting a bacterial cell's viability. In applications where complete eradication of bacteria is necessary, self-cleaning surfaces are inadequate and active antibacterial compounds may be necessary to guarantee sterility.

Bio-inspired materials take designs found in nature and enhance, combine or utilize them in another context to provide new and improved functionalities. Take for example microscopic pillars on the topography of the cicada wing. If the wing were to be used as a mold, the resulting inverse topography – which would take the form of microscopic reservoirs – can be designed to carry antibacterial liquids. To our knowledge an antibacterial micro-reservoir topography has yet to be explored for commercial antibacterial applications. However, combining the bio-inspired micro-reservoir topography with chemical antibacterial strategies could yield immediate benefits. This notion is explored in this thesis by preparing a surface with micro-reservoirs and filling the reservoirs with antibacterial ionic liquids (ILs), or salts that melt below 100 °C. As demonstrated in this thesis, the micro-reservoir strategy holds promise and warrants further investigation.

1.6 Thesis objectives

The aim of this thesis was to employ topography and surface chemistry to propose new strategies for non-leaching surfaces that are anti-biofouling or antibacterial. Research was undertaken by combining designs inspired from nature together with principals of sustainable chemistry. Original research as fulfillment for this thesis can be divided into three chapters.

Chapter 2 is a critical review of a next-generation antibacterial approach known as mechano-bactericidal nanostructures that is based partially on the discovery of the antibacterial wings of cicada and dragonfly. Future outlook for the direction of this emerging field of antibacterial research is also provided.

Inspired by self-cleaning plants reported in literature, investigations into the hydrophobic properties of the reed canary grass leaf uncovered fascinating microscopic topographies. More specifically, wettability varies depending on a water droplet's spatial positioning on the leaf since the micro-topography of a single leaf is not uniform. This original research article is described in Chapter 3.

Chapter 4 contains experimental data of the design of a highly insoluble yet antibacterial ionic liquid to be placed within a surface patterned with micro-reservoirs. By filling micro-reservoirs with antibacterial ILs that are also hydrophobic, the release of the ILs is mitigated by their containment as well as their insoluble nature. That, combined with the fact that ILs are non-volatile, means that hydrophobic antibacterial ILs do not contribute to air pollution and do not leach into the aqueous environment.

Finally, Chapter 5 summarizes the thesis and offers suggestions for future work.

1.7 References

- [1] Andersson DI, Hughes D, *Nature Reviews Microbiology*, 2010;8:260-71.
- [2] Woolhouse M, Farrar J, *Nature*, 2014;509:555.
- [3] Blair JM, Webber MA, Baylay AJ, Ogbolu DO, Piddock LJ, *Nature Reviews Microbiology*, 2015;13:42-51.
- [4] Andersson DI, Hughes D, *Nat Rev Micro*, 2014;12:465-78.
- [5] Lewis K, Klibanov AM, *TRENDS in Biotechnology*, 2005;23:343-8.
- [6] McLean RJC, Lam JS, Graham LL, *Journal of Bacteriology*, 2012;194:6706-11.
- [7] O'Toole G, Kaplan HB, Kolter R, *Annual Reviews in Microbiology*, 2000;54:49-79.
- [8] Salwiczek M, Qu Y, Gardiner J, Strugnell RA, Lithgow T, McLean KM, Thissen H, *Trends in biotechnology*, 2014;32:82-90.
- [9] Flemming H-C, Neu TR, Wozniak DJ, *Journal of bacteriology*, 2007;189:7945-7.
- [10] Vlamakis H, Chai Y, Beaugregard P, Losick R, Kolter R, *Nature Reviews Microbiology*, 2013;11:157-68.
- [11] Banerjee I, Pangule RC, Kane RS, *Adv Mater*, 2011;23:690-718.
- [12] Christie A, Dalley R, *Barnacle biology*, 1987:419-33.
- [13] Lenhart TR, Duncan KE, Beech IB, Sunner JA, Smith W, Bonifay V, Biri B, Suflita JM, *Biofouling*, 2014;30:823-35.
- [14] Shi X, Zhu X, *Trends in Food Science & Technology*, 2009;20:407-13.

- [15] Wolcott RD, Rhoads DD, Bennett ME, Wolcott BM, Gogokhia L, Costerton JW, Dowd SE, J Wound Care, 2010;19:45-6, 8-50, 2-3.
- [16] Hasan J, Crawford RJ, Ivanova EP, Trends Biotechnol, 2013;31:295-304.
- [17] Tuson HH, Weibel DB, Soft matter, 2013;9:4368-80.
- [18] Lejeune P, Trends in microbiology, 2003;11:179-84.
- [19] Fischetti VA, Nelson D, Schuch R, Nature biotechnology, 2006;24:1508-11.
- [20] Alavidze Z, Aminov R, Betts A, Bardiau M, Bretaudeau L, Caplin J, Nino C, Coffey A, Cooper I, De Vos D, Biotechnology Journal, 2016;11:1-6.
- [21] Eydelnant IA, Tufenkji N, Langmuir, 2008;24:10273-81.
- [22] Joyce MD, Jennings MC, Santiago CN, Fletcher MH, Wuest WM, Minbiole KP, Journal of Antibiotics, 2016;69:344.
- [23] Campanac C, Pineau L, Payard A, Baziard-Mouysset G, Roques C, Antimicrobial agents and chemotherapy, 2002;46:1469-74.
- [24] Barthlott W, Neinhuis C, Planta, 1997;202:1-8.
- [25] Cassie A, Baxter S, Transactions of the Faraday Society, 1944;40:546-51.
- [26] Gao L, McCarthy TJ, Langmuir, 2006;22:2966-7.
- [27] Bixler GD, Bhushan B, Critical Reviews in Solid State and Materials Sciences, 2015;40:1-37.

Chapter 2: Nanodarts, nanoblades, and nanospikes: Mechano-bactericidal nanostructures and where to find them

Traditional antibacterial agents target bacteria through chemical-based approaches. Within the past decade, another antibacterial approach has emerged: one which employs nanostructure geometry to deliver lethal mechanical forces causing bacterial cell death. “Mechano-bactericidal” nanostructures are either designed as suspended colloids (such as carbon nanotubes or graphene nanosheets) or surface nanotopography (such as nanopillars or nanospikes). These mechano-bactericidal strategies are seldom compared despite offering mutually beneficial insights. This manuscript bridges the knowledge gap between the two strategies of mechano-bactericidal design and offers insights for future directions in this novel and multidisciplinary field. The manuscript was researched and drafted by N. Lin and edited by P. Berton, C. Moraes, R.D. Rogers and N. Tufenkji and is currently under peer-review in the journal *Advances in Colloid and Interface Science* with the title: “Nanodarts, nanoblades, and nanospikes: Mechano-bactericidal nanostructures and where to find them.” As the title suggests, many mechano-bactericidal nanostructures, particularly those that contribute to surface topographies, are found in nature.

2.1 Abstract

Over the past ten years, a next-generation approach to combat bacterial contamination has emerged: one which employs nanostructure geometry to deliver lethal mechanical forces causing bacterial cell death. In this review, we first discuss advances in both colloidal and topographical nanostructures shown to exhibit such “mechano-bactericidal” mechanisms of action. Next, we highlight work from pioneering research groups in this area of antibacterials. Finally, we provide suggestions for unexplored research topics that would benefit the field of mechano-bactericidal nanostructures. Traditionally, antibacterial materials are loaded with antibacterial agents with the

expectation that these agents will be released in a timely fashion to reach their intended bacterial metabolic target at a sufficient concentration. Such antibacterial approaches, generally categorized as chemical-based, face design drawbacks as compounds diffuse in all directions, leach into the environment, and require replenishing. In contrast, due to their mechanisms of action, mechano-bactericidal nanostructures can benefit from sustainable opportunities. Namely, mechano-bactericidal efficacy needs not replenishing since they are not consumed metabolically, nor are they designed to release or leach compounds. For this same reason, however, their action is limited to the bacterial cells that have made direct contact with mechano-bactericidal nanostructures. As suspended colloids, mechano-bactericidal nanostructures such as carbon nanotubes and graphene nanosheets can pierce or slice bacterial membranes. Alternatively, surface topography such as mechano-bactericidal nanopillars and nanospikes can inflict critical membrane damage to microorganisms perched upon them, leading to subsequent cell lysis and death. Despite the infancy of this area of research, materials constructed from these nanostructures show remarkable antibacterial potential worthy of further investigation.

2.2 Introduction

Bacterial contamination is detrimental to industrial processes and hazardous to human health. The undesirable presence of bacteria is traditionally eliminated by chemical-based approaches relying on the diffusive release of antibacterial agents [1]. Today, these agents are loaded, coated, or impregnated into a myriad of materials for industrial applications and consumer products alike. However, systems designed to release antibacterial agents result in the leaching of said agents into the environment. In addition to unintended toxicity jeopardizing indigenous organisms, leached compounds produce a sublethal background dose that can foster the

development of resistance mechanisms [2, 3]. Even if these environmental and health aspects are overlooked, from a product design perspective, release-based antibacterial materials in practice are often ineffective. Their burst-release kinetics are initially highly toxic but concentration decreases rapidly, thus requiring replenishment or replacement, and released compounds ultimately do not reach the intended targets at a sufficient concentration since diffusion is uncontrolled and directionless [4, 5].

Novel, non-diffusive strategies to prevent bacterial proliferation are therefore highly sought after and are a focal point in current antibacterial research [1, 2, 6, 7]. For example, covalently functionalized, non-leaching antibacterial coatings have been designed to mitigate the excessive release of compounds into the environment [2, 8]. However, even when a surface is chemically unfavorable, ions and macromolecules such as proteins and polysaccharides secreted by bacteria or from the local environment can form a “conditioning film” on the surface. This acts to mask antibacterial functional groups so that adhesion and bacterial proliferation can proceed, rendering the covalently functionalized material inefficient [9, 10].

Innovative studies over the past ten years have led to a next-generation bactericidal approach which acts through physico-mechanical means. The typical size of an individual bacterium is on the order of 1 μm , with much of its cellular components in the nanoscale range. These components and their biological functions have proven to be greatly influenced when contact is made with other nanoscale materials in their environment [11-13]. Certain nanoscale structures and geometries have unique abilities of inhibiting, injuring, or even lethally inactivating a bacterial cell upon contact. The lattermost of these materials, henceforth known as “mechano-bactericidal nanostructures,” can be prepared as dispersed nanoparticles suspended in media, referred to as colloids, or fabricated as surface nanotopography (Figure 1). Mechano-bactericidal

colloids and mechano-bactericidal nanotopographies are seldom compared despite new colloidal insights potentially being beneficial to those studying nanotopography, and vice versa. This review bridges the knowledge gap between the two strategies of mechano-bactericidal nanostructures. By doing so, we hope to illuminate existing themes and offer potential research directions for the future.

The immediate advantage of mechano-bactericidal nanostructures over traditional, chemical-based antibacterial agents stems from their physical interactions with bacteria. As they are not designed to release antibacterial compounds, aforementioned drawbacks associated with diffusion losses are not of primary concern. However, their non-diffusive design is also the primary limitation in their potential application, as they can only inactivate bacteria that have made direct contact with the mechano-bactericidal nanostructures. Ideally, the most effective antibacterial surface would instantly eliminate adhered cells before proliferation can occur [14]. In general, this has been the case for substrates featuring mechano-bactericidal nanostructures. In particular, nanostructures designed with sharper and higher aspect ratio geometries have been shown to rapidly eliminate adhered bacteria within mere minutes of contact. The focus herein lies in the mechano-bactericidal mechanisms of action upon such contact. Proof-of-concept demonstrations by pioneering research groups are also highlighted. The fabrication techniques to produce nanoscale colloids versus topographies are vastly different from one another and therefore described here only in brief, as we focus on the lethal interactions between bacteria and mechano-bactericidal nanostructures.

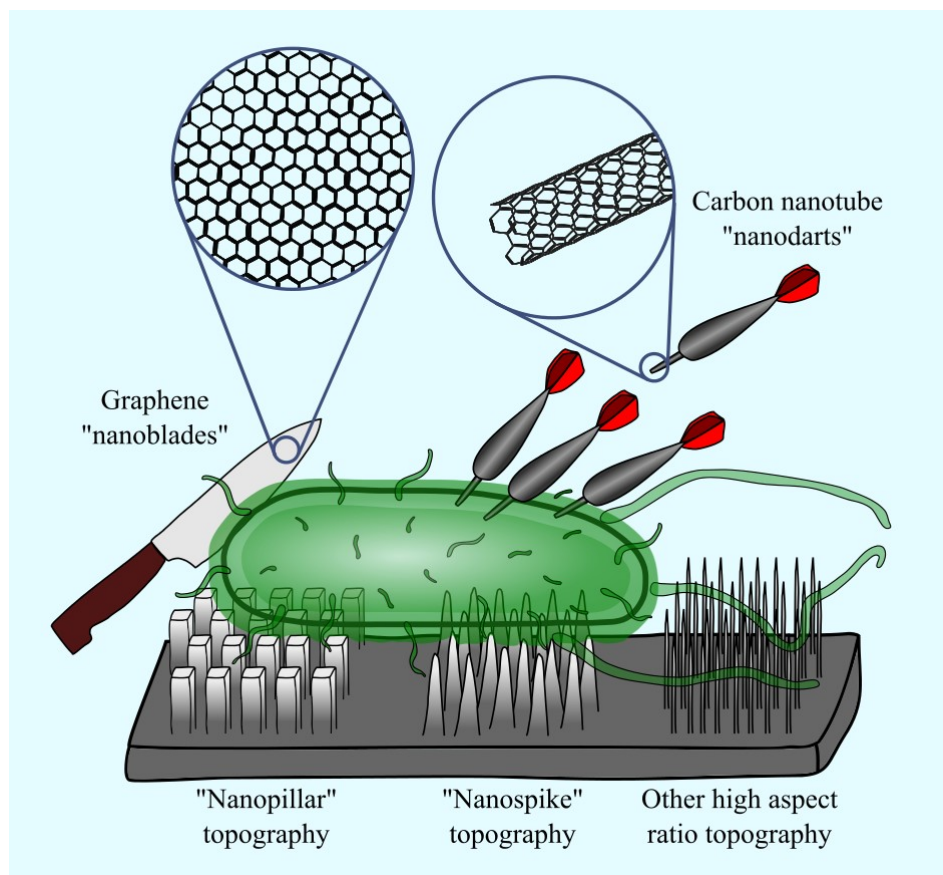


Figure 1: Mechano-bactericidal nanostructures can be designed to act as suspended colloidal systems, as is the case for carbon nanotubes and graphene nanosheets, or patterned as surface nanotopography, such as nanopillars and nanospikes. Note that the different components of this graphic are not drawn to scale.

2.3 Nanodarts and nanoblades as mechano-bactericidal colloids

In this section, we introduce suspended colloids that act as mechano-bactericidal nanostructures. Current knowledge of such colloids is mostly limited to studies of carbon nanotubes (CNTs) and graphene materials. Comprehensive reviews on the fabrication of CNTs [15, 16] or graphene [17, 18] as well as their biological interactions are available but do not emphasize the mechano-bactericidal mechanisms discussed herein. Conventional antibacterial assays [19, 20] demonstrate the mechano-bactericidal activity of these colloidal nanostructures under typical incubation conditions, whereas computational simulations offer insights into

underlying biological interaction between an individual colloid and a model cell membrane lipid bilayer.

2.3.1 CNTs as nanodarts

In 2007, Elimelech *et al.* reported the first direct evidence of the mechano-bactericidal mode of action: single walled carbon nanotubes (SWCNTs) were demonstrated to severely pierce and damage the cell membrane of *Escherichia coli* as a result of direct contact, hinting at the potential of SWCNTs as antibacterial materials [21]. In their study, metal toxicity and oxidative stress were ruled out due to the pristine nature of the preparation. In contrast, studies with multi-walled CNTs (MWCNTs) showed that, compared to aggregates of SWCNTs, bactericidal efficacy by aggregates of MWCNT were not as pronounced, but that direct contact between *E. coli* cells and CNTs was necessary for inactivation in both cases [22, 23]. Leakage of genetic material following cell membrane destruction was quantified, as were levels of stress factor-associated mRNA gene products. Both experiments once again pointed to the superior antibacterial efficacy of SWCNTs. Their results suggest that direct contact due to the high aspect ratio geometry of SWCNTs was primarily responsible for the bactericidal effect. Furthermore, higher specific surface area of SWCNTs enable more interaction opportunities with membranes of cells compared to MWCNTs, leading to increased occurrences of membrane piercing events by the ends of nanotubes [22]. Similarly, Chen *et al.* found thin and rigid SWCNTs induced more significant piercing, needle-like damage to the membranes of gut bacteria than MWCNTs [24].

Liu *et al.* increased the antibacterial contact area available by preparing pristine and individually dispersed, one-dimensional (1D) SWCNTs 8.3 Å in diameter. They concluded that these SWCNTs primarily act as “nanodarts” to pierce bacterial cells, while cell death due to inhibitory effects of oxidative stress and toxic impurities were minimal [25]. Increased

antibacterial rates were achievable simply by changing the shaking speed of the flasks during incubation with SWCNTs, thereby increasing the frequency and intensity delivered via the mechano-bactericidal SWCNTs. The group evaluated survival of both Gram-positive (*Bacillus subtilis* and *Staphylococcus aureus*) and Gram-negative (*E. coli* and *Pseudomonas aeruginosa*) bacteria and found SWCNTs exhibited higher antibacterial activity toward Gram-positive cells. They reasoned that the natural complexity of Gram-negative bacteria (characterized by inner and outer membranes sandwiching a peptidoglycan layer) made it harder for nanodarts to penetrate. The presence of complex appendages and functional groups protruding from the outer membrane of Gram-negative bacteria possibly acts as a shielding layer akin to steric hindrance, lessening the direct impact and interaction between colloidal nanostructures and Gram-negative bacteria. The same group later used a sharp 2 nm atomic force microscope (AFM) tip to mimic an individual collision event between a cell and a SWCNT and found that a singular collision between a CNT and a cell is insufficient to induce lethal damage. Instead, antibacterial activity would require the cumulative effect of a large number of individually dispersed nanodart-membrane interactions over time [26]. Table 1 lists representative studies attributing bacterial cell death to the direct physical interactions with CNTs.

Table 1: CNTs as mechano-bactericidal colloids

Colloid	Mechano-bactericidal nanostructure (d: diameter)	Summary of findings	Reference
CNTs	SWCNT aggregates (mean tube d: 0.9 nm)	First evidence of bacterial (<i>E. coli</i>) cell damage and death by direct contact with CNTs	Kang <i>et al.</i> [21]
CNTs	SWCNT aggregates (mean tube d: 0.9 nm, length: 2 μ m) and MWCNT aggregates (mean tube d: 30 nm, length: 70 μ m)	Diameter of CNTs is a key factor: SWCNTs are much more toxic to <i>E. coli</i> than MWCNTs.	Kang <i>et al.</i> [22]
CNTs	Various MWCNT aggregates	Higher toxicity towards <i>E. coli</i> is observed with uncapped, debundled, short and dispersed MWCNTs.	Kang <i>et al.</i> [23]

	(mean tube d: 17 – 35 nm, length: 2.3 – 91 μm)		
CNTs	Individually dispersed pristine SWCNT nanodarts (mean tube d: 0.83 nm, length: 1 μm)	Found physical puncture on bacteria (Gram- negatives: <i>P. aeruginosa</i> and <i>E. coli</i> , Gram- positives: <i>S. aureus</i> and <i>B. subtilis</i>) caused by nanodarts improved by individually dispersing SWCNTs, increasing SWCNT concentration, and elevating shake speed of incubation.	Liu <i>et al.</i> [25]
Carbon nanomaterials	SWCNTs (outer d: 1-2 nm, length: 30 μm), MWCNTs (outer d: 8 nm, length: 30 μm), GO ^a , rGO ^a , fullerene (C ₆₀)	Needle-like SWCNTs and knife-like GO had strongest antibacterial activity against copper- resistant <i>Ralstonia solanacearum</i> by damaging cell walls whereas the ball-like C ₆₀ did not show significant antibacterial activity.	Wang <i>et al.</i> [27]

On the one hand, experimental assays evaluate efficacy of mechano-bactericidal nanostructures in conventional incubation conditions to monitor bacterial proliferation. However, direct observations in these studies are limited to the use of microscopy at static time points that offer only discrete glimpses of the process. Simulation techniques, on the other hand, offer more comprehensive explanations as to how nanomaterials interact with modeled cell membranes, albeit modeling efforts investigate lipid bilayer membranes and cannot represent the complexities of a bacterial membrane with a peptidoglycan cell wall and cellular appendages. The model of choice for the majority of simulations is coarse grained molecular dynamics, which combines a cluster of atoms, molecules, or chemical groups into one particle to reduce computational cost [28, 29]. Through modeling, Yang *et al.* established that penetrating capability of anisotropic nanoparticles across a lipid bilayer is determined by the contact area between the particle and bilayer. For this reason, penetration becomes more difficult when the possible contact area of cylindrical nanoparticles increases [30]. Simulations of individual interactions of a CNT with a cell's lipid bilayer membrane are generally in agreement that a CNT would first enter a cell through either ends of the tube structure, likely in a near-perpendicular manner [31-35]. For instance, Wallace *et al.* used steered molecular dynamics to pull a SWCNT through a lipid bilayer, finding less pulling force was required when orientation of the SWCNT was perpendicular to the bilayer compared to

a parallel orientation [33]. After initial insertion, additional destructive intermolecular interactions with lipid molecules would arise, leading to lipids being extracted from the rest of the bilayer, for instance, or the formation of lipid micelles [34]. Figure 2 shows a selection of SEM images highlighting destruction of cell membranes by CNTs as well as modeling experiments investigating a singular membrane insertion event of a SWCNT.

Mechano-bactericidal penetration does not fully explain the observed antibacterial effect of CNTs. The energy required for a CNT to fully and spontaneously penetrate through a membrane is quite high [36, 37], not to mention other nanoscale interactions are also at play. Through modeling and experimentation, it is known that engineered nanomaterials can interact with the bacterial cell membrane by adsorbing onto the membrane, passing through it, extracting its lipids, inducing pore formation, or activating membrane receptor proteins [38-41]. Like most other antibacterial nanomaterials, CNTs offer numerous antibacterial interactions depending on their design parameters and environmental influences [42-44]. Pasquini *et al.* found SWCNTs functionalized with chemical moieties that compacted CNT aggregates indirectly decreased cytotoxicity [45]. Vecitis *et al.* suggested that piercing is merely the first of three steps leading to CNTs' overall antibacterial mechanism. The second step being the perturbation of the rest of the cell membrane, followed by the third and last step of CNT structure-dependent bacterial oxidation [44].

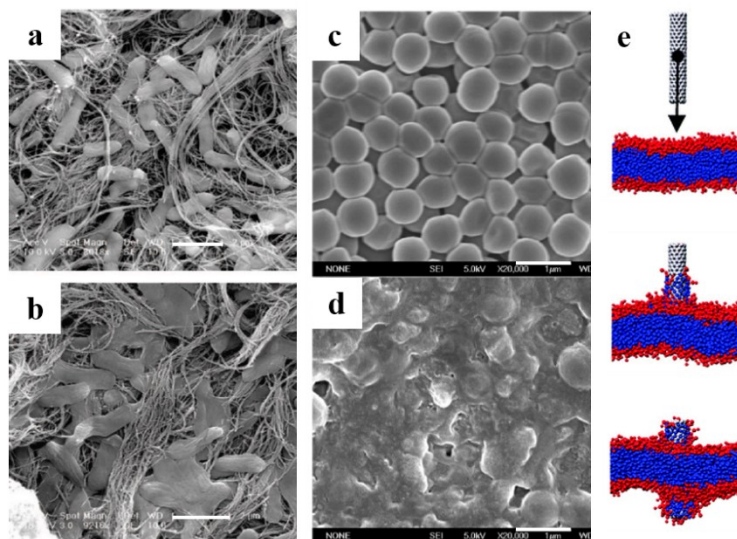


Figure 2. SEM images of *E. coli* cells exposed to (a) MWCNT aggregates for 60 min (scale bar: 2 μm) (b) and SWCNT aggregates for 60 min (scale bar: 2 μm), which produced higher mechano-bactericidal properties due to enhanced specific surface area available for contact. SEM images of *S. aureus* (c) incubated without SWCNTs (scale bar: 1 μm) (d) and after 2 h-incubation with pristine and dispersed SWCNTs (scale bar: 1 μm) show compromised cellular integrity. (e) Steered molecular dynamics pulling a SWCNT through a lipid bilayer reveals a perpendicular orientation requires less force to pull through compared to pulling CNT oriented in parallel. Lipids creep up the wall of the SWCNT during insertion and extracted lipids eventually block the tube ends. Images a), (b) adapted with permission from ref [22], copyright (2008) American Chemical Society (ACS), (c), (d) adapted with permission from ref [25], copyright (2009) ACS, (e), adapted with permission from [33], copyright (2008) ACS.

2.3.2 Graphene sheets as nanoblades

Aside from CNTs, another class of colloidal suspensions frequently reported to physically induce cell damage is graphene nanomaterials – truly two-dimensional (2D) sheet-like nanomaterials consisting of a single layer of carbon atoms arranged hexagonally. For the purposes of this review, graphene, its derivatives (such as graphene oxide (GO)), and other chemically-modified graphene nanosheet structures are broadly referred to as graphene family nanomaterials (GFNs). As GFNs are also high aspect ratio, low-dimensional nanomaterials, they were predicted to share certain antibacterial mechanisms observed in CNTs [46]. Akhavan *et al.* laid GO “nanowalls” on stainless steel substrates via electrophoretic deposition; the randomly oriented GO

nanosheets, some of which were nearly perpendicular with respect to the substrate, provided sharp edges on the surface available for bacterial interaction [46]. *E. coli* and *S. aureus* were used as Gram-negative and Gram-positive bacterial models, respectively. Nanowalls exhibited stronger antibacterial activities against *S. aureus* as shown by colony forming unit (CFU) enumeration and quantification of cytoplasmic RNA leakage. The group reasoned that the lack of outer membrane in Gram-positive bacteria made it more sensitive to the direct contact with the sharp edges of nanowalls, echoing the increased antibacterial susceptibility of Gram-positive bacteria to mechano-bactericidal colloids previously observed with CNTs [46]. In elucidating how GFNs interact with cell membranes, Lu *et al.* magnetically aligned GO nanosheets in a vertical orientation with respect to the substrate, finding the vertical orientation to exhibit enhanced antibacterial activity against *E. coli* compared to random and horizontal orientations [47]. Based on the limited generation of reactive oxygen species (ROS), they attributed antibacterial properties to a combination of direct electron transfer and nanosheet penetration due to the increased density of edges of the vertically aligned GO. Liu *et al.* found that sharp edges of GFNs induce significant membrane stress towards *E. coli* [48], comparable to earlier mechano-bactericidal studies involving sharp SWCNTs. Experimental observations by other groups concluded that efflux or leakage of intracellular genetic material was further evidence for mechanical disruption of bacterial membranes by graphene, GO, and reduced GO [27, 49-52].

Computational simulations confirmed this hypothesized membrane interaction mechanism, commonly reported as “insertion mode” or “penetration mode” [53-59]. Li *et al.* used coarse-grained molecular dynamics and all-atom molecular dynamics to reveal that membrane piercing by GFN blade-like (or knife-like) materials is initiated at rough asperities, or sharp corners, of the graphene sheets [53]. A comprehensive study by Tu *et al.* experimentally assessed membrane

damage of *E. coli* by dispersed GO, then revealed via simulations that GO can spontaneously insert through different methods of entry into both the outer and inner *E. coli* membranes [54]. Table 2 lists representative studies attributing bacterial cell death to direct physical insertion with GFNs.

Table 2. GFNs as mechano-bactericidal colloids

Colloid	Mechano-bactericidal nanostructure (d: diameter)	Summary of findings	Reference
GFNs	GO and reduced graphene deposited on stainless steel	Found direct contact between cell membrane and extremely sharp edges of deposited graphene were more effective against Gram-positive <i>S. aureus</i> compared to Gram-negative <i>E. coli</i> .	Akhavan <i>et al.</i> [46]
GFNs	GO (thickness: ~ 0.8 nm) magnetically-immobilized and vertically aligned on glass	Vertical alignment of GO nanosheets increased density of edges causing enhanced physical <i>E. coli</i> membrane penetration and chemical oxidation by electron transfer.	Lu <i>et al.</i> [47]
GFNs	Graphite (size: 6.87 μm), graphite oxide (size: 6.28 μm), reduced GO (size: 2.75 μm), GO (size: 0.31 μm)	<i>E. coli</i> incubated with dispersions of GFNs then assessed by SEM showed cell damage after direct contact (similar to CNTs) but cell death was due to a combination of membrane damage and oxidative stress.	Liu <i>et al.</i> [48]
GFNs	GO (mean thickness: 1 nm)	GO caused integrity loss of cell membrane and cell wall of dental pathogens (<i>Streptococcus mutans</i> , <i>Fusobacterium nucleatum</i> , <i>Porphyromonas gingivalis</i>) based on TEM, attributed to physical mechanism of GO which insert/cut through membranes and destructively extract phospholipids.	He <i>et al.</i> [52]
Carbon nanomaterials	SWCNTs (outer d: 1-2 nm, length: 30 μm), MWCNTs (outer d: 8 nm, length: 30 μm), GO ^a , rGO ^a , fullerene (C ₆₀)	Needle-like SWCNTs and knife-like GO had strongest antibacterial activity against copper-resistant <i>Ralstonia solanacearum</i> by damaging cell walls whereas the ball-like C ₆₀ did not show significant antibacterial activity.	Wang <i>et al.</i> [27]

However, the edge-first penetration of GFNs leading to their mechano-bactericidal action is not unanimously accepted; investigation into the physical interactions with GFNs is further complicated by the orientation of nanosheets upon contact, the density of edges, degree of asperities, and GFN size. These factors combined with theoretical modeling suggest that GFNs perhaps act more than as a simple blade [60]. Researchers have shown, for example, that by destructively extracting membrane lipids, the basal plane of GO contributes more significantly to

overall bactericidal properties than the blade-like penetration mechanism [61, 62]. Mangadlao *et al.* eliminated edge penetration effects by immobilizing flat GO sheets whose edges were embedded in a poly(ethylene terephthalate) (PET) substrate [63]. This surface still inactivated *E. coli*, indicating that mechano-bactericidal mechanisms may not contribute major antibacterial activity and that lateral dimension of nanosheets must be taken into account. The insertion, penetration, or “nanoblade” mechano-bactericidal mode of action represents one of a handful of mechanisms frequently reported in the interaction of GFNs with biological materials. Other commonly reported antibacterial mechanisms that act simultaneously upon contact include oxidative stress initiated by ROS or by charge transfer. For instance, Perreault *et al.* found that oxidative stress of GO was also size-dependent such that smaller GO sheets were more antimicrobial due to their high defect density [64]. Chong *et al.* showed light-induced oxidative stress accelerates electron transfer from bacterial biomolecules to the surface of GO, resulting in the reduction of GO while also causing cell destruction [65]. Pore formation induced by GFNs, which leads to osmotic imbalance and subsequent cell death is also possible [66].

It is clear that the extent to which the mechano-bactericidal activity contributes to overall antibacterial efficacy is still contested [60, 67-69]. Size-dependency also influences membrane interactions, as GFNs are nearly atomically thin in one dimension but the other two dimensions are typically large [53]. Through simulations, Dallavalle *et al.* suggested through molecular dynamics modeling that small sheets with a high degree of asperities tend to pierce membranes with ease, whereas intermediate-sized sheets require optimal orientation and larger sheets were more likely to sit flat atop membranes [55]. Instead of piercing, these larger GFNs would instead adsorb on the membrane causing upturning of the phospholipid molecules. Figure 3 provides depictions of some GFN-membrane interactions. Experimentally, size-dependent interactions have

focused on mammalian cell culture as opposed to bacterial systems. For instance, Sanchez *et al.* [17] suggests a critical lateral dimension to be approximately 5 μm in mammalian cell interactions with GFNs. Few-layer-graphene smaller than that can readily insert through the eukaryotic cell membranes and become internalized by human macrophages, whereas the cells would adsorb and wrap around larger graphene sheets. Whether this could lead to inflammation following mammalian uptake of GFNs is unknown [17]. These insights offer a glimpse into how mechano-bactericidal colloids would impact human health, which must be evaluated before deployment.

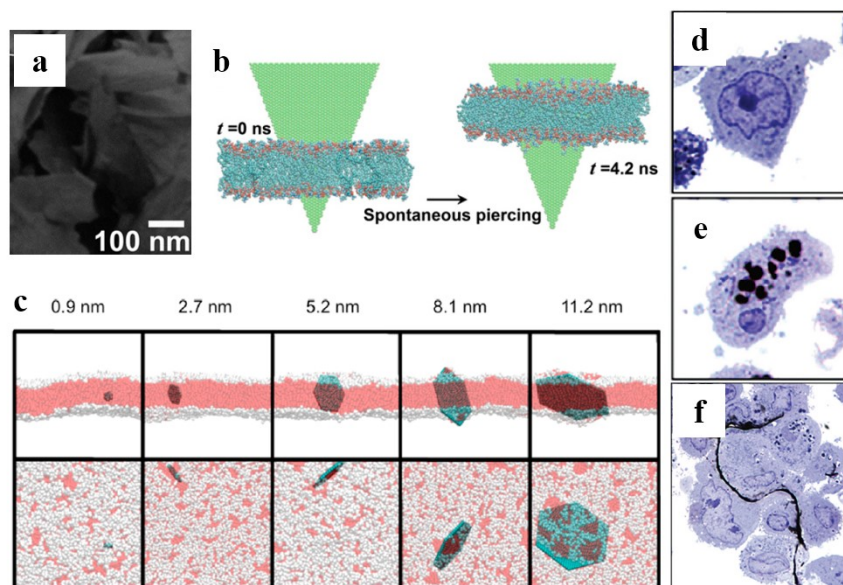


Figure 3. (a) Deposited GO nanosheets, some of which were standing perpendicular with respect to the substrate, killed *S. aureus* and *E. coli*. (b) All-atom molecular dynamics simulations of a monolayer graphene across a lipid bilayer shows corner asperities spontaneously pierce the membrane. (c) Other simulations found only smaller GFNs pierce membranes, whereas larger sheets would adhere flat atop the membrane. Further indications of a lateral dimension size-dependency in cellular interactions with GFNs can be observed when comparing at magnification of 1000 \times (d) untreated human macrophages to (e) cells treated with 550 nm GFN, which are readily internalized by the cell, while (f) 25 μm GFNs wrap around cells instead of penetrating through the membrane. Image (a) adapted with permission from ref [46], copyright (2010) ACS, (b) adapted with permission from ref [53], copyright (2013) National Academy of Sciences, (c) adapted with permission from ref [55], copyright (2015) ACS, (d)-(f) adapted with permission from ref [17], copyright (2012) ACS.

2.3.3 Other colloidal mechano-bactericidal nanostructures

In areas of research where nanomaterials interact with biological components, such as cell membranes, the terms nanoknife and nanoblade are used interchangeably to describe graphene materials to provide imagery for the edge-first insertion mechanism and 2D graphene nanosheet itself. The use of nanodart to describe mechano-bactericidal carbon nanotubes appears to be limited in literature, and thus far specifically refers to CNTs. Comparisons with other 1D materials would confirm whether the nanodart effect is a ubiquitous trait across all 1D nanomaterials. For instance, only one published computational simulation of cellular interactions with boron nitride nanotubes (BNNTs) exists [70]. According to this study, spontaneous insertion of BNNTs (considered to be more stable and inert than CNTs) into the lipid membrane can occur but the nanotube could stay within the bilayer without further disruption. Early investigations into yet other nanoparticles have indicated physico-mechanical interactions at play. For example, Penders *et al.* evaluated gold nanoparticles of similar sizes but of different shapes and concluded that spheres did not cause antibacterial activity. Rather, nanoflowers possessed shape-dependent antibacterial activity but were innocuous towards mammalian cell behavior [71]. Similarly, copper oxide nanoparticles and nanosheets with irregular edges were shown by Gilbertson *et al.* to possess physical and chemical toxicity [72]. The nanosheets would orient parallel to the cell membrane, suggesting bactericidal interaction to originate from rotation.

Lastly, CNTs and GFNs represent mechano-bactericidal colloids for which a strong body of knowledge exists on their fabrication and geometric modification. Current lack of understanding prevents the conclusive claim of mechano-bactericidal efficacy for other colloids. It is worth noting that early applications employing these CNTs and GFNs did not have antibacterial applications in mind [21, 73, 74]. Rather, their mechanical, electronic, and structural properties

allowed diverse uses which eventually overlapped into biological and microbiological research. As others have pointed out, substances categorized as 1D- or 2D- or 2D layered-nanomaterials, both naturally occurring or synthetic, are expansive [13, 75]. Other nanomaterials that are atomically thin and possess high aspect ratio exist as well (e.g., chalcogenide nanosheets such as tungsten disulfide or molybdenum disulfide or exfoliated bismuth selenide, etc.). It is reasonable to hypothesize that these under-represented nanomaterials too have the potential to deliver mechano-antibacterial efficacy but simply have yet to be explored in this context. In doing so, however, researchers should be wary of the presence of impurities, which are often difficult to eliminate but need to be accounted for in any antibacterial experiments.

2.4 Nanopillars, nanospikes, and other mechano-bactericidal nanotopographies

The first mechano-bactericidal nanotopography described in literature was of natural origin [76]. Since then, a handful of other natural surfaces have demonstrated similar mechano-bactericidal activity, inspiring biomimetic efforts to replicate these surfaces on artificial substrates. Here, we summarize research efforts in mechano-bactericidal nanotopographies and their proposed modes of action to highlight established concepts as well as questions that remain. For additional reading, Elbourne *et al.* [5] recently prepared a comprehensive review of antibacterial surfaces.

2.4.1 Mechano-bactericidal nanotopographies in nature

Ivanova *et al.* were the first to report a surface lethal to bacterial cells purely through mechanical means [76], retroactively referring to this mechanism as mechano-bactericidal [77-80]. The title of this review borrows the same terminology. The nanostructured surface in question was the wing of the cicada insect *Psaltoda claripennis*, which possesses a topography consisting of spherically capped nanopillars. Electron microscopy of the cicada wing revealed spherically capped nanopillars 200 nm tall with a 100 nm wide base that tapered off to 60 nm at the cap with

ordered periodicity of 170 nm between the center of two pillars [76]. *P. aeruginosa* cells that adhered to the wing's nanotopography were rapidly killed independent of surface chemistry – a factor which was ruled out after wings sputter-coated with 10 nm of gold maintained the same bactericidal efficacy.

Wings of several species of cicada, dragonfly, as well as damselfly have been discovered to possess mechano-bactericidal nanopillar or nanospike topographies (Table 3 summarizes the reports of natural mechano-bactericidal surfaces to date). It is hypothesized that the bactericidal activity of these insect wings represents an evolutionary function to prevent accumulation of microbial matter such as biofilms, thereby maintaining the insects' lightweight stature during flight [76, 81, 82]. Curiously, the skin of gecko lizards is bactericidal in the same manner because of their nanotipped hairs termed spinules [83-85], suggesting evolutionary convergence. SEM by Watson *et al.* revealed individual spinules of the skin of the gecko *Lucasium steindachneri* to be 4 μm long with slight curvature and spherically capped with radius of 10-30 nm. Since exposure to moisture (which carry microorganisms) or environmental contaminants in their habitat is continuous and unavoidable, geckos likely possess self-cleaning and mechano-bactericidal nanotopography as a protective mechanical barrier [85]. Figure 4 showcases some natural mechano-bactericidal surfaces such as cicada wing, dragonfly wing, and gecko skin.

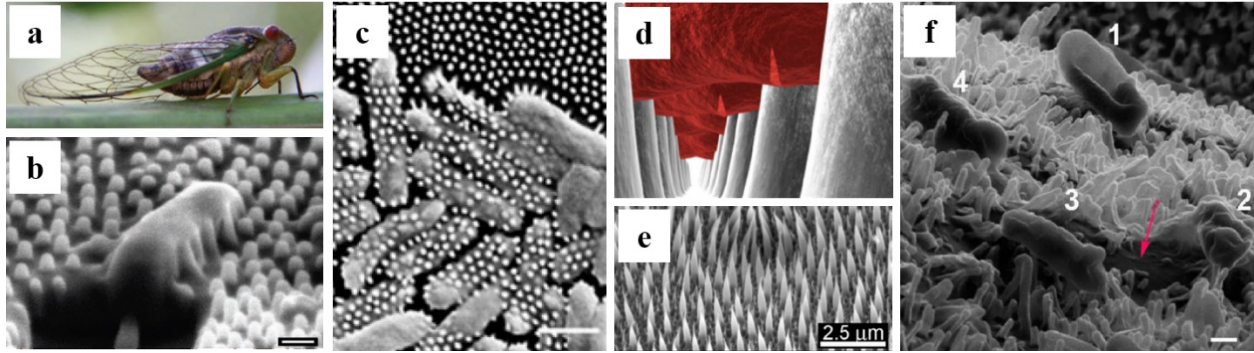


Figure 4. The wing of the (a) cicada insect was the first reported mechano-bactericidal nanotopography. (b) SEM image of a *P. aeruginosa* cell sinking between nanopillars of cicada wing (scale bar: 200 nm).

(c) Aerial view of nanopillars of cicada wing inducing mechano-bactericidal mode of action on *P. aeruginosa* leading to cell rupture (scale bar: 200 nm) (d) Biophysical modeling of the outer layer of rod-shaped bacterial reveal nanopillars do not pierce. Instead, suspended regions of membrane rupture. (e) Mechano-bactericidal nanotopography was also observed on the spinules of gecko skin. (f) Another proposed mechanism is that high adhesive forces between cellular EPS and the nanopillars (of dragonfly wing) as well as shear forces caused by struggling bacteria cause death (scale bar: 200 nm). Images (a), (b) adapted with permission from ref [76], copyright (2012) John Wiley and Sons, (c) adapted with permission from ref [86], copyright (2013) Springer, (d) adapted with permission from ref [87], copyright (2013) Elsevier, (e) adapted with permission from ref [84], (2017) Nature Publishing Group, (f) adapted with permission from ref [81], copyright (2017) ACS.

2.4.2 Topographical geometry influences mechano-bactericidal efficacy

Hasan *et al.* found the nanopillar topography of the *P. claripennis* cicada wing to be highly efficient against Gram-negative bacteria (*P. aeruginosa*, *E. coli*, *Pseudomonas fluorescens*, *Branhamella catarrhalis*). It appears that bacteria initially sank down onto the wing nanotopography, spread between nanopillars, then suddenly experienced a short downward displacement, as detected by AFM, indicative of lethal rupture of the cell. Most attached cells were killed in this manner in under 5 minutes [76]. However, the same wing was not particularly effective against Gram-positive species (*B. subtilis*, *S. aureus*, *Planococcus maritimus*) [86]. Thus, bacterial cell wall and outer membrane were suggested to play decisive roles in the cell-surface interaction. It is well-known that, compared to Gram-negative species, Gram-positive bacteria

have characteristically thick peptidoglycan layers, generating more rigid, stress-bearing outer surfaces [86, 88].

Pogodin *et al.* performed biophysical simulations of Gram-negative and Gram-positive bacteria and their interactions with nanopillars to show that it is the region of the cell membrane stretched between two neighboring nanopillars that leads to critical rupture [87]. Importantly, cells are not pierced directly as was the case with SWCNTs described in the previous section. Rather, Gram-negative cells adhered to the nanopillar surface and critically deformed and were ultimately killed by the nanopillars of the wing. In contrast, morphology of Gram-positive cells was largely unchanged and remained viable due to their increased rigidity. It appears the thicker cell wall of Gram-positive bacteria would require greater deformational stress than what the cicada nanopillars can inflict. Other simulations were largely in agreement, suggesting that Gram-negative cell death was thermodynamically possible on nanopillars whereas the geometry needs optimization to rupture Gram-positive bacteria [89, 90]. There is discrepancy in proposed approaches to optimize the nanopillar geometry. Simulations by Li *et al.* called for increasing nanopillar distribution density, the radius and the height of nanopillars to enhance the adhesion contact area available for critical stretching [90]. Meanwhile, Xue *et al.* suggested sharper nanopillars with increased spacing would result in the increased bacterial membrane surface tension necessary for Gram-positive rupture [89]. Experimental results from Fisher *et al.* agreed with the latter approach, finding sharp diamond nanocones on silicon substrate arranged in a non-uniform array of decreased distribution density were more bactericidal towards *P. aeurignosa* compared to uniformly arranged, high density nanocones [91]. In contrast, Linklater *et al.* and Kelleher *et al.*, assessing silicon nanopillars and cicada wing nanopillars respectively, found densely packed nanopillars to be more bactericidal [79, 92]. Dickson *et al.* fabricated nanopillars constructed of poly(methyl

methacrylate) (PMMA) of varying periodicity. Their findings indicate optimal nanopillar spacing lies between 130 and 380 nm against *E. coli* proliferation, whereas periodicity of 600 nm caused noticeably less cell death [93]. The optimal spacing to produce the most bactericidal nanotopography remains unclear and under investigation.

Nonetheless, it is generally unanimous in literature that increasing the height and sharpness of the nanopillars, thereby enhancing the aspect ratio, improves bactericidal efficacy. This notion was definitively demonstrated by Ivanova *et al.* [94]. Biomimicking dragonfly wings, which possessed longer pillars with sharper tips, the group fabricated longer, sharper, high aspect ratio pillars with black silicon (referred to as “nanospikes”) via reactive-ion etching. Nanospikes were 20-80 nm in diameter with height of 500 nm and randomly distributed and were able to achieve increased cell wall stress resulting in bactericidal efficacy against Gram-negative and Gram-positive bacteria. Even highly resilient *B. subtilis* endospores were killed at a rate of ~140,000 spores per minute per cm² [94]. Thus, despite not directly piercing bacterial cells, enhancement of the aspect ratio of nanopillars and nanospikes results in greater mechano-bactericidal efficacy, mirroring the trend of sharper CNTs and thinner GFNs discussed above also being more effective. In this case, longer and sharper nanospikes provide the necessary deformation and stress to the highly rigid cell walls of Gram-positive bacteria and endospores.

2.4.3 Bacterial motility can influence mechano-bactericidal efficacy

There is evidence to suggest bacterial motility, rather than cell rigidity, plays the determining role in bactericidal action. Bandara *et al.* assessed bactericidal nanopillars of dragonfly wings and observed that dead adhered cells leaked cytoplasmic material which appeared characteristically flattened [81]. Observations with helium ion microscopy showed cell death soon after attachment. At this point, membrane wrinkling and beginning of cytoplasm leakage was also

observed. Upon initial attachment, cell morphology appeared flattened and finally, cytoplasm completely leaked and the cell sank into the nanopillars causing loss of cell integrity. However, rather than cells being critically stretched between two pillars, cell death was attributed to the combination of high adhesive force between pillars and the extracellular polymeric substances (EPS) on the exterior of bacterial cells as well as the strong shear forces generated as adhered bacteria – still alive at this point – push, pull, and struggle upon the unfavorable topography that cause cell death [81]. Diu *et al.* assessed three highly motile bacteria (*P. aeruginosa*, *E. coli*, and *B. subtilis*) and three low- or non-motile species (*S. aureus*, *Enterococcus faecalis*, and *Klebsiella pneumonia*) on a titanium substrate covered with titania nanowires [95]. Their observations implicate motility as the determining factor: significant bactericidal activities occurred for motile bacteria whereas little or negligible activity was observed for low-motility bacteria. This explanation corroborates well with conclusions made by Kelleher *et al.* [92], who established that the greater number of nanostructures with which cells come into contact, the greater the bactericidal activity, as motility along the surface naturally introduces more contact. In relation to motility, Sengstock *et al.* proposed that cell division during bacterial proliferation could explain the observed difference in antibacterial activity between *E. coli* and *S. aureus* [96]. Namely, *E. coli* multiply by elongating, which requires horizontal movement of the cell body attached to the nanostructures. In contrast, *S. aureus* divide along three planes, resulting in some daughter cells clustering above the original cells thus escaping direct contact with the nanostructured surface [97].

The physico-mechanical forces of cicada nanopillars have also shown lethality against the eukaryotic microorganism *Saccharomyces cerevisiae* (yeast) [98], hinting at broad-spectrum efficacy against microorganisms in general. Despite inherent differences in yeast cell wall

structure, ruptured yeast cells resembled the morphology of ruptured bacteria others have reported. Observations of “puddles” were reported and hypothesized to derive from leaked yeast cytoplasm. Notably, these findings raise doubts over motility being the primary mechanism behind microbial cell death since *S. cerevisiae* cells do not possess propulsion mechanisms and are considered non-motile. It is also wholly possible that cell wall rigidity as well as motility, whether through movement or cell division, play combined roles in cell death but the influence of each factor is not well understood.

Table 3. Natural mechano-bactericidal nanotopographies

Material	Mechano-bactericidal nanostructure (h: height; d: diameter)	Summary of findings	Reference
Cicada wing	Nanopillars (h: 200 nm, base d: 100 nm, tip d: 60 nm)	First reported example of mechano-bactericidal nanotopography but only effective against <i>P. aeruginosa</i> .	Ivanova <i>et al.</i> [76]
Cicada wings (3 species)	Nanopillars (h: 241 nm, d: 156 nm; h: 182 nm, d: 159 nm; h: 182 nm, d: 207 nm)	Antibacterial against <i>Pseudomonas fluorescens</i> (Gram-negative). The more nanostructures cells come into contact with, the greater the bactericidal activity, suggesting reducing pitch and diameter of features are more effective.	Kelleher <i>et al.</i> [92]
Cicada (2 species) and dragonfly wings	Hemispheres (h: 84 nm, width: 167 nm), spherically capped cones (h: 183 nm, base width: 104 nm, cap width: 57 nm), spherically capped cylinders (h: 241 nm, width: 53 nm)	Strains of <i>Saccharomyces cerevisiae</i> (yeast) experience rupture similar to bacterial cell death despite differences in cell wall structure. Adhesion of cell to the nanostructured topography stretches and distorts it with cell derived material or debris flowing and “puddling” into topography.	Nowlin <i>et al.</i> [98]
Cicada wing and PMMA	Wing nanopillars (h: 210 nm, d: 60 nm), PMMA nanopillars (h: 300 nm, d: 215 nm; h: 300 nm, d: 190 nm; h: 210 nm, tip d: 70 nm)	First polymer mechano-bactericidal nanotopography. Smaller, closely spaced (between 130 – 380 nm) PMMA nanopillars were optimally bactericidal against <i>E. coli</i> .	Dickson <i>et al.</i> [93]
Dragonfly wing and silicon	Wing nanopillars (h: 240 nm, d: < 90 nm) and nanospikes (h: 240 nm, d: < 30 nm). Silicon nanospikes (h: 279 nm, d: 62 nm), nanospikes (h: 433 nm, d: 80 nm), nanospikes:	Effective against Gram-negative (<i>P. aeruginosa</i>) and Gram-positive (<i>B. subtilis</i>) bacteria and endospores. First reported artificial and biomimetic mechano-bactericidal nanotopography. Effective against <i>P. aeruginosa</i> and <i>B. subtilis</i> bacteria and <i>B. subtilis</i> endospores.	Ivanova <i>et al.</i> [94]

	(h: 612 nm, d: 93 nm)		
Dragonfly wings (3 species)	Nanopillars (h: 200-300 nm, d: 80 nm)	Assessed <i>P. aeruginosa</i> , <i>B. subtilis</i> and endospores to show species-dependent trend in bactericidal efficiency depending on evolution.	Mainwaring <i>et al.</i> [82]
Dragonfly wing	Bimodal, short nanopillars (h: 189 nm, d: 37 nm) and tall nanopillars (h: 311 nm, d: 57 nm)	Using <i>E. coli</i> , suggested cell membrane damage is a combination of strong adhesion between nanopillars and bacterium as well as shear forces due to movement of adhered bacterium during struggle on nanopillars	Bandara <i>et al.</i> [81]
Damselfly wing	Nanoprotrusions (h: 433 nm, tip d: 48 nm)	Young and late-stationary phase bacterial cells (<i>P. aeruginosa</i> , <i>S. aureus</i>) were most susceptible. Mature cells were more resilient.	Truong <i>et al.</i> [80]
Gecko skin	Spinules (h: < 4 μ m, terminating with spherical cap of small radius of curvature \sim 10-30 nm)	Gecko skin kills <i>P. gingivalis</i> (Gram-negative) but demonstrated eukaryotic cell compatibility with human dental pulp stem cells.	Watson <i>et al.</i> [85]
Gecko skin and epoxy resin replica	Spinules (h: 2-4 μ m)	Death of <i>S. mutans</i> and <i>P. gingivalis</i> (Gram-negative) is caused by cell compression and stretching. More successful against Gram-negative than Gram-positive bacteria.	Li <i>et al.</i> [83]
Gecko skin and biopolymer blend replica	Spinules (h: 1-4 μ m and taper to <50 nm nanotip)	A biotemplating method to replicate the spinules covering gecko lizard skin is described. Gut bacteria cultivated on natural and replica gecko skin experienced rupture and death on spinules.	Green <i>et al.</i> [84]

2.4.4 Biomimetic and bio-inspired nanotopographies

In addition to insect wings and gecko skin, biomimetic artificial nanotopography constructed from silicon, titanium, PMMA, biopolymer blends, gold, and diamond have also demonstrated mechano-bactericidal efficacy. Collectively, works described in this section emphasize mechano-bactericidal nanostructures as antibacterial agents independent of chemistry. As is true for their natural counterparts, the spacing between two adjacent structures as well as the aspect ratio of the structures of an artificial nanotopography are critical factors in antibacterial efficacy. Spacing dictates the number of nanostructures an adhered cell is subjected to, as well as the degree of deformation experienced by the membrane regions between adjacent nanostructures, while enhancing the aspect ratio of nanotopography features leads to higher mechano-bactericidal efficiency. Table 4 summarizes experimental studies describing natural as well as biomimetic mechano-bactericidal topographies. After bacterial incubation with mechano-bactericidal

nanotopography, a trend among these studies is the characteristically flattened or sunken cell morphology observed by SEM, sometimes accompanied by visible puddles of cytoplasmic leakage and loss of cell integrity.

For artificial biomimetic nanotopography, black silicon nanospikes pioneered by Ivanova *et al.* have made the most progress in demonstrating applicability. To date, the black silicon nanospikes from Ivanova *et al.* represents the only mechano-bactericidal nanotopography that has also proven *in vivo* biocompatibility [99]. Implanting the black silicon substrate in mice showed that the nanostructured surface produced minor tissue reaction, whereas a smooth, nontextured silicon induced a greater inflammatory reaction. Black silicon nanospikes have undoubtedly shown great promise but the use of silicon is scarce in biomedical applications due to its brittle nature. As titanium materials are heavily favored for implants, mechano-bactericidal titanium substrates hold a more promising future but these have not been evaluated *in vivo*. The possibility of irritation or inflammation as a result of mechano-bactericidal titania nanowires [95, 100], for example, needs to be addressed.

Table 4. Biomimetic and bio-inspired mechano-bactericidal nanotopographies

Material	Mechano-bactericidal nanostructure (h: height; d: diameter)	Summary of findings	Reference
Gecko skin and epoxy resin replica	Spinules (h: 2-4 μm)	Death of <i>S. mutans</i> and <i>P. gingivalis</i> (Gram-negative) is caused by cell compression and stretching. More successful against Gram-negative than Gram-positive bacteria.	Li <i>et al.</i> [83]
Gecko skin and biopolymer blend replica	Spinules (h: 1-4 μm and taper to <50 nm nanotip)	A biotemplating method to replicate the spinules covering gecko lizard skin is described. Gut bacteria cultivated on natural and replica gecko skin experienced rupture and death on spinules.	Green <i>et al.</i> [84]
Silicon	Nanopillars (h: 279 nm, d: 62 nm; h: 433 nm, d: 80 nm; h: 612 nm, d: 93 nm)	Time-dependent plasma etching of silicon produces different heights. Incubation with Gram-positive <i>S. aureus</i> and Gram-negative <i>P. aeruginosa</i> showed smaller, more densely packed pillars exhibit greatest bactericidal activity.	Linklater <i>et al.</i> [79]
Silicon	Nanopillars (h: \sim 652 nm, d: \sim 100 nm)	Substrate preinfected with <i>P. aeruginosa</i> or <i>S. aureus</i> then incubated with fibroblast cells	Pham <i>et al.</i> [99]

		prevented bacterial colonization while enabling eukaryotic proliferation. The substrate did not trigger <i>in vivo</i> inflammatory response in mice.	
Silicon	Nanospikes (h: 500 nm, d: 95 nm)	A microfluidic device incorporating bactericidal black silicon substratum was effective in killing <i>E. coli</i> and <i>P. aeruginosa</i> under fluid flow.	Wang <i>et al.</i> [101]
Silicon	Nanopillars (d: 150-200 nm)	Nanopillars prepared by maskless plasma etching were bactericidal against <i>E. coli</i> , <i>S. aureus</i> and <i>Bacillus cereus</i> (Gram-positive).	Vassallo <i>et al.</i> [102]
Titanium	Nanopillars (d: 200-300 nm) and nanospikes (d: 20 nm)	Titanium nanospikes fabricated by thermal oxidation showed 40% reduction of <i>E. coli</i> . Similar bactericidal efficacy between nanopillars and nanospikes.	Sjostrom <i>et al.</i> [103]
Titanium	Titanium (357 nm nanoroughness) and hydrothermally etched titanium (401 nm nanoroughness, nanowires 40 nm in height)	Etched titanium was more bactericidal against <i>P. aeruginosa</i> (53% viable) than <i>S. aureus</i> (80% viable). The same substrate enhanced proliferation of human fibroblast growth.	Bhadra <i>et al.</i> [104]
Titanium	Nanopillars (h: 1 μm , d: 80 nm)	Observed mechanical rupturing of <i>E. coli</i> , <i>P. aeruginosa</i> , <i>S. aureus</i> , and <i>Mycobacterium smegmatis</i> (Gram-positive) cells. Also supported attachment and proliferation of mammalian cells.	Hasan <i>et al.</i> [105]
Titanium	Sharp-edged titanium columns (h: 478 nm)	Damaged morphology of <i>E. coli</i> while morphology of <i>S. aureus</i> was unaffected. Possibly related to movement of cell body during cell division. Mammalian cells grown on nanotopography were no different than control.	Sengstock <i>et al.</i> [96]
Titania on titanium substrate	Titanium dioxide nanowire brushes (h: 3 μm , d: 100 nm), nanowire niches (h: 3 μm , d: 10-15 μm)	Selectively bactericidal against motile bacteria <i>P. aeruginosa</i> , <i>E. coli</i> , and <i>B. subtilis</i> . Non-motile <i>S. aureus</i> , <i>E. faecalis</i> and <i>K. pneumonia</i> were not strongly affected. The same surfaces were capable of guiding mammalian cell proliferation.	Diu <i>et al.</i> [95]
Titania on titanium substrate	Nanowires with spike-like structures (h: 1 μm , d: 25 nm) and brush-like structures (h: \sim 2 μm , d: 222 nm)	TiO ₂ nanowires on titanium substrates supported osteoblast and osteoclast growth and differentiation while reducing bacterial viability of <i>P. aeruginosa</i> . Killing efficiency was 30% and 58% after 1 h and 18 h, respectively.	Tsimbouri <i>et al.</i> [100]
Gold	Nanopillars (h: \sim 100 nm, d: \sim 50 nm) and other topographical nanostructures (nanoring, nanonugget)	Number of live <i>S. aureus</i> cells on all gold nanotopographies was 3 orders of magnitude lower than on flat and rough control surfaces. All three nanostructures delivered similar bactericidal performance.	Wu <i>et al.</i> [106]
Diamond on silicon wafer	Nanocones (h: 0.8-2.5 μm , width: 350-750 nm), bimodal nanocones (h: 100 nm or 3-5 μm , width: 10-40 nm).	Diamond nanocones with varying cone dimensions, non-uniform array and decreased density was more bactericidal than highly dense nanocone surface against <i>P. aeruginosa</i> . Morphological damage varied despite cell death.	Fisher <i>et al.</i> [91]
Diamond coated nanopillared silicon wafer	Short silicon needles (h: 1 μm) or long silicon needles (h: 15-20 μm) both coated with 10 nm nanodiamond	Bactericidal properties of diamond-coated silicon needles against <i>P. aeruginosa</i> was evident after 1 hour (13% dead compared to 2% flat control). Cells appeared to be damaged by nanofeatures, appearing flat and non-turgid.	May <i>et al.</i> [107]
GO film	Various highly wrinkled and rough GO (h: 0.74-2.1 μm)	Wrinkled GO films prepared by vacuum filtration of GO suspensions form mechanically robust GO	Zou <i>et al.</i> [108]

	depending on roughness, width of each wall of wrinkles: 7.75-15.2 μm)	“traps” resulting in damage to the cell membranes of <i>E. coli</i> , <i>S. aureus</i> , and <i>M. smegmatis</i> caused by increased oxidative stress and physical piercing or laceration.	
Zeolitic imidazolate framework (ZIF) on various substrates	ZIF Nano-daggers (h: > 1 μm , 2 μm thick with sharp nanotips)	High bactericidal activity against <i>E. coli</i> , <i>S. aureus</i> , and <i>Candida albicans</i> (fungi) hypothesized to be caused by enhanced cell adhesion by positively charged ZIF followed by killing by rigid and sharp nano-dagger tips.	Yuan <i>et al.</i> [109]

2.4.5 Tissue cell interactions with mechano-bactericidal nanotopographies

Most cells in human tissues (aside from blood cells) are anchorage-dependent and are influenced by surface topography [110]. Anchorage and subsequent mammalian tissue healing and regeneration can be promoted through the patterning of nanotopography. In fact, implant surfaces are sometimes nanoroughened intentionally for this very reason [111, 112]. Thus, there potentially exists an elusive “sweet-spot” that maximizes tissue cell growth while minimizing bacterial proliferation. To that end, Ivanova *et al.* pre-infected the black silicon nanospike substrate with pathogenic bacteria, then seeded with monkey kidney tissue cells. The substrate was able to inhibit bacterial proliferation while simultaneously promoting tissue growth [99]. A handful of other nanotopographies have also demonstrated selective inhibition of bacteria while also supporting eukaryotic cell growth [85, 95, 96, 100, 104, 105]. These findings are of particular importance as they show that on an optimally engineered implant surface, tissue cells can win what is known as “the race for the surface” [113]. In brief, the race describes the onset of surface colonization of an implant material. If initially won out predominantly by host tissue cells, the implant will be protected from invading pathogens, allowing tissue integration to proceed. However, if initial bacterial colonization dominates over host tissue, severe inflammatory response leading to subsequent biofilm infection symptoms would arise, which would require explant and additional surgical efforts [113, 114]. Figure 5 depicts several biomimetic mechano-bactericidal

nanotopography, some of which selectively inhibition bacteria while supporting eukaryotic cell growth.

Why are nanopillar and nanospike topographies consistently lethal against bacterial cells yet capable of supporting tissue growth? Rigidity (and flexibility) of cell membranes is perhaps the critical difference. Compared to eukaryotes, bacteria are typically more rigid due to the prokaryotic peptidoglycan layer rendering bacterial cells incapable of accommodating the nanotopographies described in this section [12]. Hanson *et al.* used transmission electron microscopy to show that eukaryotic cells are capable of stretching and distorting to accommodate the shape of the nanopillars without compromising intracellular material [115]. Xu *et al.* fabricated high aspect ratio, hollow alumina nanostraws (100 nm in diameter, 1 mm in height) bound to a polycarbonate substrate. They determined penetration of Chinese hamster ovary cells sitting atop the surface by the nanostraws as a relatively rare occurrence – approximately 1 in 15 nanostraws induced penetration [116]. Similarly, fibroblast cells on an array of gallium phosphide vertical nanowires (3.9 μm height, 4 nanowires per μm^2) akin to a “bed-of-nails” were fully motile, resided on top of the nanowires, and were morphologically similar to cells on control substrates [117]. Xie *et al.* modeled cell adhesion on an array of nanowires, concluding nanowire geometry and cell stiffness as critical factors [118]. Moreover, stiffer eukaryotic cells are more sensitive as a result of high stress concentration at the nanowire tips, thus the penetration force required is low. While their study did not extend to prokaryotes, their conclusions help to explain the high bactericidal efficiency of nanotopography due to the stiff peptidoglycan layer in bacteria. However, by that logic, Gram-positive bacteria with thicker peptidoglycans would be more sensitive to mechano-bactericidal nanotopography, which is not the case experimentally.

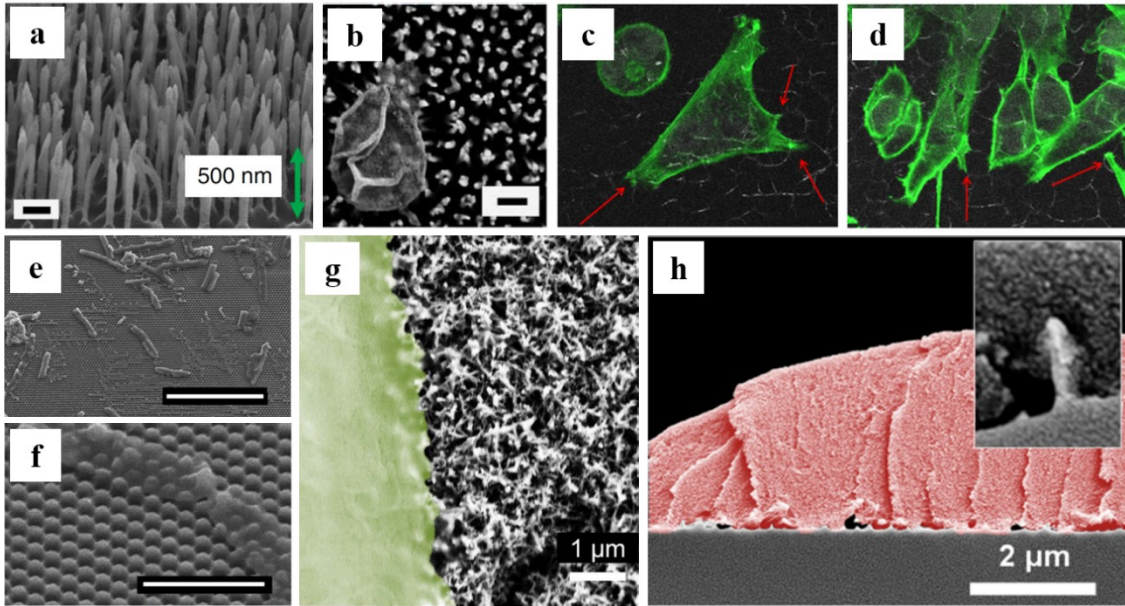


Figure 5. (a) Black silicon nanospikes fabricated by Ivanova et al. exhibit high aspect ratio capable of killing Gram-negative and Gram-positive bacteria and even (b) highly rigid endospores (scale bar: 200 nm). After four-day incubation upon bactericidal titania nanowire surfaces, (c) and (d), lamellipodia of mammalian cells migrated into pockets designed for mammalian cell interaction (scale bar not reported). (e) PMMA nanopillars were able to kill bacteria adhered to it (scale bar: 10 μm) with (f) 130 – 380 nm spacing between pillars being the optimally bactericidal (scale bar: 2 μm). (g) Anchorage points of a fibroblast cell interacting with mechano-bactericidal titanium nanowire surface. (h) The flexible membrane of mammalian cells can accommodate mechano-bactericidal nanotopography. Images (a), (b) adapted with permission from ref [94], copyright (2013) Nature Publishing Group, (c), (d) adapted with permission from ref [95], copyright (2014) Nature Publishing Group, (e), (f) adapted with permission from ref [93], copyright (2015) AIP Publishing LLC, (g) adapted with permission from ref [104], copyright (2015) Nature Publishing Group, (h) adapted with permission from ref [99], copyright (2016) ACS.

2.5 Future outlook

Collectively, the research community commands immense knowledge over nanofabrication techniques. Only a small handful of these techniques have been applied to mechano-bactericidal materials so far. In anticipation of an influx of work in this field of antibacterial research, we urge researchers to report or tabulate all available measurements of their nanostructures' dimensions. This is especially important since there is no consensus in terminology of reported nanostructures. For example, a “nanospike” topography carries connotation and

imagery of sharper, higher aspect ratio protrusions compared to a “nanopillar” topography but no systematic categorization exists to distinguish the two. Moreover, neither of the two terms can convey height or periodicity, critical factors related to efficacy of a mechano-bactericidal nanotopography. Similarly, lateral size of atomically thin GFNs influence their interactions with cell membranes but the term “nanoknife” cannot express this property.

The very nature of mechano-bactericidal colloids in their dispersed form means they are unfortunately impractical in certain applications. Furthermore, their discharge can be harmful to the environment and to human health. CNTs, GFNs, and engineered nanomaterials in general can enter the body via skin penetration, inhalation, ingestion, or biomedical implantation [17]. Gilbertson *et al.* asserted that the bactericidal properties of dispersed CNTs can be a benefit or a hazardous liability depending on their intended use [45, 119, 120]. Immobilization of these colloids onto surfaces would open future possibilities while minimizing their dispersal. Indeed, we note a recent shift in the literature from studying bacterial interactions with dispersed CNTs to the incorporation of these nanomaterials in filters for water purification. Recent advances in antifouling filtration membranes are reviewed in Werber *et al.* [121] and Zhang *et al.* [122]. Immobilizing mechano-bactericidal colloids blurs the line between bactericidal mechanisms of colloids versus mechanisms of nanotopography, which makes knowledge exchange between researchers studying these two systems even more important. It is reasonable to suggest that membrane-piercing interactions of CNTs can be retained even as they are surface-immobilized but efficacy and contribution of mechano-bactericidal activity to the overall antibacterial activity observed would likely change as a result.

For mechano-bactericidal nanotopographies, highly ordered fabrication is not trivial but Nowlin *et al.* have recently outlined a set of useful lithography techniques [123]. Once constructed,

their use becomes attractive as they are easy to manipulate, more predictable and more effective than release-based approaches to controlling both bacterial and eukaryotic cell growth [112]. Medically-relevant mechano-bactericidal prototypes constructed from PMMA or titanium offer great promise. Abiotic devices intended to interface with the human body (e.g., catheters or intravenous injection ports) are frequently infected and in need of constant replacement, and could perhaps benefit most from what mechano-bactericidal nanotopography has to offer. The design of the urinary catheter, for example, has remained the same since the 1930s and while antibacterial coatings reduce the risk of catheter-associated urinary tract infections, the efficacy cannot be maintained [124]. Applying mechano-bactericidal nanotopography on the inner surface of the catheter could prove highly effective. An elegant microfluidic design by Wang *et al.* using black silicon nanospikes as a substrate demonstrates that mechano-bactericidal nanotopography can function even under fluid flow [101]. In any case, how human cells interact and remodel in the presence of the same nanotopography still needs to be understood.

Whether a surface is directly patterned with mechano-bactericidal nanotopography, or if it is prepared by immobilizing mechano-bactericidal colloids, their practical limitation is the same. Namely, only bacteria that have made direct contact with the surface will be inactivated. In other words, they can prevent bacterial proliferation on the surface of interest but cannot sterilize the bulk environment surrounding the surface. Conversely, as antibacterial surfaces that do not release chemicals, mechano-bactericidal nanostructures offer opportunities to develop sustainable antimicrobial materials. Black silicon nanospikes, for example, cannot be consumed metabolically nor are they lost through diffusion. Thus, if the surface is not damaged, mechano-bactericidal materials can be reused indefinitely when cleaned. The same can be said for surface-immobilized mechano-bactericidal colloids. Thus far, no reports on the cleaning and reuse of mechano-

bactericidal materials have been published. It is safe to say that the cleaning regiment must consistently remove surface fouling in the form of adsorbed macromolecules (e.g., proteins, polysaccharides), accumulated dead bacteria or debris at no detriment to the mechano-bactericidal nanostructures.

Lastly, to truly harness its sustainable potential, we suggest an exciting area of research resides in the reproduction of nanostructures onto natural biopolymers. Cellulose and chitin are the first and second most abundant biopolymers, respectively [125, 126]. Both are sourced from renewable origins; cellulose is sourced from plant matter while chitin is extracted from insect or crustacean exoskeletons [127]. Interestingly, the wings of the cicada insect, the inspiration that prompted all subsequent mechano-bactericidal nanotopographies to date, is composed mainly of chitin [76, 128]. Considerable efforts have already been made in the fabrication of bioactive substrates composed of cellulose and chitin [129-132]. Both these biopolymers have long been explored as drug delivery substrates and tissue engineering scaffolds [133-135] and could incorporate mechano-bactericidal nanotopography as a new function. Constructing antibacterial topographies onto such biodegradable, nontoxic, tuneable biopolymer films extracted directly from renewable resources would further improve the sustainable outlook of mechano-bactericidal materials.

2.6 Concluding perspectives

Mechano-bactericidal colloids and mechano-bactericidal nanotopography differ from one another in terms of the specific mechanism(s) of physical damage. 1D, 2D, or near-2D colloidal materials are so thin that they pierce and slice bacterial cell membranes thereby lethally compromising membrane integrity and causing membrane destruction. Compared to Gram-negative bacteria, it seems the less complicated cell membranes of Gram-positive bacteria (which

lack outer membranes as well as membrane-associated proteins) causes them to be more susceptible to mechano-bactericidal effects of CNTs and GFNs. For CNTs specifically, the thinner in diameter and higher the aspect ratio, the stronger the antibacterial properties. The same trend is true for GFNs featuring higher degrees of sharp edge-asperities. Conversely, the mechanism of action for a surface topography of nanopillars is hypothesized to be very different. Although under debate, there is evidence to suggest lethal shear forces stemming from motility of certain bacteria species or movement atop the nanotopography associated with cells that struggle. Another explanation is that regions of cell membranes perched between two pillars experience deformation leading to critical membrane stress and cell rupture. Since Gram-positive cells have stiffer peptidoglycan layers, they were not critically deformed by mechano-bactericidal nanotopography until enhanced aspect ratio of nanospikes was achieved.

Thus, in both colloids and nanotopography, increasing the aspect ratio by creating sharper or thinner nanostructures improves antibacterial efficacy. In either case, cell morphology observable via SEM appears flattened with loss of integrity accompanied by leakage of cytoplasmic matter. Since mechano-bactericidal rely heavily on said morphology observations, preparations of bacterial samples for SEM should strongly consider the use of critical point drying (CPD). Air-drying, which almost all mechano-bactericidal reports have employed, leads to distortion of the cells under observation that could be misconstrued as effects of mechano-bactericidal nanostructures. CPD is widely recognized as the most correct method to observe biological samples as it causes the least amount of alterations to the cell morphology under investigation [136, 137].

Studies to date have favored a select few Gram-positive and Gram-negative bacterial models while other infectious microorganisms of interest such as fungi or even viruses have not

been adequately assessed. Investigations of these microorganisms with known mechano-bactericidal materials would establish their efficacy as broad-spectrum antimicrobials while providing insight in the exact role of the stiff peptidoglycan layer and by extension, the role of the cell membrane. Indeed, many other differences exist between Gram-positive and Gram-negative cells. The presence (or absence) of outer surface proteins and other biomacromolecules such as lipopolysaccharides could play a role. The difference in thickness of the peptidoglycan between Gram-positive and Gram-negative bacteria is likely insufficient to fully encompass the mechano-bactericidal interactions. Even within Gram-positive bacteria, peptidoglycan thickness is not uniform – the peptidoglycan of *E. coli* is nearly three times thicker than that of *P. aeruginosa* despite both being Gram-negative bacteria [138].

A comprehensive understanding of the underlying interactions between biological systems and mechano-bactericidal nanostructures must be well established before widespread application. Their environmental fate and transformation when discharged must also be considered. Toxic reagents or byproducts during synthesis of certain nanomaterials will need to be evaluated as well. No doubt, the ideal scenario is one in which risk towards health and safety is minimized while antibacterial efficacy is maximized. At this moment, the mechanism of action of colloidal mechano-bactericidal systems and its consequence on bacterial cell-surface interactions remain confounding. The same can be said for mechano-bactericidal nanotopography. Fully understanding the bacterial interactions with mechano-bactericidal nanostructures in the future will help define optimal geometry and dimensions. Finally, design of these nanomaterials must conform to the principles of green chemistry [139] in order to accelerate their deployment as next-generation antibacterial products.

2.7 Acknowledgements

The authors thank A. Valiei, V. Maisuria, N. Yousefi, and C. King for helpful discussions.

This research was undertaken, in part, thanks to funding from the Canada Excellence Research Chairs Program (RDR), the Canada Research Chairs Program (NT, CM), the NSERC Discovery Program (RDR and NT) and the Eugenie Ulmer Lamothe fund at McGill University (NL).

2.8 Conflicts of interest

The authors declare no competing conflicts of interest.

2.9 References

- [1] Hasan J, Crawford RJ, Ivanova EP. Antibacterial surfaces: the quest for a new generation of biomaterials. *Trends Biotechnol.* 2013;31:295-304. <http://dx.doi.org/10.1016/j.tibtech.2013.01.017>.
- [2] Lewis K, Klibanov AM. Surpassing nature: rational design of sterile-surface materials. *Trends Biotechnol.* 2005;23:343-8. <https://doi.org/10.1016/j.tibtech.2005.05.004>.
- [3] Andersson DI, Hughes D. Microbiological effects of sublethal levels of antibiotics. *Nat Rev Micro.* 2014;12:465-78. <http://dx.doi.org/10.1038/nrmicro3270>.
- [4] Cloutier M, Mantovani D, Rosei F. Antibacterial coatings: challenges, perspectives, and opportunities. *Trends Biotechnol.* 2015;33:637-52. <https://doi.org/10.1016/j.tibtech.2015.09.002>.
- [5] Elbourne A, Crawford RJ, Ivanova EP. Nano-structured antimicrobial surfaces: From nature to synthetic analogues. *J Colloid Interface Sci.* 2017;508:603-16. <https://doi.org/10.1016/j.jcis.2017.07.021>.
- [6] Blair JM, Webber MA, Baylay AJ, Ogbolu DO, Piddock LJ. Molecular mechanisms of antibiotic resistance. *Nat Rev Microbiol.* 2015;13:42-51. <http://dx.doi.org/10.1038/nrmicro3380>.
- [7] Perros M. A sustainable model for antibiotics. *Science.* 2015;347:1062-4. <http://dx.doi.org/10.1126/science.aaa3048>.
- [8] Banerjee I, Pangule RC, Kane RS. Antifouling coatings: recent developments in the design of surfaces that prevent fouling by proteins, bacteria, and marine organisms. *Adv Mater.* 2011;23:690-718. <http://dx.doi.org/10.1002/adma.201001215>.
- [9] Tuson HH, Weibel DB. Bacteria–surface interactions. *Soft Matter.* 2013;9:4368-80. <http://dx.doi.org/10.1039/C3SM27705D>.
- [10] Lejeune P. Contamination of abiotic surfaces: what a colonizing bacterium sees and how to blur it. *Trends Microbiol.* 2003;11:179-84. [http://dx.doi.org/10.1016/S0966-842X\(03\)00047-7](http://dx.doi.org/10.1016/S0966-842X(03)00047-7).
- [11] Bazaka K, Crawford RJ, Ivanova EP. Do bacteria differentiate between degrees of nanoscale surface roughness? *Biotechnol J.* 2011;6:1103-14. <http://dx.doi.org/10.1002/biot.201100027>.
- [12] Anselme K, Davidson P, Popa A, Giazon M, Liley M, Ploux L. The interaction of cells and bacteria with surfaces structured at the nanometre scale. *Acta Biomater.* 2010;6:3824-46. <https://doi.org/10.1016/j.actbio.2010.04.001>.
- [13] Wang Z, Zhu W, Qiu Y, Yi X, von dem Bussche A, Kane A, et al. Biological and environmental interactions of emerging two-dimensional nanomaterials. *Chem Soc Rev.* 2016;45:1750-80. <http://dx.doi.org/10.1039/C5CS00914F>.

- [14] Rizzello L, Galeone A, Vecchio G, Brunetti V, Sabella S, Pompa PP. Molecular response of *Escherichia coli* adhering onto nanoscale topography. *Nanoscale Res Lett.* 2012;7:1. <http://dx.doi.org/10.1186/1556-276X-7-575>.
- [15] Smith SC, Rodrigues DF. Carbon-based nanomaterials for removal of chemical and biological contaminants from water: a review of mechanisms and applications. *Carbon.* 2015;91:122-43. <https://doi.org/10.1016/j.carbon.2015.04.043>.
- [16] Johnston HJ, Hutchison GR, Christensen FM, Peters S, Hankin S, Aschberger K, et al. A critical review of the biological mechanisms underlying the in vivo and in vitro toxicity of carbon nanotubes: The contribution of physico-chemical characteristics. *Nanotoxicology.* 2010;4:207-46. <http://dx.doi.org/10.3109/17435390903569639>.
- [17] Sanchez VC, Jachak A, Hurt RH, Kane AB. Biological Interactions of Graphene-Family Nanomaterials: An Interdisciplinary Review. *Chemical Res Toxicol.* 2012;25:15-34. <http://dx.doi.org/10.1021/tx200339h>.
- [18] Mao HY, Laurent S, Chen W, Akhavan O, Imani M, Ashkarran AA, et al. Graphene: promises, facts, opportunities, and challenges in nanomedicine. *Chem Rev.* 2013;113:3407-24. <http://dx.doi.org/10.1021/cr300335p>.
- [19] Seil JT, Webster TJ. Antimicrobial applications of nanotechnology: methods and literature. *Int J Nanomedicine.* 2012;7:2767-81. <http://dx.doi.org/10.2147/IJN.S24805>.
- [20] Reller LB, Weinstein M, Jorgensen JH, Ferraro MJ. Antimicrobial Susceptibility Testing: A Review of General Principles and Contemporary Practices. *Clin Infect Dis.* 2009;49:1749-55. <http://dx.doi.org/10.1086/647952>.
- [21] Kang S, Pinault M, Pfefferle LD, Elimelech M. Single-walled carbon nanotubes exhibit strong antimicrobial activity. *Langmuir.* 2007;23:8670-3. <http://dx.doi.org/10.1021/la701067r>.
- [22] Kang S, Herzberg M, Rodrigues DF, Elimelech M. Antibacterial effects of carbon nanotubes: size does matter! *Langmuir.* 2008;24:6409-13. <http://dx.doi.org/10.1021/la800951v>.
- [23] Kang S, Mauter MS, Elimelech M. Physicochemical determinants of multiwalled carbon nanotube bacterial cytotoxicity. *Environ Sci Technol.* 2008;42:7528-34. <http://dx.doi.org/10.1021/es8010173>.
- [24] Chen H, Wang B, Gao D, Guan M, Zheng L, Ouyang H, et al. Broad-Spectrum Antibacterial Activity of Carbon Nanotubes to Human Gut Bacteria. *Small.* 2013;9:2735-46. <http://dx.doi.org/10.1002/sml.201202792>.
- [25] Liu S, Wei L, Hao L, Fang N, Chang MW, Xu R, et al. Sharper and faster “nano darts” kill more bacteria: a study of antibacterial activity of individually dispersed pristine single-walled carbon nanotube. *ACS Nano.* 2009;3:3891-902. <http://dx.doi.org/10.1021/nn901252r>.
- [26] Liu S, Ng AK, Xu R, Wei J, Tan CM, Yang Y, et al. Antibacterial action of dispersed single-walled carbon nanotubes on *Escherichia coli* and *Bacillus subtilis* investigated by atomic force microscopy. *Nanoscale.* 2010;2:2744-50. <http://dx.doi.org/10.1039/c0nr00441c>.
- [27] Wang X, Liu X, Han H. Evaluation of antibacterial effects of carbon nanomaterials against copper-resistant *Ralstonia solanacearum*. *Colloids Surf B Biointerfaces.* 2013;103:136-42. <http://dx.doi.org/10.1016/j.colsurfb.2012.09.044>.
- [28] Wu L, Jiang X. Recent developments in methodology employed to study the interactions between nanomaterials and model lipid membranes. *Anal Bioanal Chem.* 2016;408:2743-58. <http://dx.doi.org/10.1007/s00216-015-9157-5>.
- [29] Jimenez-Cruz CA, Kang S-g, Zhou R. Large scale molecular simulations of nanotoxicity. *Wiley Interdiscip Rev Syst Biol Med.* 2014;6:329-43. <http://dx.doi.org/10.1002/wsbm.1271>.

- [30] Yang K, Ma Y-Q. Computer simulation of the translocation of nanoparticles with different shapes across a lipid bilayer. *Nat Nanotechnol.* 2010;5:579-83. <http://dx.doi.org/10.1038/nnano.2010.141>.
- [31] Shi X, Kong Y, Gao H. Coarse grained molecular dynamics and theoretical studies of carbon nanotubes entering cell membrane. *Acta Mechanica Sinica.* 2008;24:161-9. <https://doi.org/10.1007/s10409-007-0131-0>.
- [32] Shi X, von dem Bussche A, Hurt RH, Kane AB, Gao H. Cell entry of one-dimensional nanomaterials occurs by tip recognition and rotation. *Nat Nanotechnol.* 2011;6:714-9. <http://dx.doi.org/doi:10.1038/nnano.2011.151>.
- [33] Wallace EJ, Sansom MS. Blocking of carbon nanotube based nanoinjectors by lipids: a simulation study. *Nano Lett.* 2008;8:2751-6. <http://dx.doi.org/10.1021/nl801217f>.
- [34] Lelimosin M, Sansom MS. Membrane perturbation by carbon nanotube insertion: pathways to internalization. *Small.* 2013;9:3639-46. <http://dx.doi.org/10.1002/smll.201202640>.
- [35] Kraszewski S, Bianco A, Tarek M, Ramseyer C. Insertion of short amino-functionalized single-walled carbon nanotubes into phospholipid bilayer occurs by passive diffusion. *PLoS One.* 2012;7:e40703. <https://doi.org/10.1371/journal.pone.0040703>.
- [36] Yaron PN, Holt BD, Short PA, Lösche M, Islam MF, Dahl KN. Single wall carbon nanotubes enter cells by endocytosis and not membrane penetration. *J Nanobiotechnol.* 2011;9:45. <https://doi.org/10.1186/1477-3155-9-45>.
- [37] Pogodin S, Baulin VA. Can a Carbon Nanotube Pierce through a Phospholipid Bilayer? *ACS Nano.* 2010;4:5293-300. <http://dx.doi.org/10.1021/nn1016549>.
- [38] Negoda A, Liu Y, Hou W-C, Corredor C, Moghadam BY, Musolff C, et al. Engineered nanomaterial interactions with bilayer lipid membranes: screening platforms to assess nanoparticle toxicity. *Int J of Biomed Nanosci and Nanotechnol.* 2013;3:52-83. <https://doi.org/10.1504/IJBNN.2013.054512>.
- [39] Moghadam BY, Hou W-C, Corredor C, Westerhoff P, Posner JD. Role of Nanoparticle Surface Functionality in the Disruption of Model Cell Membranes. *Langmuir.* 2012;28:16318-26. <http://dx.doi.org/10.1021/la302654s>.
- [40] Suresh AK, Pelletier DA, Doktycz MJ. Relating nanomaterial properties and microbial toxicity. *Nanoscale.* 2013;5:463-74. <http://dx.doi.org/10.1039/C2NR32447D>.
- [41] Wang L, Hu C, Shao L. The antimicrobial activity of nanoparticles: present situation and prospects for the future. *Int J Nanomedicine.* 2017;12:1227-49. <http://dx.doi.org/10.2147/IJN.S121956>.
- [42] Holt BD, Dahl KN, Islam MF. Cells take up and recover from protein-stabilized single-wall carbon nanotubes with two distinct rates. *ACS Nano.* 2012;6:3481-90. <http://dx.doi.org/10.1021/nn300504x>.
- [43] Arias LR, Yang L. Inactivation of Bacterial Pathogens by Carbon Nanotubes in Suspensions. *Langmuir.* 2009;25:3003-12. <http://dx.doi.org/10.1021/la802769m>.
- [44] Vecitis CD, Zodrow KR, Kang S, Elimelech M. Electronic-Structure-Dependent Bacterial Cytotoxicity of Single-Walled Carbon Nanotubes. *ACS Nano.* 2010;4:5471-9. <http://dx.doi.org/10.1021/nn101558x>.
- [45] Pasquini LM, Hashmi SM, Sommer TJ, Elimelech M, Zimmerman JB. Impact of Surface Functionalization on Bacterial Cytotoxicity of Single-Walled Carbon Nanotubes. *Environ Sci Technol.* 2012;46:6297-305. <http://dx.doi.org/10.1021/es300514s>.
- [46] Akhavan O, Ghaderi E. Toxicity of graphene and graphene oxide nanowalls against bacteria. *ACS Nano.* 2010;4:5731-6. <http://dx.doi.org/10.1021/nn101390x>.

- [47] Lu X, Feng X, Werber JR, Chu C, Zucker I, Kim J-H, et al. Enhanced antibacterial activity through the controlled alignment of graphene oxide nanosheets. *Proc Natl Acad Sci USA*. 2017. <http://dx.doi.org/10.1073/pnas.1710996114>.
- [48] Liu S, Zeng TH, Hofmann M, Burcombe E, Wei J, Jiang R, et al. Antibacterial activity of graphite, graphite oxide, graphene oxide, and reduced graphene oxide: membrane and oxidative stress. *ACS Nano*. 2011;5:6971-80. <http://dx.doi.org/10.1021/nn202451x>.
- [49] Musico YLF, Santos CM, Dalida MLP, Rodrigues DF. Surface modification of membrane filters using graphene and graphene oxide-based nanomaterials for bacterial inactivation and removal. *ACS Sustainable Chem Eng*. 2014;2:1559-65. <http://dx.doi.org/10.1021/sc500044p>.
- [50] Chen J, Peng H, Wang X, Shao F, Yuan Z, Han H. Graphene oxide exhibits broad-spectrum antimicrobial activity against bacterial phytopathogens and fungal conidia by intertwining and membrane perturbation. *Nanoscale*. 2014;6:1879-89. <http://dx.doi.org/10.1039/c3nr04941h>.
- [51] Chen J, Wang X, Han H. A new function of graphene oxide emerges: inactivating phytopathogenic bacterium *Xanthomonas oryzae* pv. *Oryzae*. *J Nanopart Res*. 2013;15:1-14. <https://doi.org/10.1007/s11051-013-1658-6>.
- [52] He J, Zhu X, Qi Z, Wang C, Mao X, Zhu C, et al. Killing dental pathogens using antibacterial graphene oxide. *ACS Appl Mater Interfaces*. 2015;7:5605-11. <http://dx.doi.org/10.1021/acsami.5b01069>.
- [53] Li Y, Yuan H, von dem Bussche A, Creighton M, Hurt RH, Kane AB, et al. Graphene microsheets enter cells through spontaneous membrane penetration at edge asperities and corner sites. *Proc Natl Acad Sci USA*. 2013;110:12295-300. <http://dx.doi.org/10.1073/pnas.1222276110>.
- [54] Tu Y, Lv M, Xiu P, Huynh T, Zhang M, Castelli M, et al. Destructive extraction of phospholipids from *Escherichia coli* membranes by graphene nanosheets. *Nat Nanotechnol*. 2013;8:594-601. <http://dx.doi.org/10.1038/nnano.2013.125>.
- [55] Dallavalle M, Calvaresi M, Bottoni A, Melle-Franco M, Zerbetto F. Graphene can wreak havoc with cell membranes. *ACS Appl Mater Interfaces*. 2015;7:4406-14. <http://dx.doi.org/10.1021/am508938u>.
- [56] Wang J, Wei Y, Shi X, Gao H. Cellular entry of graphene nanosheets: the role of thickness, oxidation and surface adsorption. *RSC Adv*. 2013;3:15776-82. <http://dx.doi.org/10.1039/C3RA40392K>.
- [57] Titov AV, Král P, Pearson R. Sandwiched graphene–membrane superstructures. *ACS Nano*. 2009;4:229-34. <http://dx.doi.org/10.1021/nn9015778>.
- [58] Guo R, Mao J, Yan L-T. Computer simulation of cell entry of graphene nanosheet. *Biomaterials*. 2013;34:4296-301. <https://doi.org/10.1016/j.biomaterials.2013.02.047>.
- [59] Luan B, Huynh T, Zhao L, Zhou R. Potential Toxicity of Graphene to Cell Functions via Disrupting Protein–Protein Interactions. *ACS Nano*. 2015;9:663-9. <http://dx.doi.org/10.1021/nn506011j>.
- [60] Zou X, Zhang L, Wang Z, Luo Y. Mechanisms of the antimicrobial activities of graphene materials. *J Am Chem Soc*. 2016;138:2064-77. <http://dx.doi.org/10.1021/jacs.5b11411>.
- [61] Hui L, Piao J-G, Auletta J, Hu K, Zhu Y, Meyer T, et al. Availability of the basal planes of graphene oxide determines whether it is antibacterial. *ACS Appl Mater Interfaces*. 2014;6:13183-90. <http://dx.doi.org/10.1021/am503070z>.
- [62] Yi X, Gao H. Cell interaction with graphene microsheets: near-orthogonal cutting versus parallel attachment. *Nanoscale*. 2015;7:5457-67. <http://dx.doi.org/10.1039/c4nr06170e>.

- [63] Mangadlao JD, Santos CM, Felipe MJL, de Leon ACC, Rodrigues DF, Advincula RC. On the antibacterial mechanism of graphene oxide (GO) Langmuir-Blodgett films. *Chem Commun.* 2015;51:2886-9. <http://dx.doi.org/10.1039/C4CC07836E>.
- [64] Perreault F, de Faria AF, Nejati S, Elimelech M. Antimicrobial Properties of Graphene Oxide Nanosheets: Why Size Matters. *ACS Nano.* 2015;9:7226-36. <http://dx.doi.org/10.1021/acsnano.5b02067>.
- [65] Chong Y, Ge C, Fang G, Wu R, Zhang H, Chai Z, et al. Light-Enhanced Antibacterial Activity of Graphene Oxide, Mainly via Accelerated Electron Transfer. *Environ Sci Technol.* 2017;51:10154-61. <http://dx.doi.org/10.1021/acs.est.7b00663>.
- [66] Pham VTH, Truong VK, Quinn MDJ, Notley SM, Guo Y, Baulin VA, et al. Graphene Induces Formation of Pores That Kill Spherical and Rod-Shaped Bacteria. *ACS Nano.* 2015;9:8458-67. <http://dx.doi.org/10.1021/acsnano.5b03368>.
- [67] Soroush A, Rice D, Rahaman MS, Perreault F. Antimicrobial Properties of Graphene Nanomaterials: Mechanisms and Applications. *Graphene-based Materials in Health and Environment*: Springer; 2016. p. 287-322. https://doi.org/10.1007/978-3-319-45639-3_10.
- [68] Palmieri V, Papi M, Conti C, Ciasca G, Maulucci G, De Spirito M. The future development of bacteria fighting medical devices: the role of graphene oxide. *Expert Rev Med.* 2016;13:1013-9. <http://dx.doi.org/10.1080/17434440.2016.1245612>.
- [69] Ji H, Sun H, Qu X. Antibacterial applications of graphene-based nanomaterials: Recent achievements and challenges. *Adv Drug Deliv Rev.* 2016;105:176-89. <https://doi.org/10.1016/j.addr.2016.04.009>.
- [70] Thomas M, Enciso M, Hilder TA. Insertion Mechanism and Stability of Boron Nitride Nanotubes in Lipid Bilayers. *J Phys Chem B.* 2015;119:4929-36. <http://dx.doi.org/10.1021/acs.jpcc.5b00102>.
- [71] Penders J, Stolzoff M, Hickey DJ, Andersson M, Webster TJ. Shape-dependent antibacterial effects of non-cytotoxic gold nanoparticles. *Int J Nanomedicine.* 2017;12:2457. <http://dx.doi.org/10.2147/IJN.S124442>.
- [72] Gilbertson LM, Albalghiti EM, Fishman ZS, Perreault F, Corredor C, Posner JD, et al. Shape-Dependent Surface Reactivity and Antimicrobial Activity of Nano-Cupric Oxide. *Environ Sci Technol.* 2016;50:3975-84. <http://dx.doi.org/10.1021/acs.est.5b05734>.
- [73] Allen MJ, Tung VC, Kaner RB. Honeycomb carbon: a review of graphene. *Chem Rev.* 2009;110:132-45. <http://dx.doi.org/10.1021/cr900070d>.
- [74] De Volder MFL, Tawfick SH, Baughman RH, Hart AJ. Carbon Nanotubes: Present and Future Commercial Applications. *Science.* 2013;339:535-9. <http://dx.doi.org/10.1126/science.1222453>.
- [75] Xu M, Liang T, Shi M, Chen H. Graphene-like two-dimensional materials. *Chem Rev.* 2013;113:3766-98. <http://dx.doi.org/10.1021/cr300263a>.
- [76] Ivanova EP, Hasan J, Webb HK, Truong VK, Watson GS, Watson JA, et al. Natural bactericidal surfaces: mechanical rupture of *Pseudomonas aeruginosa* cells by cicada wings. *Small.* 2012;8:2489-94. <http://dx.doi.org/10.1002/sml.201200528>.
- [77] Ivanova EP, Crawford RJ. *Antibacterial Surfaces*: Springer; 2015. <http://dx.doi.org/10.1007/978-3-319-18594-1>.
- [78] Nguyen DH, Pham VT, Al Kobaisi M, Bhadra C, Orłowska A, Ghanaati S, et al. Adsorption of Human Plasma Albumin and Fibronectin onto Nanostructured Black Silicon Surfaces. *Langmuir.* 2016;32:10744-51. <http://dx.doi.org/10.1021/acs.langmuir.6b02601>.

- [79] Linklater DP, Nguyen HKD, Bhadra CM, Juodkazis S, Ivanova EP. Influence of nanoscale topology on bactericidal efficiency of black silicon surfaces. *Nanotechnology*. 2017;28:245301. <http://dx.doi.org/10.1088/1361-6528/aa700e>.
- [80] Truong VK, Geeganagamage NM, Baulin VA, Vongsvivut J, Tobin MJ, Luque P, et al. The susceptibility of *Staphylococcus aureus* CIP 65.8 and *Pseudomonas aeruginosa* ATCC 9721 cells to the bactericidal action of nanostructured *Calopteryx haemorrhoidalis* damselfly wing surfaces. *Appl Microbiol Biotechnol*. 2017;1-8. <http://dx.doi.org/10.1007/s00253-017-8205-9>.
- [81] Bandara CD, Singh S, Afara IO, Tesfamichael T, Wolff A, Ostrikov K, et al. Bactericidal Effects of Natural Nanotopography of Dragonfly Wing on *Escherichia coli*. *ACS Appl Mater Interfaces*. 2017. <http://dx.doi.org/10.1021/acsami.6b13666>.
- [82] Mainwaring DE, Nguyen SH, Webb H, Jakubov T, Tobin M, Lamb RN, et al. The nature of inherent bactericidal activity: insights from the nanotopology of three species of dragonfly. *Nanoscale*. 2016;8:6527-34. <http://dx.doi.org/10.1039/C5NR08542J>.
- [83] Li X, Cheung GS, Watson GS, Watson JA, Lin S, Schwarzkopf L, et al. The nanotipped hairs of gecko skin and biotemplated replicas impair and/or kill pathogenic bacteria with high efficiency. *Nanoscale*. 2016;8:18860-9. <http://dx.doi.org/10.1039/C6NR05046H>.
- [84] Green DW, Lee KK-H, Watson JA, Kim H-Y, Yoon K-S, Kim E-J, et al. High Quality Bioreplication of Intricate Nanostructures from a Fragile Gecko Skin Surface with Bactericidal Properties. *Sci Rep*. 2017;7. <http://dx.doi.org/10.1038/srep41023>.
- [85] Watson GS, Green DW, Schwarzkopf L, Li X, Cribb BW, Myhra S, et al. A gecko skin micro/nano structure—A low adhesion, superhydrophobic, anti-wetting, self-cleaning, biocompatible, antibacterial surface. *Acta Biomater*. 2015;21:109-22. <http://dx.doi.org/10.1016/j.actbio.2015.03.007>.
- [86] Hasan J, Webb HK, Truong VK, Pogodin S, Baulin VA, Watson GS, et al. Selective bactericidal activity of nanopatterned superhydrophobic cicada *Psaltoda claripennis* wing surfaces. *Appl Microbiol Biotechnol*. 2013;97:9257-62. <http://dx.doi.org/10.1007/s00253-012-4628-5>.
- [87] Pogodin S, Hasan J, Baulin Vladimir A, Webb Hayden K, Truong Vi K, Phong Nguyen The H, et al. Biophysical Model of Bacterial Cell Interactions with Nanopatterned Cicada Wing Surfaces. *Biophys J*. 2013;104:835-40. [10.1016/j.bpj.2012.12.046](http://dx.doi.org/10.1016/j.bpj.2012.12.046).
- [88] Filloux A, Whitfield C. Editorial: The many wonders of the bacterial cell surface. *FEMS Microbiol Rev*. 2016;40:161-3. <http://dx.doi.org/10.1093/femsre/fuv047>.
- [89] Xue F, Liu J, Guo L, Zhang L, Li Q. Theoretical study on the bactericidal nature of nanopatterned surfaces. *J Theor Biol*. 2015;385:1-7. <http://dx.doi.org/10.1016/j.jtbi.2015.08.011>.
- [90] Li X. Bactericidal mechanism of nanopatterned surfaces. *Phys Chem Chem Phys*. 2016;18:1311-6. <http://dx.doi.org/10.1039/c5cp05646b>.
- [91] Fisher LE, Yang Y, Yuen M-F, Zhang W, Nobbs AH, Su B. Bactericidal activity of biomimetic diamond nanocone surfaces. *Biointerphases*. 2016;11:011014. <http://dx.doi.org/10.1116/1.4944062>.
- [92] Kelleher SM, Habimana O, Lawler J, O'Reilly B, Daniels S, Casey E, et al. Cicada wing surface topography: An investigation into the bactericidal properties of nanostructural features. *ACS Appl Mater Interfaces*. 2015;8:14966-74. <http://dx.doi.org/10.1021/acsami.5b08309>.
- [93] Dickson MN, Liang EI, Rodriguez LA, Vollereaux N, Yee AF. Nanopatterned polymer surfaces with bactericidal properties. *Biointerphases*. 2015;10:021010. <http://dx.doi.org/10.1116/1.4922157>.
- [94] Ivanova EP, Hasan J, Webb HK, Gervinskis G, Juodkazis S, Truong VK, et al. Bactericidal activity of black silicon. *Nat Commun*. 2013;4. <http://dx.doi.org/10.1038/ncomms3838>.

- [95] Diu T, Faruqui N, Sjöström T, Lamarre B, Jenkinson HF, Su B, et al. Cicada-inspired cell-instructive nanopatterned arrays. *Sci Rep.* 2014;4:7122. <http://dx.doi.org/10.1038/srep07122>.
- [96] Sengstock C, Lopian M, Motemani Y, Borgmann A, Khare C, Buenconsejo PJS, et al. Structure-related antibacterial activity of a titanium nanostructured surface fabricated by glancing angle sputter deposition. *Nanotechnology.* 2014;25:195101. <http://dx.doi.org/10.1088/0957-4484/25/19/195101>.
- [97] Tzagoloff H, Novick R. Geometry of cell division in *Staphylococcus aureus*. *J Bacteriol.* 1977;129:343-50.
- [98] Nowlin K, Boseman A, Covell A, LaJeunesse D. Adhesion-dependent rupturing of *Saccharomyces cerevisiae* on biological antimicrobial nanostructured surfaces. *J R Soc Interface.* 2015;12:20140999. <http://dx.doi.org/10.1098/rsif.2014.0999>.
- [99] Pham VT, Truong VK, Orłowska A, Ghanaati S, Barbeck M, Booms P, et al. "Race for the surface": eukaryotic cells can win. *ACS Appl Mater Interfaces.* 2016;8:22025-31. <http://dx.doi.org/10.1021/acsami.6b06415>.
- [100] Tsimbouri P, Fisher L, Holloway N, Sjöstrom T, Nobbs A, Meek RD, et al. Osteogenic and bactericidal surfaces from hydrothermal titania nanowires on titanium substrates. *Sci Rep.* 2016;6. <http://dx.doi.org/10.1038/srep36857>.
- [101] Wang X, Bhadra CM, Dang THY, Buividas R, Wang J, Crawford RJ, et al. A bactericidal microfluidic device constructed using nano-textured black silicon. *RSC Adv.* 2016;6:26300-6. <http://dx.doi.org/10.1039/C6RA03864F>.
- [102] Vassallo E, Pedroni M, Silvetti T, Morandi S, Toffolatti S, Angella G, et al. Bactericidal performance of nanostructured surfaces by fluorocarbon plasma. *Mater Sci Eng C Mater Biol Appl.* 2017;80:117-21. <http://dx.doi.org/10.1016/j.msec.2017.05.111>.
- [103] Sjöström T, Nobbs AH, Su B. Bactericidal nanospine surfaces via thermal oxidation of Ti alloy substrates. *Mater Lett.* 2016;167:22-6. <https://doi.org/10.1016/j.matlet.2015.12.140>.
- [104] Bhadra CM, Truong VK, Pham VT, Al Kobaisi M, Seniutinas G, Wang JY, et al. Antibacterial titanium nano-patterned arrays inspired by dragonfly wings. *Sci Rep.* 2015;5:16817. <http://dx.doi.org/10.1038/srep16817>.
- [105] Hasan J, Jain S, Chatterjee K. Nanoscale Topography on Black Titanium Imparts Multi-biofunctional Properties for Orthopedic Applications. *Sci Rep.* 2017;7:41118. <http://dx.doi.org/10.1038/srep41118>.
- [106] Wu S, Zuber F, Brugger J, Maniura-Weber K, Ren Q. Antibacterial Au nanostructured surfaces. *Nanoscale.* 2016;8:2620-5. <http://dx.doi.org/10.1039/C5NR06157A>.
- [107] May P, Clegg M, Silva T, Zanin H, Fatibello-Filho O, Celorrio V, et al. Diamond-coated 'black silicon' as a promising material for high-surface-area electrochemical electrodes and antibacterial surfaces. *J Mater Chem B.* 2016;4:5737-46. <http://dx.doi.org/10.1039/C6TB01774F>.
- [108] Zou F, Zhou H, Jeong DY, Kwon J, Eom SU, Park TJ, et al. Wrinkled Surface-Mediated Antibacterial Activity of Graphene Oxide Nanosheets. *ACS Appl Mater Interfaces.* 2017;9:1343-51. <http://dx.doi.org/10.1021/acsami.6b15085>.
- [109] Yuan Y, Zhang Y. Enhanced biomimetic bactericidal surfaces by coating with positively-charged ZIF nano-dagger arrays. *Nanomedicine.* 2017;13:2199-077. <http://dx.doi.org/10.1016/j.nano.2017.06.003>.
- [110] Chan B, Leong K. Scaffolding in tissue engineering: general approaches and tissue-specific considerations. *Eur Spine J.* 2008;17:467-79. <http://dx.doi.org/10.1007/s00586-008-0745-3>.

- [111] Luong-Van E, Rodriguez I, Low HY, Elmouelhi N, Lowenhaupt B, Natarajan S, et al. Review: Micro-and nanostructured surface engineering for biomedical applications. *J Mater Res*. 2013;28:165-74. <https://doi.org/10.1557/jmr.2012.398>.
- [112] Jeon H, Simon CG, Kim G. A mini-review: cell response to microscale, nanoscale, and hierarchical patterning of surface structure. *J Biomed Mater Res B Appl Biomater*. 2014;102:1580-94. <http://dx.doi.org/10.1002/jbm.b.33158>.
- [113] Gristina A, Naylor P, Myrvik Q. Infections from biomaterials and implants: a race for the surface. *Med Prog Technol*. 1987;14:205-24.
- [114] Busscher HJ, Van Der Mei HC, Subbiahdoss G, Jutte PC, Van Den Dungen JJ, Zaat SA, et al. Biomaterial-associated infection: locating the finish line in the race for the surface. *Sci Transl Med*. 2012;4:153rv10. <http://dx.doi.org/10.1126/scitranslmed.3004528>.
- [115] Hanson L, Lin ZC, Xie C, Cui Y, Cui B. Characterization of the cell–nanopillar interface by transmission electron microscopy. *Nano Lett*. 2012;12:5815-20. <http://dx.doi.org/10.1021/nl303163y>.
- [116] Xu AM, Aalipour A, Leal-Ortiz S, Mekhdjian AH, Xie X, Dunn AR, et al. Quantification of nanowire penetration into living cells. *Nat Commun*. 2014;5:3613. <http://dx.doi.org/10.1038/ncomms4613>.
- [117] Persson H, Li Z, Tegenfeldt JO, Oredsson S, Prinz CN. From immobilized cells to motile cells on a bed-of-nails: effects of vertical nanowire array density on cell behaviour. *Sci Rep*. 2015;5:18535. <http://dx.doi.org/10.1038/srep18535>.
- [118] Xie X, Xu AM, Angle MR, Tayebi N, Verma P, Melosh NA. Mechanical model of vertical nanowire cell penetration. *Nano Lett*. 2013;13:6002-8. <http://dx.doi.org/10.1021/nl403201a>.
- [119] Gilbertson LM, Goodwin DG, Taylor AD, Pfefferle L, Zimmerman JB. Toward Tailored Functional Design of Multi-Walled Carbon Nanotubes (MWNTs): Electrochemical and Antimicrobial Activity Enhancement via Oxidation and Selective Reduction. *Environ Sci Technol*. 2014;48:5938-45. <http://dx.doi.org/10.1021/es500468y>.
- [120] Gilbertson LM, Melnikov F, Wehmas LC, Anastas PT, Tanguay RL, Zimmerman JB. Toward safer multi-walled carbon nanotube design: establishing a statistical model that relates surface charge and embryonic zebrafish mortality. *Nanotoxicology*. 2016;10:10-9. <http://dx.doi.org/10.3109/17435390.2014.996193>.
- [121] Werber JR, Osuji CO, Elimelech M. Materials for next-generation desalination and water purification membranes. *Nat Rev Microbiol*. 2016;1:16018. <http://dx.doi.org/10.1038/natrevmats.2016.18>.
- [122] Zhang R, Liu Y, He M, Su Y, Zhao X, Elimelech M, et al. Antifouling membranes for sustainable water purification: strategies and mechanisms. *Chem Soc Rev*. 2016;45:5888-924. <http://dx.doi.org/10.1039/C5CS00579E>.
- [123] Nowlin K, LaJeunesse DR. Fabrication of hierarchical biomimetic polymeric nanostructured surfaces. *Mol Syst Des Eng*. 2017;2:201-13. <http://dx.doi.org/10.1039/C7ME00009J>.
- [124] Feneley RCL, Hopley IB, Wells PNT. Urinary catheters: history, current status, adverse events and research agenda. *J Med Eng Technol*. 2015;39:459-70. <http://dx.doi.org/10.3109/03091902.2015.1085600>.
- [125] O'sullivan AC. Cellulose: the structure slowly unravels. *Cellulose*. 1997;4:173-207. <https://doi.org/10.1023/A:1018431705579>.
- [126] Tharanathan RN, Kittur FS. Chitin — The Undisputed Biomolecule of Great Potential. *Critical reviews in food science and nutrition*. 2003;43:61-87. <http://dx.doi.org/10.1080/10408690390826455>.

- [127] Younes I, Rinaudo M. Chitin and chitosan preparation from marine sources. Structure, properties and applications. *Mar Drugs*. 2015;13:1133-74. <http://dx.doi.org/10.3390/md13031133>.
- [128] Chandran R, Williams L, Hung A, Nowlin K, LaJeunesse D. SEM characterization of anatomical variation in chitin organization in insect and arthropod cuticles. *Micron*. 2016;82:74-85. <http://dx.doi.org/10.1016/j.micron.2015.12.010>.
- [129] Turner MB, Spear SK, Holbrey JD, Rogers RD. Production of bioactive cellulose films reconstituted from ionic liquids. *Biomacromolecules*. 2004;5:1379-84. <http://dx.doi.org/10.1021/bm049748q>.
- [130] Qin Y, Lu X, Sun N, Rogers RD. Dissolution or extraction of crustacean shells using ionic liquids to obtain high molecular weight purified chitin and direct production of chitin films and fibers. *Green Chem*. 2010;12:968-71. <http://dx.doi.org/10.1039/C003583A>.
- [131] Swatloski RP, Spear SK, Holbrey JD, Rogers RD. Dissolution of cellulose with ionic liquids. *J Am Chem Soc*. 2002;124:4974-5. <http://dx.doi.org/10.1021/ja025790m>.
- [132] King C, Shamshina JL, Gurau G, Berton P, Khan NFAF, Rogers RD. A platform for more sustainable chitin films from an ionic liquid process. *Green Chem*. 2017;19:117-26. <http://dx.doi.org/10.1039/C6GC02201D>.
- [133] Muzzarelli RA. Chitins and chitosans for the repair of wounded skin, nerve, cartilage and bone. *Carbohydr Polym*. 2009;76:167-82. <https://doi.org/10.1016/j.carbpol.2008.11.002>.
- [134] Khor E, Lim LY. Implantable applications of chitin and chitosan. *Biomaterials*. 2003;24:2339-49. [https://doi.org/10.1016/S0142-9612\(03\)00026-7](https://doi.org/10.1016/S0142-9612(03)00026-7).
- [135] Müller FA, Müller L, Hofmann I, Greil P, Wenzel MM, Staudenmaier R. Cellulose-based scaffold materials for cartilage tissue engineering. *Biomaterials*. 2006;27:3955-63. <https://doi.org/10.1016/j.biomaterials.2006.02.031>.
- [136] Fischer ER, Hansen BT, Nair V, Hoyt FH, Dorward DW. *Scanning Electron Microscopy. Current Protocols in Microbiology: John Wiley & Sons, Inc.*; 2005. <http://dx.doi.org/10.1002/9780471729259.mc02b02s25>.
- [137] Bray D. Critical Point Drying of Biological Specimens for Scanning Electron Microscopy. In: Williams JR, Clifford AA, (editors). *Supercritical Fluid Methods and Protocols*. Totowa, NJ: Humana Press; 2000. p. 235-43. <http://dx.doi.org/10.1385/1-59259-030-6:235>.
- [138] Matias VR, Al-Amoudi A, Dubochet J, Beveridge TJ. Cryo-transmission electron microscopy of frozen-hydrated sections of *Escherichia coli* and *Pseudomonas aeruginosa*. *J Bacteriol*. 2003;185:6112-8. <http://dx.doi.org/10.1128/JB.185.20.6112-6118.2003>.
- [139] Gilbertson LM, Zimmerman JB, Plata DL, Hutchison JE, Anastas PT. Designing nanomaterials to maximize performance and minimize undesirable implications guided by the Principles of Green Chemistry. *Chem Soc Rev*. 2015;44:5758-77. <http://dx.doi.org/10.1039/C4CS00445K>.

Chapter 3: Anisotropic and metastable hydrophobicity of the leaf canary grass leaf

The previous chapter highlighted numerous mechano-bactericidal topographies found on the surface of animals and insects. Some plant surfaces, on the other hand, are highly hydrophobic as a result of surface chemistry and physical topography. While not mechano-bactericidal per se, these plant surfaces do possess anti-biofouling properties. How a droplet of water wets the surface of a complex plant topography is nontrivial. A detailed understanding of such wetting behavior has implications in the design of future biomimetic anti-biofouling materials. This manuscript is currently under preparation for submission to a peer-reviewed journal. Experimental work was performed by N. Lin who was assisted by V. Uong. Data analysis was conducted by N. Lin and R.J. Hill. The manuscript was drafted by N. Lin and P. Berton while R.J. Hill, R.D. Rogers and N. Tufenkji provided guidance and supervision throughout the project and in manuscript editing.

3.1 Abstract

The reed canary grass (*Phalaris arundinacea*) possesses a complex leaf topography. In addition to longitudinal grooves and a dense coverage of waxy nanocrystals, the underside of the leaf is decorated with oriented arrays of microscopic trichomes (plant epidermal outgrowths). An individual reed canary grass trichome resembles a ratchet structure that tapers asymmetrically to a sharp tip but the trichome's size and organization is highly dependent on spatial positioning. Due to the complexity of its topography, the wettability of the reed canary grass leaf is nontrivial. In our assessment, we found the leaf to be nearly superhydrophobic. Waxy nanocrystals and trichomes combined to enhance surface roughness, achieving water contact angles as high as 147°. Unidirectional wettability was observed but only at the tip region of the leaf. This can be attributed to the leaf narrowing at the leaf tip (causing longitudinal grooves to furrow thereby increasing

surface roughness). The ability to control the direction of a water droplet's motion is advantageous in self-cleaning surfaces and devices requiring precise fluid transport such as microfluidics or biomedical sensors. Time-dependent contact angle measurements revealed that the leaf's hydrophobicity is metastable. Initially, water droplets exist in a semi-suspended state supported by air pockets somewhere between the Cassie-Baxter and Wenzel state of wettability, but droplets collapse into the Wenzel state over time. Insights gained from this study are useful for biomimetic and bio-inspired designs.

3.2 Introduction

The wettability of plant surfaces has garnered immense research attention in the past few decades. Arguably the most well-studied plant surface, the lotus leaf consists of nanoscale waxy crystalloid protrusions on top of microscale convex cells [1]. This hierarchical topography prevents droplets of water from wetting the leaf surface [2, 3]. Instead, water droplets roll off with ease, carrying with them any biotic or abiotic contaminants. The result is the superhydrophobic lotus leaf which appears to stay clean at all times, a phenomenon aptly referred to as the “lotus” effect or the “self-cleaning” effect [1].

The leaf of the rice plant, too, is well-known for its superhydrophobic properties. Whereas the lotus leaf's topography is homogeneous throughout, the rice leaf features macro- and microscale grooves running longitudinally along the length of the leaf blade [4]. Droplets of water preferentially roll along the length of the leaf since it is energetically favorable to move in directions parallel to the longitudinal grooves. In contrast, large energy barriers need to be overcome if a droplet of water is to move in a direction perpendicular to the grooves. Thus, the rice leaf's superhydrophobicity is said to be anisotropic [4-7]. In addition to self-cleaning or anti-fouling applications [8], such control over a water droplet's direction of motion is of particular

interest in devices requiring precise fluid transport, as is the case for microfluidics or biomedical sensors [9]. Biological reagents such as blood or DNA are usually limited in quantity and highly valuable. In these scenarios, anisotropic surfaces that offer control over liquid handling, fluid motion or drag reduction to minimize the loss of reagents would be highly advantageous.

Recently, Guo *et al.* found that the ryegrass leaf exhibits unidirectional wettability such that the leaf sheds water droplets preferentially in one direction [10]. The ryegrass leaf topography consists of grooves similar to the rice leaf but also possesses microscopic arrays of oriented trichomes (plant epidermal outgrowths). Each trichome resembles a ratchet structure that tapers asymmetrically from the base of the leaf into a curved, sharpened tip. It was proposed that a droplet of water moving in the direction opposite the collective orientation of the trichomes' tips would experience partial pinning by the tips. Conversely, moving along the same direction as the tips is energetically favorable as a water droplet would not be pinned and would then shed off from the leaf easier. The surface of the ryegrass leaf was therefore suggested to be biologically designed by nature to influence wettability [10].

Trichomes perform a myriad of physiological and ecological functions and have recently attracted the interest of researchers in the fields of biomimicry and bio-inspiration, culminating in a 2017 review by Liu *et al.* which discusses some bio-inspired designs based on trichomes [11]. A review of the literature indicates that for grass-type plants, trichomes are not usually known for influencing wettability and are instead associated with plant defense by inhibiting insect movement. Whether taper-ratchet trichomes have the evolutionary purpose of anisotropic wettability as suggested by Guo *et al.* is therefore unclear.

Herein, we investigated the wettability of the reed canary grass leaf (*Phalaris arundinacea*), which has been shown to resist insects with its trichomes [12]. Macroscopically, the

leaf is similar to the rice leaf and the ryegrass leaf as they are all thin and blade-like with visible longitudinal grooves characteristic of grass-type plants. Microscopically, the underside of the reed canary grass leaf features taper-ratchet trichomes that individually bear resemblance to those of the ryegrass. The size and organization of the trichomes are highly complex and directly related to their spatial positioning on the leaf. Trichomes growing from the ridges of the grooves appear to be small near the base of the leaf but steadily become larger and even self-organized into oriented overlapping arrays near the tip of the leaf. Longitudinal grooves are indicative of anisotropic wettability similar to the rice leaf while the oriented nature of the trichomes suggest potential unidirectional wettability of the ryegrass leaf. How a moving water droplet wets the reed canary grass leaf is nontrivial due to the complexity and spatial variation of its topography. Insights gained from this study are useful for future biomimetic and bio-inspired designs.

3.3 Experimental

3.3.1 Sample preparation

Reed canary grass (*Phalaris arundinacea*) leaves were obtained from the location 45°30'17.5"N, 73°34'28.6"W within the campus of McGill University (Montreal, Quebec, Canada). Leaves were cut from the plants as-needed. For experiments, leaves were blown with pressurized air for 10 seconds before experiments to remove debris. Experiments were completed within an hour of removing the leaves from the plant to ensure leaves did not dry or warp during experiments. No additional cleaning preparations were undertaken to minimize potential damage or modification to the leaf surface. To eliminate seasonal variation in plant morphology, experiments were carried out between May to September of 2017.

3.3.2 Leaf topography characterization and wettability measurements

Variable-pressure scanning electron microscopy (SEM, Hitachi SU-3500, Hitachi High Technologies, Tokyo, Japan), also referred to as environmental scanning electron microscopy (E-SEM), was performed on leaf samples still in their native hydrated state without the need for conductive coating or fixation. Voltage of 3-5 kV, spot of 40-50, and pressure of 30-60 Pa produced optimal E-SEM observations. For cross-sectional examinations of the leaf, samples were cut orthogonally and observed by tilting the SEM sample holder to 80°. Length measurements of topographical features of the leaf were conducted with the image processing software ImageJ (National Institutes of Health, Maryland, U.S.).

The static contact angles of droplets of deionized (DI) water deposited upon sample surfaces were measured with a contact angle apparatus (OCA15, Dataphysics Instruments GmbH, Filderstadt, Germany). Droplets 3 μL in volume were dispensed by a 30-gauge blunt-end needle (outer diameter: 0.3 mm, SAI Infusion Technologies, Illinois, U.S.) affixed to a syringe. Measurements were obtained immediately after deposition unless otherwise stated. Advancing and receding contact angle measurements were conducted by dispensing and withdrawing additional water with the syringe into the initial 3 μL drop at a rate of 0.1 $\mu\text{L}/\text{s}$.

To evaluate potential unidirectional wetting preferences, two methods were performed. First, a 3 μL droplet of DI water was deposited onto the leaf sample surface. Immediately following and without removing the needle from the droplet, an additional 15 μL of water was dispensed at a rate of 0.3 $\mu\text{L}/\text{s}$, causing the droplet to advance. Afterwards, the same 15 μL was withdrawn from the droplet at a rate of 0.3 $\mu\text{L}/\text{s}$. In a second method, 2 μL droplets were deposited onto leaf sample surfaces and allowed to evaporate over time at ambient temperature ($\sim 21^\circ\text{C}$) and pressure (~ 1 atm). The purpose of the slow evaporation process is twofold. First, it provides insights into

the dynamics of a receding droplet. Second, it evaluates the metastability of the hydrophobicity of the leaf. Contact angle measurements and representative images were taken throughout the evaporation process.

3.4 Results and discussion

3.4.1 Leaf topography characterization

Macroscopically, the appearance of the reed canary grass plant (Figure 2a) is characteristic of many other grass-type plants: its leaves are long, narrow, blade-like, and protrude from a central stem. Apart from grooves that run longitudinally along the entire length of the leaf blade, observations by E-SEM did not identify discernible topographical structures on the top (abaxial) surface of the leaf (Figure 2b and Figure 3a).

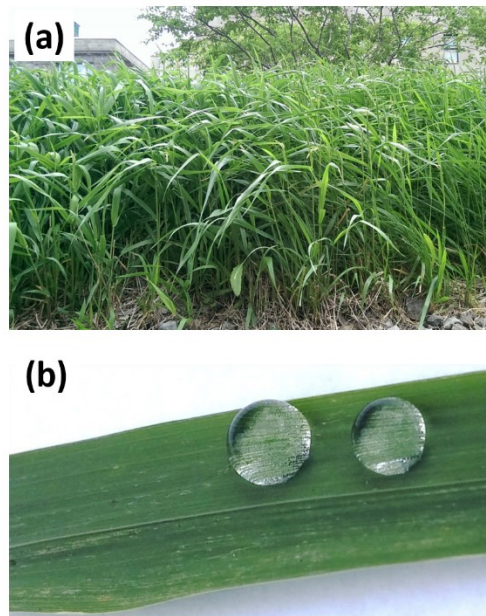


Figure 2. The reed canary grass has (a) blade-like leaves protruding from its stem. (b) Leaves have visible longitudinal grooves along the entire length of the leaf blade.

The underside (adaxial) surface of the leaf is far more complex. In addition to the longitudinal grooves, the underside features arrays of trichomes that can be described as ratchet structures which taper in a curved and asymmetric manner ending with sharp points as seen in Figure 3b. Most trichomes grow out of the ridges of the grooves although some protrude from the troughs of the grooves (Figure 3b, c). Moreover, trichomes near the base of the leaf (i.e., the leaf region that is closest to the stem of the plant), appear widely distributed and small in size (Figure 3d). However, trichomes on the ridge of the grooves gradually grow larger and eventually begin to overlap one another especially at the tip region of the leaf. In Figure 3e, it is evident that they collectively orient to point towards the tip of the leaf (away from the stem) in a self-organized manner. In comparison, trichomes growing out of the groove troughs do not change in size and are relatively unorganized. Finally, the entire underside of the leaf is densely covered with waxy nanocrystals (Figure 3f) except for the trichomes themselves. Detailed size measurements are provided in the ESI along with additional E-SEM images (Figures S1-S9) of topographical features. The collective orientation of the trichomes contribute to roughness that can be felt via tactile touch. In fact, the leaf is rough and abrasive near the tip but as tactile motion moves towards the base of the leaf, the abrasive sensation decreases and is hardly noticeable at the base.

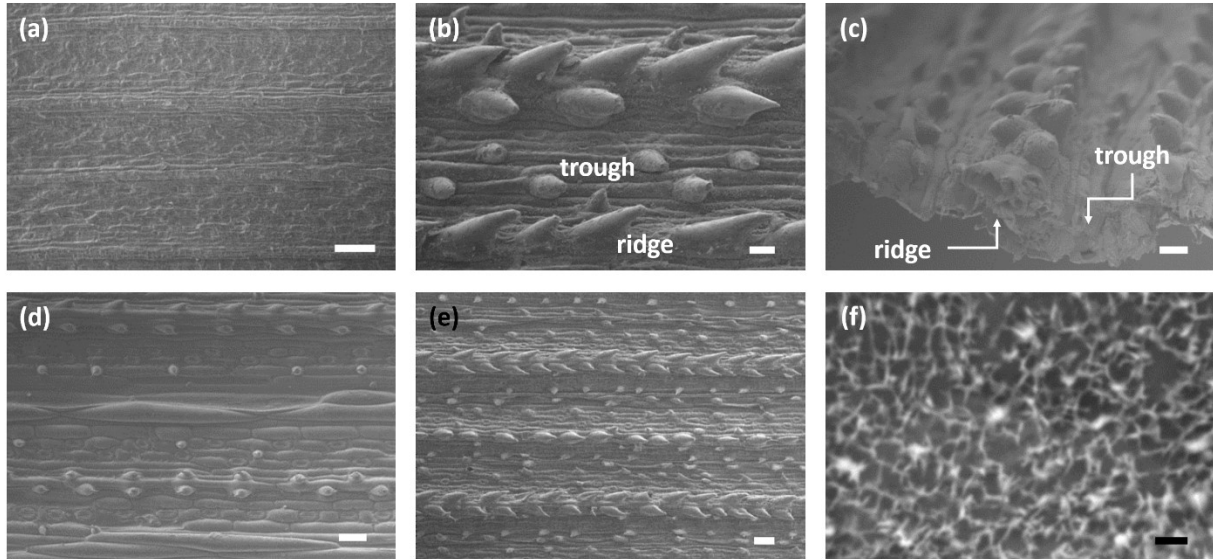


Figure 3. E-SEM of leaf topography reveals (a) longitudinal grooves on the top surface of the leaf (scale bar: 100 μm). (b) Taper-ratchet trichomes viewed at 60° tilt (scale bar: 20 μm) (c) ridges of grooves (scale bar: 20 μm), (d) trichomes are small near the base of the leaf (scale bar: 50 μm), (e) but grow larger near the tip of the leaf (scale bar: 50 μm). (f) Dense layer of waxy nanocrystals cover the underside of the leaf (scale bar: 1 μm).

Average static contact angle measurements of water droplets deposited on the top and underside surface of the leaf are shown in Figure 4. Since E-SEM observations revealed that the topography of the leaf changes depending on the location on the leaf surface, the experiment was conducted at three representative regions on both sides of each leaf: the region near the stem (base), middle region of the leaf (mid), and the tip of the leaf (tip). Two trends are apparent in Figure 4 that can be rationalized by considering the differences in topographies from region to region.

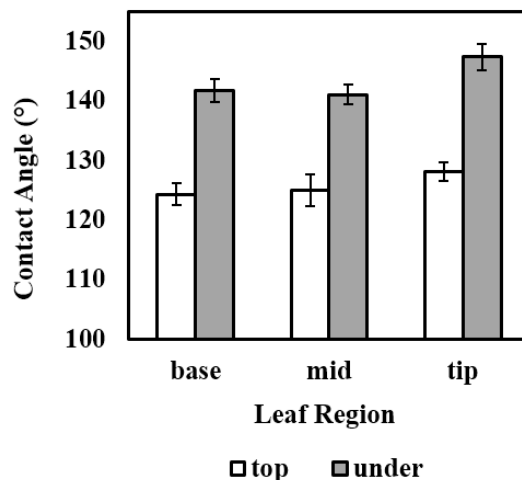


Figure 4. Average static contact angle measurements of the reed canary grass leaf

First, compared to the top surface, the underside of the leaf is more hydrophobic—just short of the superhydrophobic contact angle threshold of 150° . Microscale trichomes and nanoscale waxy crystals, both of which exist exclusively on the leaf’s underside, combine to form a highly roughened surface which promotes hydrophobicity and traps air pockets. During our evaluation of contact angle hysteresis (CAH), defined as the difference between advancing and receding contact angles [13], we observed that droplets on the underside of the leaf recede in discrete de-pinning, re-pinning and de-pinning events. This repeated “jumping” motion is indicative of some air pockets trapped within microscopic cavities due to surface roughness. Therefore, the underside of the leaf resides in a partially-suspended wettability state somewhere between the Cassie-Baxter and Wenzel states of wettability (see ESI for details) [14-16].

Second, the tip regions are more hydrophobic than the rest of the leaf. Examining the topography at the tip regions reveals that the periodicity of the grooves at the leaf tip is smaller than the rest of the leaf. Most likely, since the leaf narrows more dramatically at the tip, grooves

in this region also narrow accordingly. The result is the reduced periodicity of the grooves (Tables S3 and S4) as well as increased depth of grooves observable by E-SEM due to the furrowing of the grooves as they “compress.” This trend is visible in Figure 6, where the base and mid regions of the underside of the leaf have nearly the same groove periodicity and topography, but the periodicity at the tip region is noticeably reduced contributing to a rougher surface. In addition, trichomes on the underside of the leaf are more prominent near the tip (Figure 5c), again enhancing roughness and providing microscopic cavities at the tip region, whereas trichomes at the base and mid regions of the leaf are sparser and do not contribute as much to the topography.

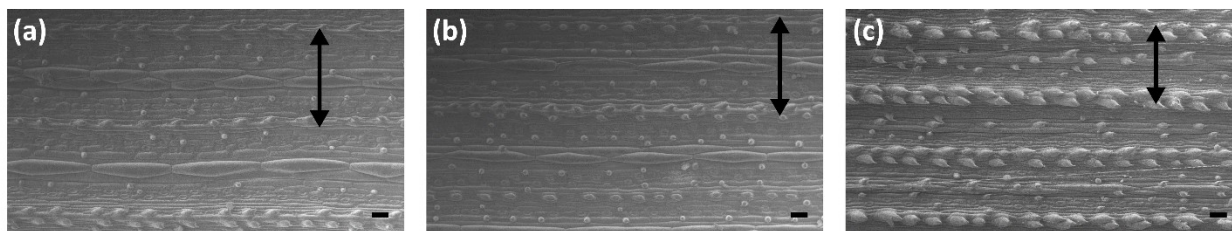


Figure 5: E-SEM images show grooves at the (a) base, (b) mid, and (c) tip regions of the underside of the leaf. In (a) and (b) the arrows have the same width $\sim 290 \mu\text{m}$ whereas the arrow in (c) represents $\sim 210 \mu\text{m}$. The scale bar is $50 \mu\text{m}$ in all cases.

3.4.2 Anisotropic wettability

There are several approaches to assess potential directional wettability of a moving droplet of water. Dynamic dispensing/withdrawing of a droplet at a fixed rate as well as evaporation experiments were favored in this study. These experiments, when captured by a camera, provide clarity into the advancing and/or receding contact lines during gradual droplet motion. The pinning dynamics of the receding contact line are especially important as they have been shown to dictate anisotropic wettability on ratcheted surfaces [17]. As a general note, techniques such as sliding

angle or vibrational experiments produce dramatic results. However, they cannot offer the same level of clarity into the changes of the contact lines since movement by the equipment or the droplet itself during its motion can blur the captured images.

In dynamic dispensing/withdrawing, we first deposited 3 μL droplets of water on leaf samples. An additional 15 μL was dispensed into and then withdrawn from each droplet to induce advancing and receding droplet motions, respectively. Again, the experiment was conducted at three representative regions on both sides of each leaf due to the spatially-changing topography of the leaf. The process was captured by a camera positioned perpendicular to the longitudinal grooves of the leaf. Therefore, any observed movement in the left or right direction with respect to the page represents movement in either direction parallel to the grooves. For the sake of consistency, moving towards the left-hand side of the page is to move in the direction towards the base of the leaf (which is also the direction against the oriented tips of the trichomes for the underside of the leaf). Similarly, moving towards the right-hand side is to move towards the tip of the leaf, akin to moving along the direction of the trichome tips. Results from dispensing/withdrawing experiments are displayed in Figure 6.

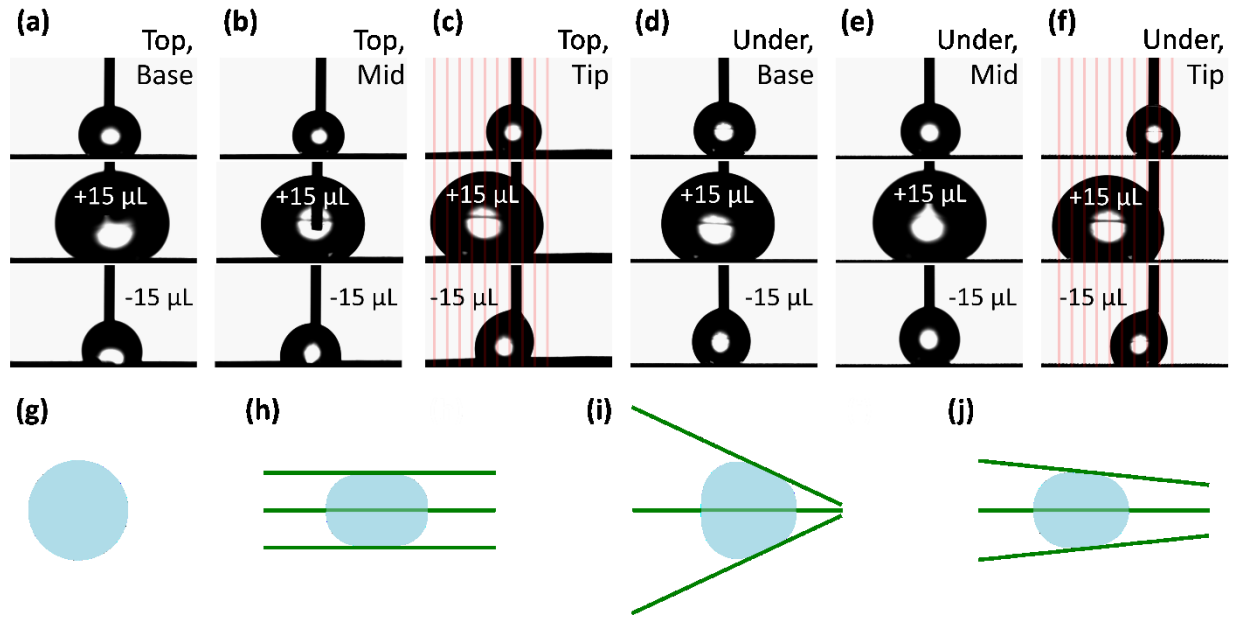


Figure 6: Images (a) – (f) display 3 μL droplets of water before dynamic dispensing, after dispensing, and after withdrawing on various regions of the leaf. A water droplet's advancing behavior is schematically represented for (g) a smooth surface, (h) a grooved surface, (i) an exaggerated, non-parallel grooved surface, and (j) a more realistic non-parallel grooved surface similar to the grooves of the leaf.

There is no apparent preference of droplet movement towards either direction of the leaf for the base and mid regions of the leaf. This is true for the top surface (Figure 6a, b) and the underside (Figure 6d, e) of the leaf. For the top surface, this was predictable as there were no topographical features that would act as energy barriers to produce unidirectional preferences. Longitudinal grooves impart anisotropic wettability but would have little impact on the movement of droplets parallel to the grooves as there are no topographical structures that would cause pinning. The underside of the leaf features oriented trichomes yet no apparent directional preference was observed either (in the base and mid regions). Based on findings by Guo *et al.* of unidirectional wetting by the taper-ratchet trichomes of the ryegrass, we expected the droplet to experience pinning by the tips of the trichomes' collective orientation. This would make movement towards the tip of the leaf more energetically favorable. It is possible that, while the reed canary grass

trichomes are in fact oriented, their overall surface coverage was insufficient to produce observable, macroscopic effects on directional wettability. Another possibility lies in the presence of the smaller set of poorly-ordered trichomes (which are absent in the ryegrass leaf) that grow from the trough of the grooves that may have contributed randomness to the surface topography.

Unidirectional wettability was observed on the tip regions for both the top (Figure 6c) and underside (Figure 6f) of the leaf. Specifically, droplets consistently advanced towards the stem of the leaf. For reference, it is convenient to visualize the extent by which the droplets advanced towards one direction by comparing it to the body-width of the syringe needle (outer diameter: 0.3 mm), which we have overlaid in red lines. In Figure 6c, f, both droplets moved multiple body-widths towards the stem of the leaf. During the receding of their contact lines, again it is the left-hand sides of the droplets that move. The final equilibrium position of the droplets after the receding event, too, is noticeably off-centre, thus, the mass-centre of the droplet is not recovered.

Unidirectional wetting can not be attributed to the presence of trichomes as the top surface of the leaf is entirely void of trichomes. Rather, the leaf tip likely possesses a surface gradient due to narrowing and furrowing of the grooves at the tips. The resulting gradient of roughness produces a driving force at the tip region: moving towards the right is more hydrophobic whereas moving towards the left is less rough and therefore less hydrophobic and by association has a higher surface free energy. In addition, the gradual furrowing of the grooves also produces non-parallel grooves which could also contribute to unidirectional wetting. A droplet on a flat surface would spread homogeneously in the radial direction until it reached equilibrium, as shown in Figure 6g. The introduction of longitudinal grooves (Figure 6h) causes the spreading motion to advance in directions parallel to the grooves because advancing perpendicularly requires overcoming energy barriers. Similarly, the non-parallel grooves exaggerated in Figure 5i for demonstration impart

unidirectional wetting because movement towards the narrow side is energetically unfavorable. Figure 5j is a more realistic representation of the grooves of the reed canary grass leaf.

The dispensing/withdrawing experiment can be considered as a modified CAH experiment with a much larger change in volume. As was observed in CAH experiments, discrete “jumping” motions during the dispensing/withdrawing experiment indicate the presence of air pockets on the underside of the leaf. In Figure 6f, the entire droplet appears to shift during advancing motion again demonstrating low adhesion due to air pockets. The contact line of the right-hand side de-pinned, moved one syringe needle body-width to the left, and re-pinned at a new equilibrium position (ESI Video).

In a second set of experiments, 2 μL droplets were left to evaporate on the leaf surface to observe the dynamics of the receding motion with high precision. Naturally, a large droplet of water would produce significant hydrostatic pressure due to its mass, which would accelerate the penetration of water into the spacing between the topographical structures. However, a water droplet that is too small is difficult to deposit as it cannot overcome the surface tension of the dispensing needle. In this study, 2 μL droplets proved to be the minimum volume that still enabled us to maneuver without much difficulty. For a surface to produce anisotropy in wettability, we would expect pinning upon topographical structures in an anisotropic manner such that motion in the un-pinned direction is favorable. Take the longitudinal grooves of the leaf, for instance. When the longitudinal grooves are parallel to the camera, as is the case for Figure 7a, the droplet is decreasing in size as it evaporates but the droplet diameter is unchanged (until the very end) using its initial diameter as a reference. The entire contact line pinned to the grooves would have to de-pin for the observed diameter to decrease. Since motion is unhindered in directions parallel to the grooves, the droplet recedes such that it eventually appears elongated in the perpendicular

direction. Sometimes the elongated droplet splits down the middle when the droplet is nearly completely evaporated.

In Figure 7b, the grooves are perpendicular to the camera. As the droplet evaporates, its diameter decreases as well since no pinning occurs in the left and right direction as it recedes. If the collective asymmetry of trichomes influence wetting in a macroscopically-observable manner, one side would recede more than the other side. This was not observed during our experiments. Using the initial droplet diameter as a reference, the droplet receded against and along the trichome directions equally.

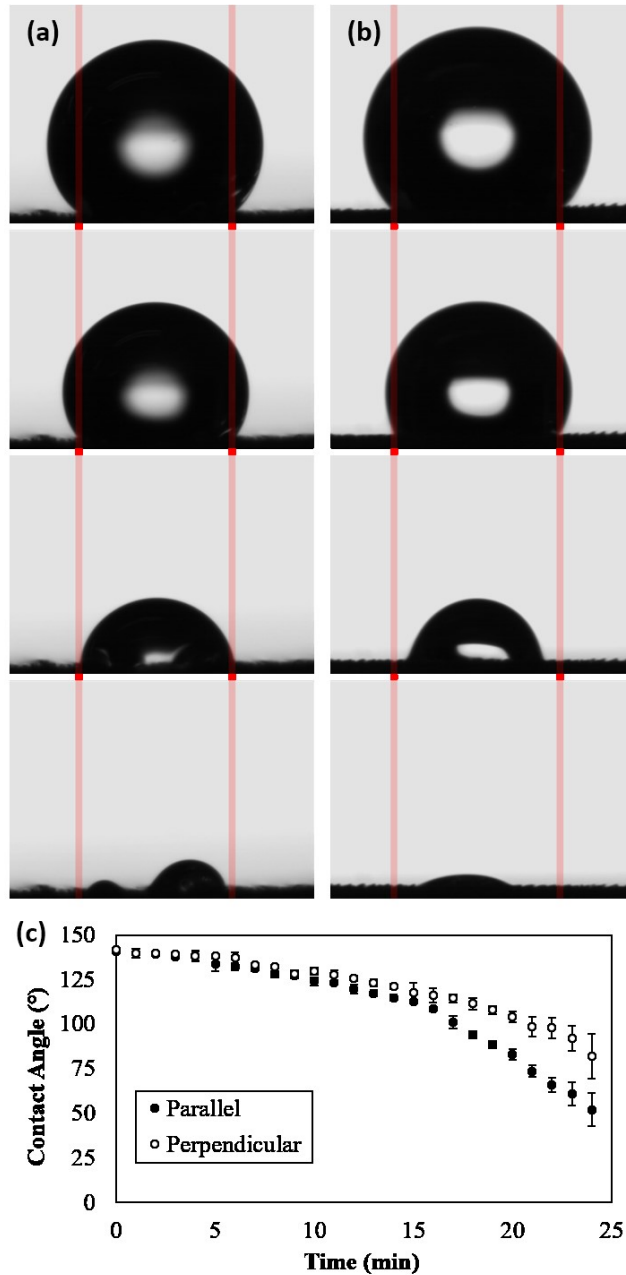


Figure 7: Evaporating droplets of water viewed from the (a) parallel and (b) perpendicular directions with respect to longitudinal grooves. Overlaid red lines represent initial droplet diameter. (c) Contact angle decreases continuously during evaporation.

3.4.3 Metastability

The underside of the reed canary grass leaf can be described as a combination of multiple topographies. The longitudinal grooves, an array of oriented trichomes growing out of the ridges

of the grooves, another array of unorganized trichomes growing out of the troughs of the grooves, and waxy nanocrystals that densely cover the surface all contribute to surface wettability. Due to this highly irregular and non-uniform nature of the underside of the reed canary grass leaf topography, we hypothesized that its near-superhydrophobic static contact angles were a transient observation. Specifically, air pockets trapped in microscopic cavities described above may not persist over time. Indeed, evaporation experiments indicated that, given sufficient time to equilibrate, water eventually penetrates the spacing between topographical structures. It's semi-suspended state of wetting is metastable and thus collapses to the Wenzel state as seen by the ever-decreasing contact angles in Figure 7c. The receding "jumping" motion described earlier is also not observed in this case, further indicating that no air pockets remain. The transition from superhydrophobic to hydrophilic is often the case for biological surfaces. If static contact angle measurements are carried out immediately upon contact with water droplets, superhydrophobicity is achievable, but air pockets are not sustained under hydrostatic pressure [18-20].

3.4.4 Physiological function of taper-ratchet trichomes

In general, trichomes perform a myriad of physiological and ecological functions but the most apparent and well-documented is their ability to mechanically resist against invasive insects [21]. In some bean plants, trichomes have even been observed to incapacitate insect locomotion by impaling them. Thus, trichomes that incapacitate insects are usually sharp or pointed or even hooked, as is the case for bean plant trichomes. Literature indicates a correlation between trichome shape, size, coverage and plant resistance to insect damage [12, 22, 23]. During our studies, we noticed the presence of aphids on the top surfaces of a leaf but none on the underside where trichomes are present (Figure S10). Transplanting the plant indoors to observe aphid proliferation, we noticed their presence persisted for weeks and infected the top surface of another leaf. The

observation was serendipitous and un-controlled but nonetheless supports the notion that reed canary grass trichomes function to mechanically resist insects. However, it is curious as to why taper-ratchet trichomes only exist on the underside of leaves, as one would expect the top surface of the leaf to benefit from insect resistance as well.

3.5 Conclusions

In this study, we sought to understand how the complex leaf topography of reed canary grass influences its wettability. Overall, the leaf was highly hydrophobic and near-superhydrophobic at the tip regions as microscopic trichomes and waxy nanocrystals combined to form a roughened surface with microscopic cavities for air pockets. Unidirectional wettability was also observed at the tip region of the leaf. As the leaf tip narrows, its longitudinal grooves gradually furrow creating a topographical and free energy gradient. Its hydrophobicity is metastable as water droplets deposited on the leaf initially reside in a partially-suspended state of wettability but equilibrate to the Wenzel state over time.

3.6 Acknowledgements

The authors thank K.M.T. Ahmmed, H. Choudhary, and Prof. Christopher Moraes for helpful discussions and Prof. Alan Watson for help in identifying reed canary grass. This research was undertaken, in part, thanks to funding from the Canada Excellence Research Chairs Program (RDR), the Canada Research Chairs Program (NT), the Natural Sciences and Engineering Research Council (NSERC) Discovery Program (RDR and NT) and the Eugenie Ulmer Lamothe fund at McGill University (NL).

3.7 Supplementary information

Table S1: Measurement of topographical features on the top surface of the leaf

Measurement (μm)	Base	Mid	Tip
Groove periodicity	298 ± 5	304 ± 3	205 ± 4

Table S2: Measurement of topographical features on the underside of the leaf

Measurement (μm)	Base	Mid	Tip
Groove periodicity	291 ± 6	288 ± 4	205 ± 4
Trichome length (trough)	23 ± 3	24 ± 4	28 ± 3
Trichome length (ridge)	36 ± 3	39 ± 2	71 ± 1
Trichome tip-to-tip (ridge)	105 ± 8	102 ± 9	65 ± 9

Figure S1: Longitudinal grooves on the top surface of the leaf

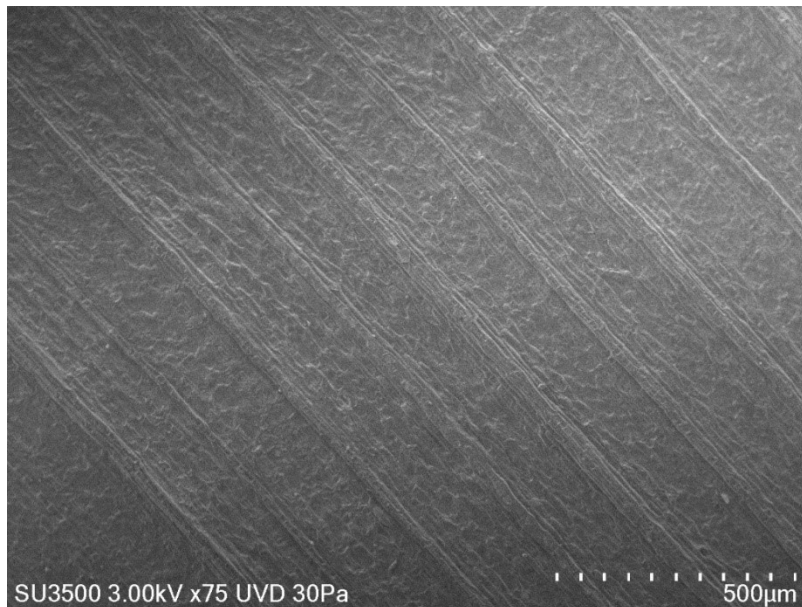


Figure S2: Trichomes are small on the underside base region of the leaf

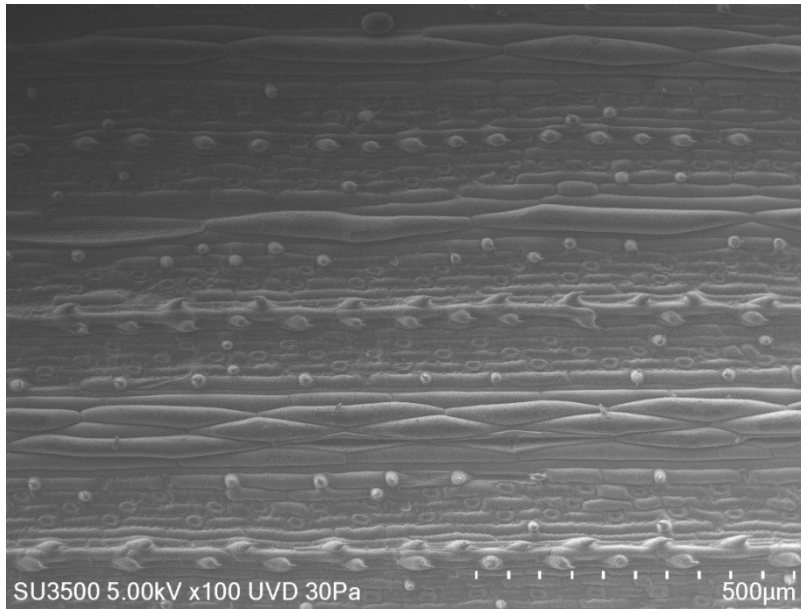


Figure S3: Trichomes growing from ridge of grooves are visibly larger and the surface is more rough at the underside tip region of the leaf

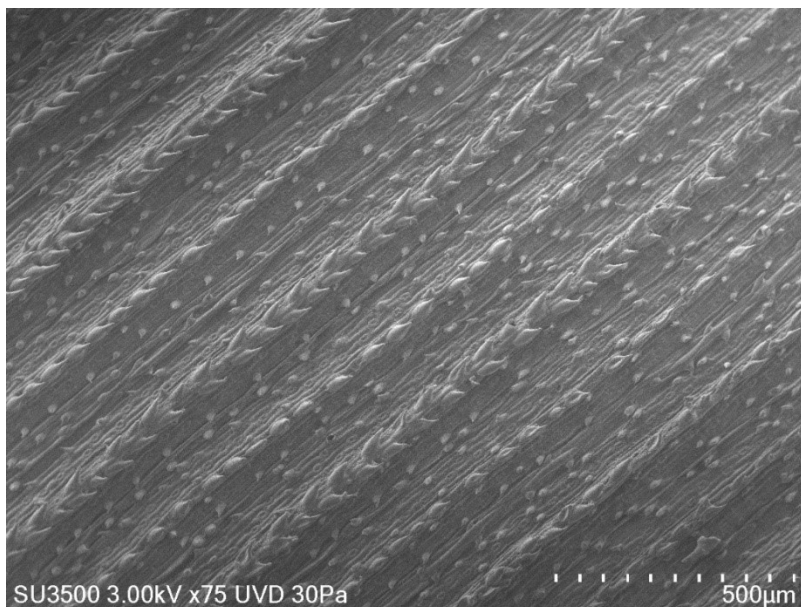


Figure S4: Trichomes growing from ridges of the grooves are large and oriented whereas trichomes growing from the troughs of the grooves are small and unorganized

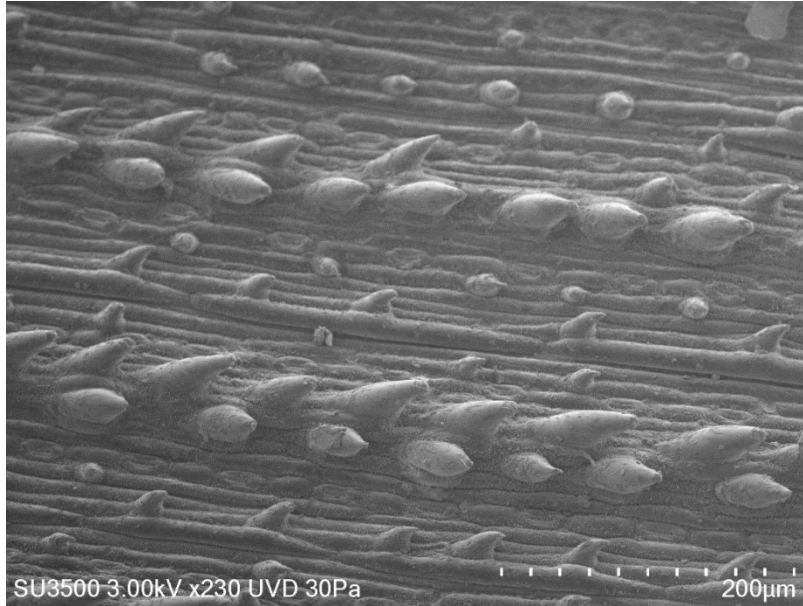


Figure S5: Close-up of the sharp, tapered point of the trichomes



Figure S6: A dense layer of waxy nanocrystals cover the leaf surface

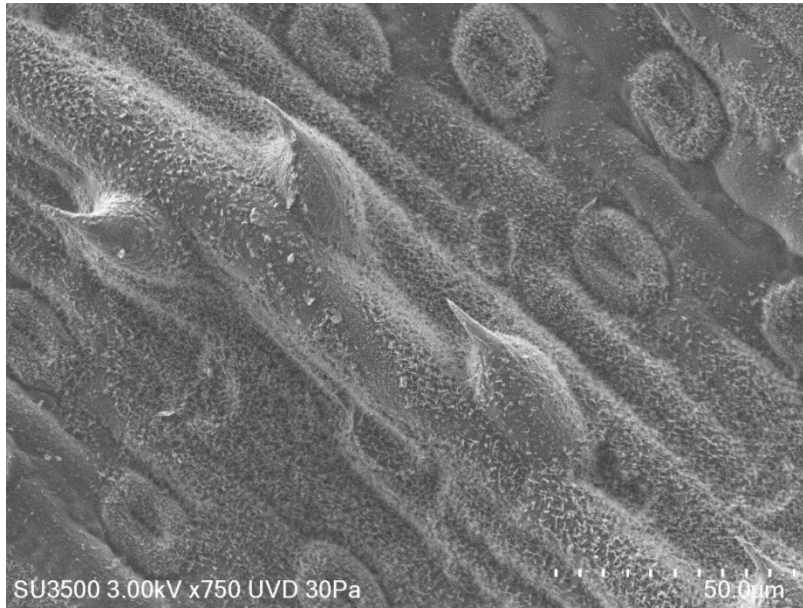


Figure S7: Close-up of waxy nanocrystals

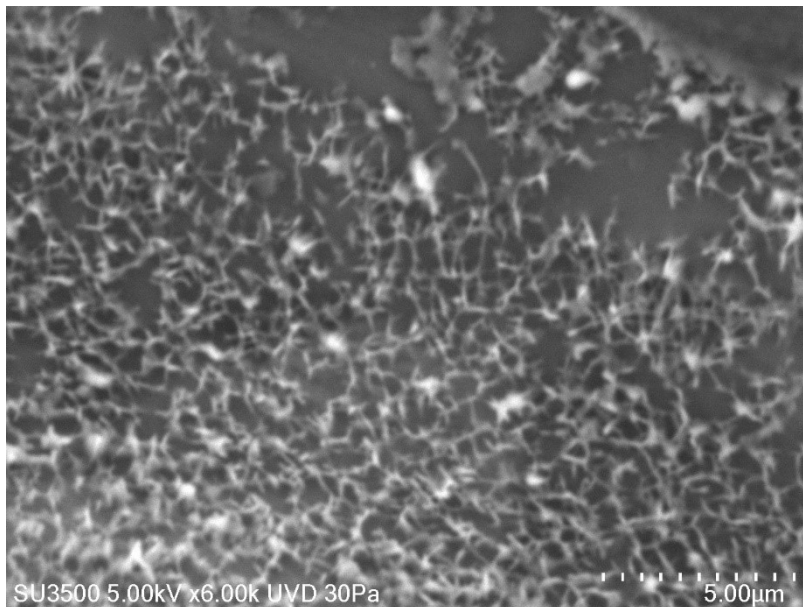


Figure S8: Cross section of the leaf with the top surface visible

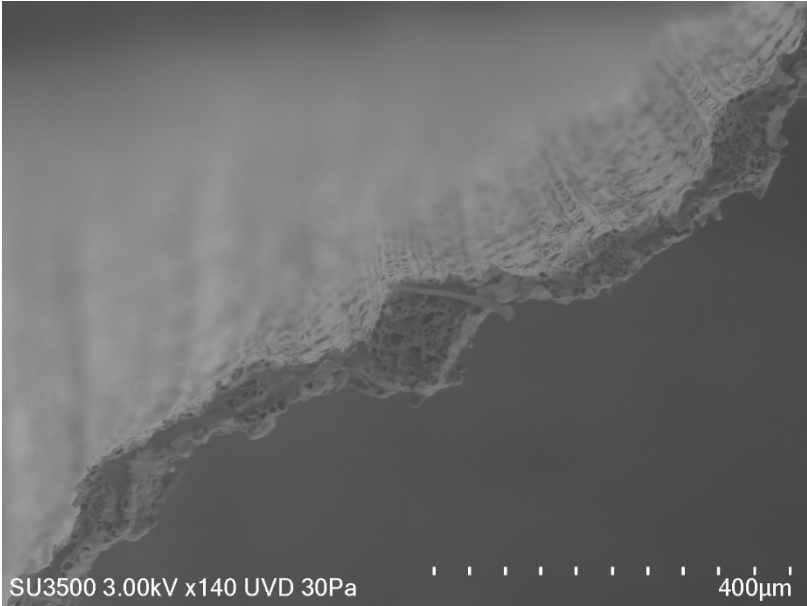
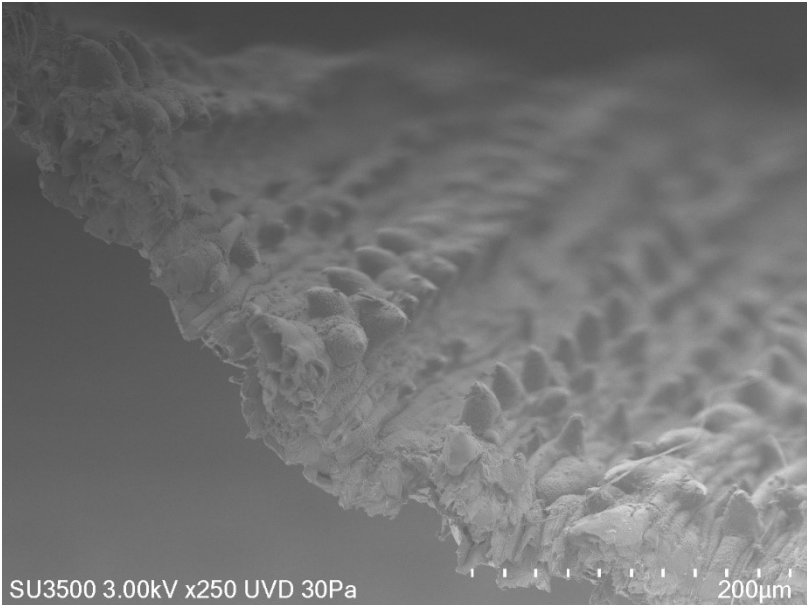


Figure S9: Cross section of the leaf with the underside visible



Supporting information:

Contact angle hysteresis (CAH) is defined as the difference between advancing and receding contact angles. In this study, advancing and receding contact angle measurements were conducted by dispensing and withdrawing additional water with the syringe into the initial 3 μL drop at a rate of 0.1 $\mu\text{L/s}$. Tables S3 and S4 indicate that CAH measurements fall between $\sim 15^\circ$ to $\sim 30^\circ$. Generally, truly superhydrophobic and self-cleaning surfaces such as the lotus leaf and the rice leaf reside in the Cassie-Baxter state of wettability wherein droplets sit upon microscopic air pockets unable to wet the surface. Usually this produces contact angles of 150° or greater in addition to low CAH (less than 10°).

Table S3: Advancing and receding angles on the top surface of the leaf

Measurement ($^\circ$)	Base	Mid	Tip
Average advancing angle	133.8 ± 1.7	134.4 ± 2.7	140.9 ± 2.8
Average receding angle	107.9 ± 2.0	108.6 ± 1.1	120.5 ± 4.2

Table S4: Advancing and receding angles on the underside of the leaf

Measurement ($^\circ$)	Base	Mid	Tip
Average advancing angle	150.7 ± 2.2	150.9 ± 2.6	155.3 ± 1.9
Average receding angle	136.1 ± 1.7	135.5 ± 3.6	140.1 ± 1.2

The Cassie-Baxter model can be described by the following equation where θ_{CB} is the apparent contact angle of a heterogeneous surface:

$$\cos\theta_{CB} = f_S \cos\theta + (1 - f_S) \cos\theta_g \quad (1)$$

Here, $f_s < 1$ is the fraction representing topographical protrusions and $(1 - f_s)$ is the fraction that corresponds to the air pockets. The contact angle on the solid surface is represented by θ while the contact angle on air, θ_g , is taken to be 180° .

In the Wenzel state of wetting, a droplet of water can still possess a high static contact angle measurement. However, the droplet fully penetrates the spaces between topographical structures so that its contact line is pinned to these structures. As a result, droplets do not easily roll about on surfaces in the Wenzel state and CAH is relatively high (more than 10°). For this reason, wetting in the Wenzel state is sometimes described as “sticky” whereas the Cassie-Baxter state is described as “slippery.”

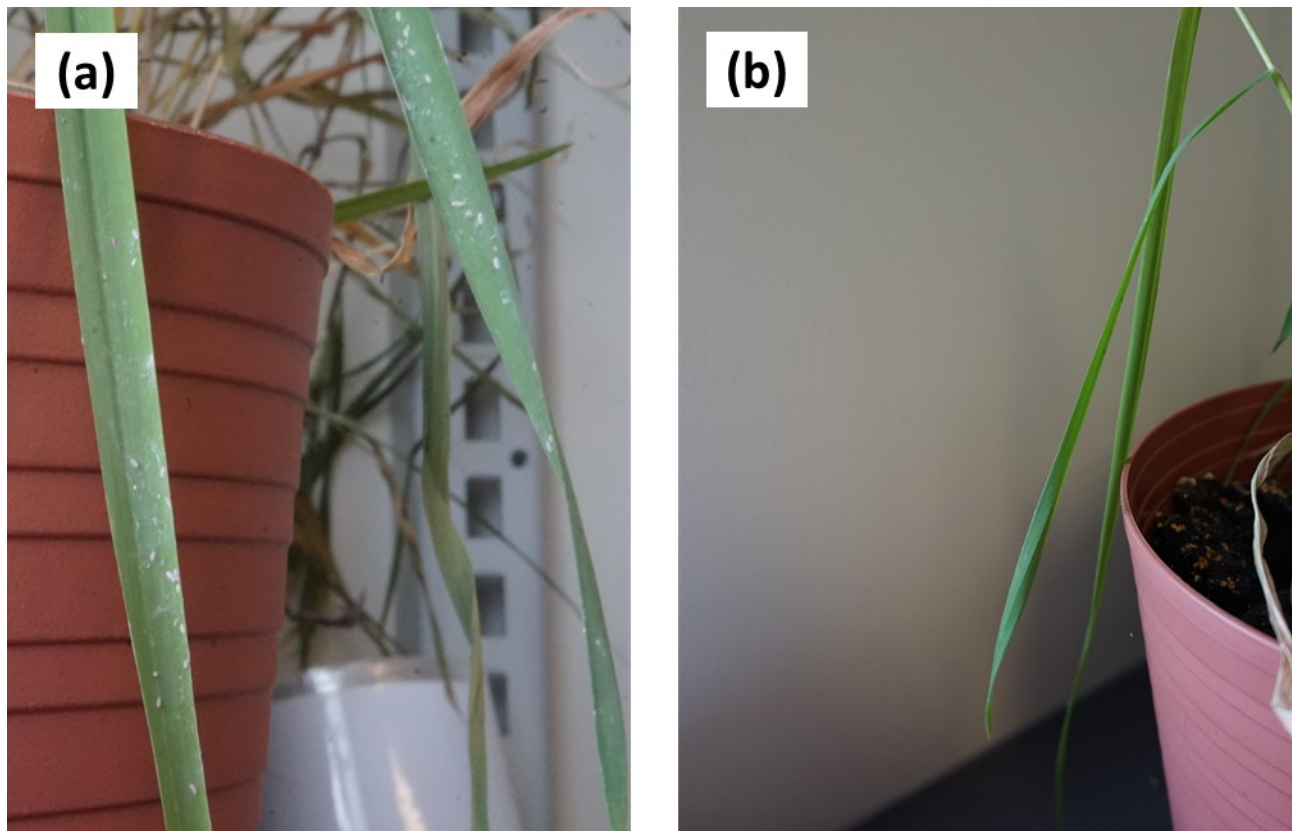
Equation 2 is known as Wenzel’s equation, where θ is the contact angle of the flat surface of the material in question. An increase in roughness, represented by the roughness factor $r > 1$ leads to an increase in the apparent contact angle θ_W .

$$\cos\theta_W = r\cos\theta \quad (2)$$

The two states of wettability can be represented by the combined general equation (Equation 3) for surfaces that exist partially between the two states of wettability:

$$\cos\theta_{CB,W} = f_s r(\cos\theta) + f_s - 1 \quad (3)$$

Figure S10: Aphids grew on the top surface of leaves but not the underside of the same leaves



3.9 References

- [1] W. Barthlott, C. Neinhuis, Purity of the sacred lotus, or escape from contamination in biological surfaces, *Planta*, 202 (1997) 1-8.
- [2] L. Gao, T.J. McCarthy, The “lotus effect” explained: two reasons why two length scales of topography are important, *Langmuir*, 22 (2006) 2966-2967.
- [3] W. Li, A. Amirfazli, Hierarchical structures for natural superhydrophobic surfaces, *Soft Matter*, 4 (2008) 462-466.
- [4] L. Feng, S. Li, Y. Li, H. Li, L. Zhang, J. Zhai, Y. Song, B. Liu, L. Jiang, D. Zhu, Superhydrophobic surfaces: from natural to artificial, *Advanced materials*, 14 (2002) 1857-1860.
- [5] D. Wu, J.N. Wang, S.Z. Wu, Q.D. Chen, S. Zhao, H. Zhang, H.B. Sun, L. Jiang, Three-Level Biomimetic Rice-Leaf Surfaces with Controllable Anisotropic Sliding, *Advanced Functional Materials*, 21 (2011) 2927-2932.
- [6] G.D. Bixler, B. Bhushan, Bioinspired rice leaf and butterfly wing surface structures combining shark skin and lotus effects, *Soft Matter*, 8 (2012) 11271-11284.
- [7] D. Xia, X. He, Y.-B. Jiang, G.P. Lopez, S. Brueck, Tailoring anisotropic wetting properties on submicrometer-scale periodic grooved surfaces, *Langmuir*, 26 (2010) 2700-2706.

- [8] T. Sun, L. Feng, X. Gao, L. Jiang, Bioinspired surfaces with special wettability, *Accounts of chemical research*, 38 (2005) 644-652.
- [9] D. Xia, L.M. Johnson, G.P. López, Anisotropic Wetting Surfaces with One-Dimensional and Directional Structures: Fabrication Approaches, Wetting Properties and Potential Applications, *Advanced Materials*, 24 (2012) 1287-1302.
- [10] P. Guo, Y. Zheng, C. Liu, J. Ju, L. Jiang, Directional shedding-off of water on natural/bio-mimetic taper-ratchet array surfaces, *Soft Matter*, 8 (2012) 1770-1775.
- [11] H. Liu, S. Liu, J. Jiaojiao, T. Lu, F. Xu, Trichome as the natural biophysical barrier for plants and its bioinspired applications, *Soft Matter*, (2017).
- [12] Y. Ling, W. Campbell, B. Haws, K. Asay, Scanning electron microscope (SEM) studies of morphology of range grasses in relation to feeding by *Labops hesperius*, *Crop science*, 25 (1985) 327-332.
- [13] P. Roach, N.J. Shirtcliffe, M.I. Newton, Progress in superhydrophobic surface development, *Soft matter*, 4 (2008) 224-240.
- [14] A. Cassie, S. Baxter, Wettability of porous surfaces, *Transactions of the Faraday Society*, 40 (1944) 546-551.
- [15] R.N. Wenzel, Resistance of solid surfaces to wetting by water, *Industrial & Engineering Chemistry*, 28 (1936) 988-994.
- [16] A. Lafuma, D. Quéré, Superhydrophobic states, *Nature materials*, 2 (2003) 457-460.
- [17] H. Kusumaatmaja, J. Yeomans, Anisotropic hysteresis on ratcheted superhydrophobic surfaces, *Soft Matter*, 5 (2009) 2704-2707.
- [18] Z. Han, J. Fu, Z. Wang, Y. Wang, B. Li, Z. Mu, J. Zhang, S. Niu, Long-term durability of superhydrophobic properties of butterfly wing scales after continuous contact with water, *Colloids and Surfaces A: Physicochemical and Engineering Aspects*, 518 (2017) 139-144.
- [19] J. Hasan, H.K. Webb, V.K. Truong, G.S. Watson, J.A. Watson, M.J. Tobin, G. Gervinskas, S. Juodkazis, J.Y. Wang, R.J. Crawford, Spatial variations and temporal metastability of the self-cleaning and superhydrophobic properties of damselfly wings, *Langmuir*, 28 (2012) 17404-17409.
- [20] X. Sheng, J. Zhang, Air layer on superhydrophobic surface underwater, *Colloids and Surfaces A: Physicochemical and Engineering Aspects*, 377 (2011) 374-378.
- [21] D.A. Levin, The role of trichomes in plant defense, *The quarterly review of biology*, 48 (1973) 3-15.
- [22] J.D. Hansen, K.H. Asay, D.C. Nielson, Feeding preference of a black grass bug, *Labops hesperius* (Hemiptera: Miridae), for 16 range grasses, *Journal of the Kansas Entomological Society*, (1985) 356-359.
- [23] G. Wagner, E. Wang, R. Shepherd, New approaches for studying and exploiting an old protuberance, the plant trichome, *Annals of Botany*, 93 (2004) 3.

Chapter 4: Micro-reservoir surfaces containing hydrophobic antibacterial ionic liquids

While anti-fouling topographies found on insects, animals and plants function adequately in nature, processes that guarantee sterility on a surface must rely on potent antibacterial compounds. How these compounds are incorporated into the material is a design choice that directly impacts its practicality, longevity and sustainability. Inspired by nature's design of topographical nanopillars of the cicada and dragonfly, we explored the use of pillars to create a mold to obtain its inverse structure: reservoirs. Once constructed, microscale reservoirs were then filled by antibacterial liquids to design a new type of antibacterial surface. In this case, instead of the bio-inspired topography itself being directly anti-biofouling or antibacterial, topography was combined with chemical approaches to prepare antibacterial surfaces. N. Lin and P. Berton designed and characterized materials for this project. N. Lin designed and conducted experiments and drafted the following chapter text while R.D. Rogers and N. Tufenkji provided supervision.

4.1 Abstract

Conventional approaches to prepare antibacterial surfaces face numerous limitations. Modern antibacterial research has turned to the modification of surface topography in combination with chemical strategies. A surface featuring reservoirs containing antibacterial liquids remains unexplored despite distinct advantages. Antibacterial micro-reservoir designs, when filled appropriately, offer long-lasting, more sustainable surfaces while reducing the unintended release of antibacterial agents into the environment. Herein, we created a micro-reservoir surface constructed from polydimethylsiloxane via micro-replication techniques. Next, the micro-reservoirs were filled with benzalkonium docusate and lidocaine docusate – hydrophobic ionic liquids that are designed to be antibacterial. The study is still ongoing but initial results are

promising. Upon closer inspection, a thin layer of residual ionic liquid remains above the surface as an artifact of the filling technique employed. It is therefore this residual layer that interacts and delivers the antibacterial effects, and not contents within the micro-reservoirs themselves. Future research aims are to scale down the design from micro- to nanoscale, identify other promising hydrophobic antibacterial ionic liquids, and eliminate the thin layer of ionic liquid so that antibacterial properties are truly a product of the micro-reservoir topography.

4.2 Introduction

Bacteria are highly effective at colonizing surfaces. Mechanisms that aid in their surface attachment include the secretion of bio-macromolecules to form a favorable “conditioning” layer as well as cellular appendages that make contact with and anchor to the surface [1]. Once attached, bacteria proliferate to form a community, referred to as a biofilm, that becomes substantially more difficult to eliminate [2, 3]. For surfaces that directly interact with the human body, bacterial contamination leads to health hazards, whereas the build-up of bacteria on surfaces of industrial relevance (biofouling) leads to significant reductions in efficiency [4].

The traditional approach to create antibacterial materials is to incorporate antibacterial agents onto the surface so that their release kills bacteria on or near it [5]. Typically, the material is prepared by soaking it in a solution of dissolved antibacterial agents [6]. However, in this strategy, the antibacterial agents can be washed away or diluted through prolonged immersion in water. Abrasion during contact with other objects could also accidentally remove the surface-bound antibacterial agents. Quick-release of water-dispersible antibacterial agents via diffusion offers a highly bactericidal dosage in the short term but such a high dose may be unintentionally toxic to a patient if the material is for biomedical applications. In the long term, most of the antibacterial agents have been released from the material. What remains can only provide a

sublethal concentration insufficient to kill bacteria, instead leading to development of antibacterial resistance [7]. Indeed, this is the case for many indwelling medical implants that are surgically inserted into a patient's body but become infected prematurely, thus often requiring explant and replacement [8].

The next-generation of antibacterial surfaces employ strategies to physically modify the surface's topography via micro- and nanofabrication [6]. Often, these strategies are inspired from nature. The lotus leaf, for example, possesses a hierarchy of micro- and nanostructures on its leaf topography that prevents a droplet of water from wetting its surface. Instead, water droplets roll off with ease, carrying with them biotic and abiotic contaminants in a phenomenon known as self-cleaning [9]. Recreating the topography of the lotus leaf is a common way to achieve superhydrophobicity on building materials such as windows and roof tiles [10]. More recently, Ivanova *et al.* discovered that the wings of cicada and dragonfly insects possess topographical nanopillars and nanospikes, respectively, that mechanically induce bacterial cell death during initial cellular attachment [11].

Although nanostructured materials have been examined for their antimicrobial properties (see Chapter 2), surfaces featuring micro- or nano-reservoirs filled with antibacterial liquids remain practically unexplored. Certainly, the appropriate antibacterial liquid will be critical to the design and performance of such a surface. First and foremost, the appropriate liquid must not evaporate quickly and must not be washed away by water, either of which would defeat the purpose of the micro-reservoir design. Ionic liquids (ILs) present one approach to address these concerns. ILs are salts that melt below 100 °C. As salts, they are composed of discrete anions and cations. Room-temperature ionic liquids (RTILs) are those that specifically exist in liquid state at ambient temperature and pressure. ILs display negligible vapor pressure and exceptional solvation potential

and are thus considered “green” alternatives to traditional volatile organic solvents. The interactions of ILs with chemical and biological systems are highly tuneable via modifications of either the cation or anion. “Designer” or “task-specific” ILs do this by combining the ideal ion pairs to provide optimal functionality for the intended application [12]. In this project, benzalkonium and lidocaine were selected as cations for their antibacterial properties and paired with the docusate anion – known for its hydrophobic nature – to design two non-volatile, dual-functional, hydrophobic antibacterial ILs (HAILs): benzalkonium docusate ([Benz][Doc]) and lidocaine docusate ([Lid][Doc]).

Conventional aqueous dilution tests to quantify antibacterial efficacy were not suitable for HAILs as they are insoluble in water due to their intended hydrophobicity. Instead, we developed a phase-separated incubation technique wherein a small volume of bacterial suspension in aqueous phase was placed directly above the IL-phase. Sampling of the aqueous phase demonstrated that both HAILs were strongly antibacterial against Gram-positive bacteria *Bacillus subtilis* and *Staphylococcus aureus* but weakly antibacterial against Gram-negative *Escherichia coli* and *Pseudomonas aeruginosa*.

We fabricated an epoxy mold featuring arrays of micropillars (300 µm diameter, 500 µm height). Using standard micro-replication techniques, polydimethylsiloxane (PDMS) was cast onto the mold to obtain the inverse topographical feature: micro-reservoirs. Antibacterial surfaces prepared by filling the micro-reservoirs with [Benz][Doc] and [Lid][Doc] show promising antibacterial results. However, the surface still requires improvement as, upon closer inspection, there exists a thin coating of HAIL above the micro-reservoir topography that was not effectively removed during filling. The observed antibacterial properties of the surface are therefore not the result of the micro-reservoir design as anticipated, but the artifact of residual coating of HAILs

above the topography. Ongoing work is focused on filling techniques that effectively eliminate this residual coating, then, scaling down the topographical features from microscale to nanoscale. Also underway is the search for a HAIL that is acutely bactericidal against Gram-positive and Gram-negative bacteria.

4.3 Experimental

4.3.1 Synthesis of ILs

For the synthesis of [Benz][Doc], benzalkonium chloride (>95% purity, Sigma Aldrich) and sodium dioctylsulfosuccinate (sodium docusate; 98% purity, Sigma Aldrich) were mixed in equimolar proportion in a round bottom flask with ~ 10 mL of deionized (DI) water. The flask was capped and stirred overnight at 60 °C. Afterwards, two phases were observed: the light phase was water that also contained unreacted sodium and chloride ions whereas the heavy phase consisted primarily of [Benz][Doc]. The latter was collected in a separatory funnel to fractionate again, then dried of moisture by rotary evaporation and then by high vacuum. The resulting [Benz][Doc], which appears transparent with a hint of ivory, was confirmed of purity by nuclear magnetic resonance (NMR) spectroscopy. Thermal stability was characterized by thermogravimetric analysis (TGA).

[Lid][Doc] was synthesized and purified according to previous reports [13-15]. Briefly, silver nitrate and sodium docusate were mixed to obtain silver docusate. Lidocainium chloride monohydrate was dissolved in methanol and silver docusate was added to this in a single equimolar portion. The mixture was filtered and the filtrate was collected as [Lid][Doc]. Volatiles were removed by rotary evaporator and the product was further dried under high vacuum to yield purified [Lid][Doc] as confirmed by NMR spectroscopy. Its appearance is also transparent with a hint of ivory.

4.3.2 Bacterial cell culture

The Gram-positive bacteria *B. subtilis* (ATCC 6633) and *S. aureus* (ATCC 25923) and the Gram-negative bacteria *E. coli* (K12 wildtype) and *P. aeruginosa* (PAO1 wildtype) were chosen for this study as model species. *S. aureus*, *E. coli* and *P. aeruginosa* are common foodborne pathogens whereas *B. subtilis* is found in soil and the human gastrointestinal tract. *S. aureus*, *E. coli* and *P. aeruginosa* are also common infectious pathogens on medical implants. Bacteria maintained in -80 °C frozen stocks were streaked on Mueller-Hinton II (MHBII) agar plates and incubated overnight at 37 °C. A single colony of each bacterial strain was selected to inoculate sterile MHBII broth, which was grown overnight at 37 °C to reach mid-exponential phase. Afterwards, bacteria were washed by centrifuging at 4000g for 5 minutes and resuspended in 0.01 M phosphate-buffered saline (PBS, pH 7.4). For all four bacterial strains, optical density at 600 nm (OD_{600}) was adjusted to ~ 0.01 in PBS unless otherwise stated.

4.3.3 Antibacterial assays

Antibacterial efficacy of [Benz][Doc] and [Lid][Doc] was demonstrated by transferring 0.1 mL of either [Benz][Doc] or [Lid][Doc] using disposable sterile syringes into individual wells of a sterile 96-well microplate. The ILs were allowed to settle to the bottom of the wells by gravity, after which 50 μ L of bacteria suspended in PBS was pipetted gently on top of the IL layer. The two phases were maintained as separate layers. Incubation was performed at ambient temperature (~ 22 °C) and pressure (~ 1 atm). The aqueous phase (bacteria suspended in PBS) from each well was sampled once by withdrawing a 20 μ L aliquot by pipette, either at 0.5, 3, or 12 h after exposure to the IL. Serial dilutions of the aliquot for cell enumeration by colony forming units (CFU) was performed on MHBII agar. Alternatively, instead of cell enumeration, the 20 μ L aliquot was used

to inoculate 180 μL of sterile MHBII broth in another 96-well microplate. To monitor cell growth kinetics, OD_{600} of this microplate was measured at intervals of 0.5 h for a total of 24 h (Infinite 200 PRO Microplate Reader, Tecan Trading AG, Mannedorf, Switzerland).

4.3.4 Preparation of micro-reservoir surface

To fabricate a micro-reservoir surface, we performed standard micro-replication techniques by first fabricating an epoxy mold (4 cm \times 4 cm in size) via additive manufacturing (Ember 3D Printer, Autodesk, USA). The mold consisted of arrays of pillars 300 μm in diameter, 500 μm in height, with spacing of 300 μm between two adjacent pillars. Biocompatible PDMS (Sylgard 184, Dow Corning, USA) was mixed at a standard 10:1 ratio of PDMS base to curing agent and degassed by a vacuum chamber then poured onto the mold and left to cure in a 60 $^{\circ}\text{C}$ oven for 3 h. Once cured, the PDMS was gently peeled from the mold to obtain micro-reservoirs of 300 μm diameter, 500 μm depth, and spacing of 300 μm . The PDMS was rinsed with ethanol and dried before further use. [Benz][Doc] or [Lid][Doc] was added in small dropwise quantities ($\sim 5 \mu\text{L}$) directly onto the PDMS surface and sterile cell-scrapers were used to spread and fill the ILs into the micro-reservoirs. To measure antibacterial efficacy of the micro-reservoir surfaces, 30 μL of bacterial suspension was placed directly onto the surface. After 0.5, 3, or 12 h of exposure, each droplet was sampled by withdrawing 20 μL and evaluated for cell enumeration in the same manner as described above.

4.4 Results and discussion

As non-volatile and water-insoluble liquids, HAILs meet both essential criteria presented above that are required to fill micro-reservoirs as antibacterial agents. [Benz][Doc] and [Lid][Doc]

were designed as dual function HAILS to impart the antibacterial properties of the respective cations in combination with the hydrophobicity of the docusate anion. Benzalkonium (Figure 12 a) is commonly used as a disinfection agent (usually in the form of benzalkonium chloride) in hospital sanitizers and as preservatives in personal care products such as mouthwashes and cosmetics. Lidocaine (Figure 12 b) also has known antibacterial effects but is mostly used as an anesthetic or nerve suppressing compound. Meanwhile, docusate (Figure 12 c) is hydrophobic and used in small quantities as a food additive or surfactant or prescribed as laxative medication since it is an excellent emollient [13]. [Benz][Doc] has not been reported in literature save for a patent application by Riisager *et al.* describing it as a biologically active IL [16]. [Lid][Doc], on the other hand, has been pioneered by Rogers *et al.* as a pharmaceutical IL. The inability for [Lid][Doc] to be absorbed trans-epidermally is particularly interesting to this study as it suggests direct human contact with an antibacterial surface prepared with [Lid][Doc] poses no long-term toxicity due to minimal uptake [15].

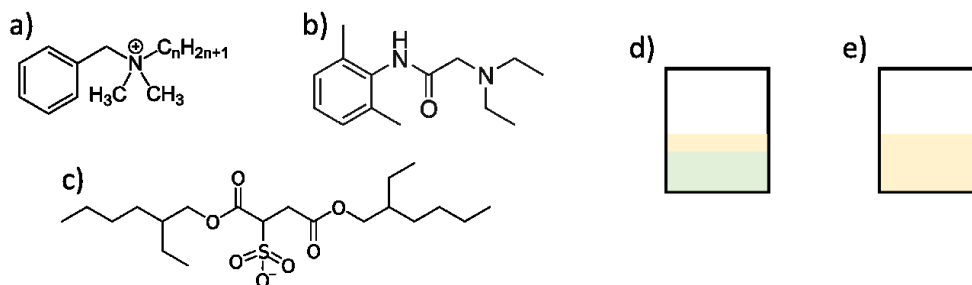


Figure 8. (a) Benzalkonium, (b) lidocaine, (c) docusate, (d) bacteria suspended in PBS (depicted in yellow) above the IL-phase (depicted in green), (e) bacteria suspended in PBS served as control.

The antibacterial activity of ILs soluble in water are usually quantified through standard dilution tests but HAILS are insoluble by design [17]. In our initial assessment of their solubilities, [Benz][Doc] or [Lid][Doc] were combined with deionized (DI) water in equal volumes and

vortexed. Both mixtures proved highly insoluble in water and quickly formed metastable emulsions upon mixing that remained for weeks. Attempts to solubilize these ILs by first introducing dimethyl sulfoxide (DMSO), Tween 80, ethanol, or methanol followed by addition of water were also unsuccessful even when additives made up as much as 20% of the total volume. While viscosity was noticeably reduced in these mixtures with additives, emulsions formed quickly nonetheless, demonstrating the highly insoluble nature of these ILs. Due to the inherent nature of water-insoluble materials, classical dilution assays are inappropriate for the quantification of their antimicrobial activity. For materials such as antimicrobial essential oils, this issue can be overcome if they can be solubilized in water containing small amounts of solvents such as DMSO or emulsifiers such as polysorbate (Tween) [18, 19]. High concentrations of solvating additives would confound antibacterial tests as solvents themselves can also have deleterious effects on cell growth. While it is possible to quantify antibacterial properties of [Benz][Doc] and [Lid][Doc] as emulsions, the number of assays available to do so are limited. Common techniques to measure bacterial concentration such as OD₆₀₀ or microscopy would experience interference from the micelles of the emulsion.

Thus, to evaluate the antibacterial efficacy of [Benz][Doc] and [Lid][Doc], 0.1 mL of either IL was transferred into individual wells of a sterile 96-well microplate. Next, 50 μ L of bacteria suspended in PBS was pipetted gently on top of the IL as depicted in Figure 12 d. The IL phase and the aqueous (bacteria in PBS) phase maintained fully phase-separated because of the highly hydrophobic nature of the ILs. This allowed for the sampling of the bacteria in the aqueous phase without contacting the ILs that are too viscous to pipette and which would have made the sampling process difficult. This technique also eliminates the need for the addition of solvents as the two phases were by design immiscible. Bacteria were exposed to either IL for 0.5, 3, or 12 h. Control

wells containing only 0.1 mL of bacteria without any ILs were also sampled for the same durations (Figure 12 e). Prolonged incubation of bacteria in PBS naturally results in cell death over time as bacteria are in a state of starvation since PBS contains no nutrients. The starvation effect proved to be too drastic in our experiments that lasted more than 12 h thus exposure times longer than this were not evaluated.

Results from cell enumeration are provided in Figure 13 a. As can be seen, when incubated only in PBS, even 12 h causes slight reductions in cell viability (except for *B. subtilis*). However, *B. subtilis* proved to be highly inactivated by both ILs. At the 3 h mark of exposure to either IL, no viable *B. subtilis* cells were detected. In fact, both ILs appear to have selective bactericidal activity against Gram-positive bacteria since no viable *S. aureus* cells were detected after 12 h either. In contrast, *E. coli* and *P. aeruginosa* were largely unaffected by [Benz][Doc] for the duration of the experiment. [Lid][Doc] inactivated all *E. coli* after 12 h, but could only impart a log reduction of ~3 to *P. aeruginosa* (99.9% inactivation).

It is important to note that the ability of benzalkonium chloride to inactivate bacteria does not normally exhibit selectivity between Gram-positive and Gram-negative cells, yet [Benz][Doc] had no effect on Gram-negative cells. Benzalkonium, like other quaternary ammonium compounds (QACs), is believed to wreak havoc on bacterial cell membranes by first displacing other positive ions near the outer membrane that are required for osmotic balance and membrane integrity. Next, it binds strongly to the negatively charged membranes leading to membrane disruption [20]. Clearly, the proximity of the docusate counter ion when it is paired with benzalkonium influences this interaction, perhaps by steric hindrance of the positively-charged ammonium. This observation is valuable for future studies looking to optimize Gram-negative antibacterial compounds and antibacterial ILs in general. Lidocaine on the other hand is already known to be less effective

against *P. aeruginosa* compared to other common nosocomial (hospital-associated) bacteria and the same trend is observed here [21, 22].

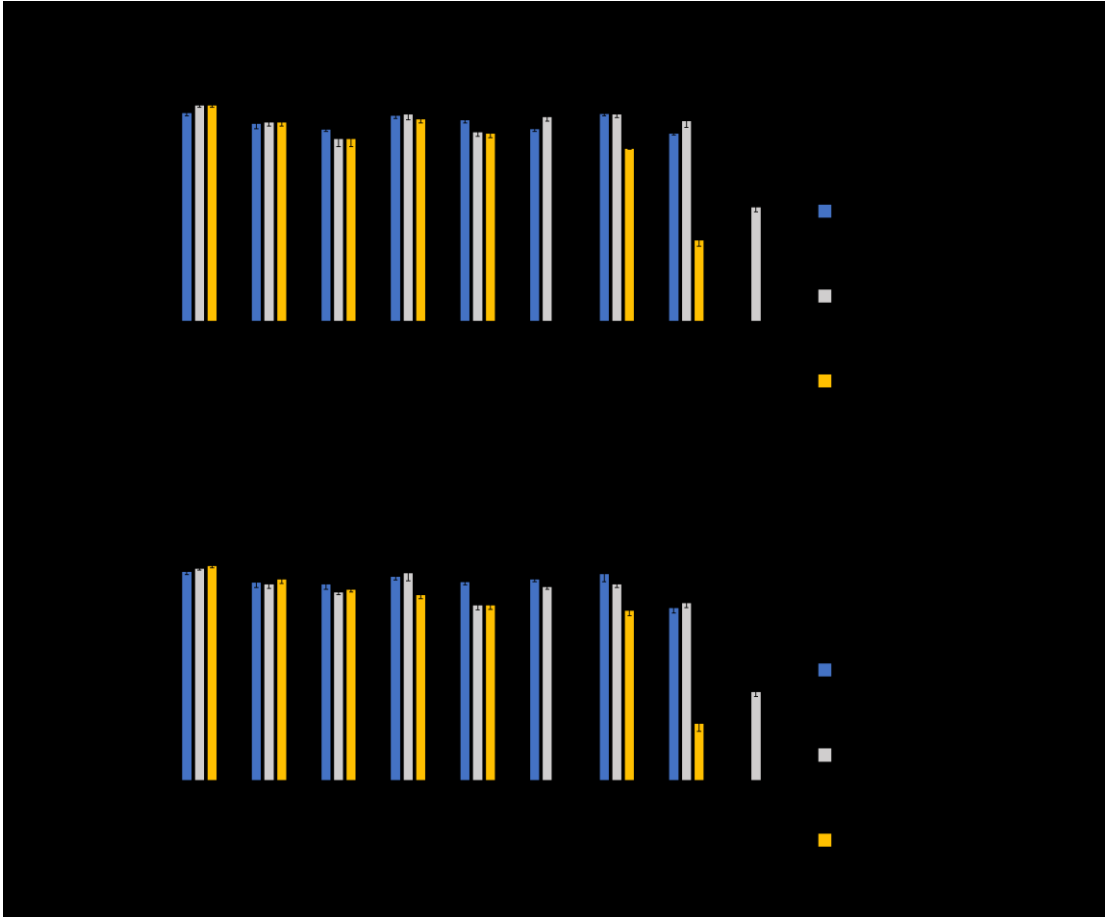


Figure 9. Bacterial cell concentrations after 0.5, 3, or 12 h incubation with PBS, [Benz][Doc], or [Lid][Doc] a) using 96-well microplate and b) using micro-reservoir PDMS. Cell concentrations below detection using standard agar plating are represented by *.

Rather than quantifying CFUs after the prescribed incubation times, samples of the aqueous phase can instead be used to inoculate sterile nutrient broth to observe cell growth kinetics. Growth kinetics as monitored by OD₆₀₀ reveal insights into the recovery of bacteria post-exposure to the ILs. This is particularly evident when comparing the growth of *P. aeruginosa* after exposure to [Benz][Doc] and [Lid][Doc]. As noted earlier, [Benz][Doc] does little to affect *P. aeruginosa*

viability when assessed by cell enumeration and the same is reflected in its growth kinetics. Growth after incubation in [Benz][Doc] appears no different than growth after incubation in PBS (Figure 14 a). Recovery of *P. aeruginosa* after exposure to [Lid][Doc], however, produces different growth kinetics (Figure 14 b). Interestingly, exposures of 0.5 h or 3 h proved somewhat deleterious despite initial exponential phase growth appearing similar to bacteria growing in PBS. Biomass levels clearly plateau faster because of initial sublethal injury. Moreover, recovery of *P. aeruginosa* after 12 h of exposure to [Lid][Doc] was observed but an extended lag phase characteristic of a low initial inoculum cell density was noted.

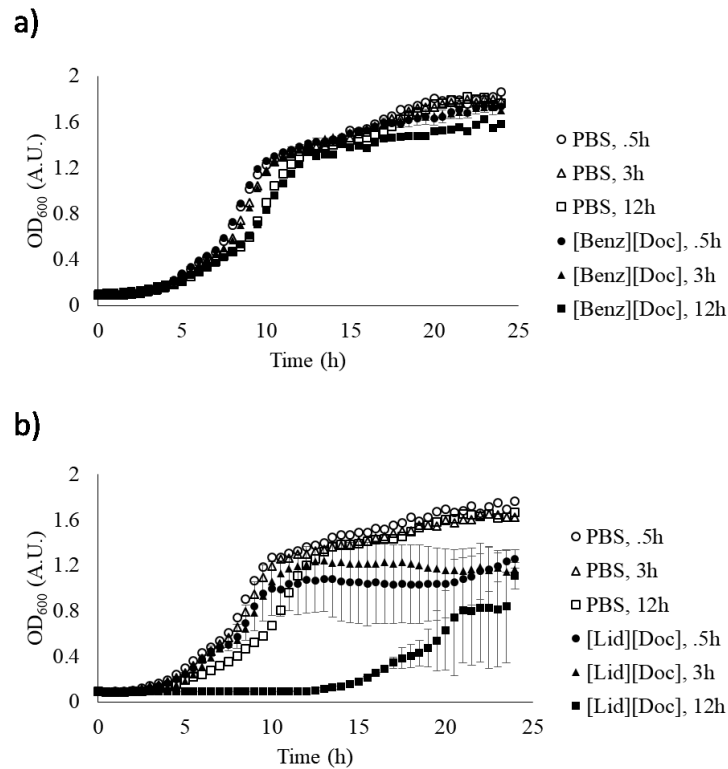


Figure 10. Growth recovery kinetics of *P. aeruginosa* post-exposure to (a) [Benz][Doc] and (b) [Lid][Doc].

HAILs can be implemented into antibacterial surface designs in several ways, as summarized in Table 1. The most obvious approach may be to apply them as a surface coating that cannot evaporate nor be washed away by water. The benefits of this design are incremental. Direct contact through tactile touch with the coating would result in an unpleasant, oily sensation. Contact abrasion would also remove the coating, which would need to be replenished. A more practical approach is to instead blend HAILs into a material of interest. For example, Choi *et al.* blended 1-ethylpyridinium docusate and tributyl(2-hydroxyethyl)phosphonium docusate into medical grade poly(vinyl chloride) (PVC) to simultaneously deliver the desirable plasticizing and antimicrobial effects on PVC [23, 24]. If, however, changes in the physicochemical properties of the bulk material are undesirable, blending ILs homogeneously into a material becomes unsuitable. Furthermore, since bacteria interact only at a surface's interface, blending antibacterial ILs throughout the entire material is unnecessary and wasteful as most of the antibacterial potential is unrealized. Only the very surface of the material needs to be prepared with antibacterial ILs and less amounts are required in this manner.

Despite the added difficulty of fabricating a micro-reservoir topography, a micro-reservoir topography containing HAILs offers numerous benefits that previous design approaches cannot. To that end, we constructed a PDMS surface featuring micro-reservoirs, then filled the reservoirs with [Benz][Doc] or [Lid][Doc]. First, uncured PDMS was poured onto a 3D-printed resin mold that featured micropillars. After curing at 60 °C to solidify the PDMS, it was peeled off to produce the inverse reservoir structures (Figure 11). Since the ILs are highly viscous, they were added to the PDMS surface dropwise then spread to distribute evenly using a clean cell scraper.

Table 1: Comparison of antibacterial surfaces prepared with HAILS

Antibacterial surface designs	Coating with water-dispersed antibacterials	Coating with HAIL	Blending with HAIL	Micro-reservoirs containing HAIL
Properties				
Evaporates	Yes	No	No	No
Washed away by water	Yes	No	No	No
Removed through abrasion	Yes	Yes	No	No
Unpleasant to touch	Yes	Yes	No	No
Quick-release action	Yes	No	No	No
Requires replenishing	Yes	Yes	No	No
Long lasting	No	No	Yes	Yes
Alters bulk material properties	No	No	Yes	No
Maximized antibacterial potential	Yes	Yes	No	Yes
Difficult fabrication process	No	No	No	Yes

In our preliminary assessment of antibacterial properties of the surface, 30 μL droplets of bacteria suspended in PBS were placed directly onto the IL-filled PDMS micro-reservoir surface. Again after 0.5, 3, or 12 h of exposure, 20 μL from each droplet was sampled by pipette. During the exposure duration, the PDMS surface was placed in an empty sterile Petri dish covered with the lid to minimize droplet evaporation and to prevent contamination. Cell enumeration (Figure 2b) indicated that the application of HAILS into micro-reservoirs does not lessen antibacterial activity as results are nearly the same as that shown in Figure 2a. The same experiment was conducted by placing bacterial droplets onto a control surface of flat PDMS untreated with IL as well as a flat PDMS surface with [Benz][Doc] or [Lid][Doc] added then scraped off using a cell scraper. On the untreated PDMS surface, little to no reduction in viability was observed, as expected, as there was no antibacterial present. However, to our surprise, the flat PDMS surface

with IL scraped off showed the same antibacterial efficacy as that of the IL-filled micro-reservoir surface. It can therefore be deduced that there is a thin coating of excess IL that is not removed from the surface during scraping. Thus, it is not the ILs within the micro-reservoirs that deliver antibacterial properties, but a thin residual layer of IL on top of the PDMS surface that is the main contributor.

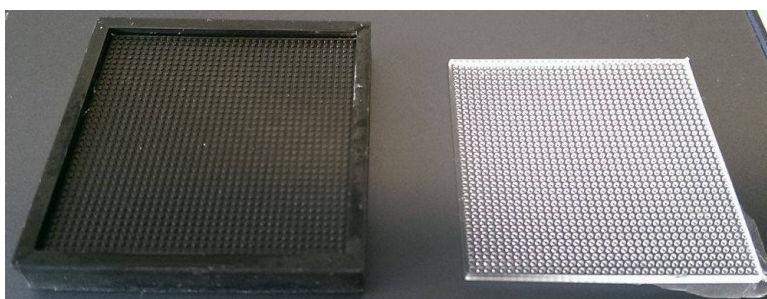


Figure 11: 3D-printed resin mold featuring pillars (left) was used to fabricate the PDMS micro-reservoir surface (right).

While not critical to the antimicrobial performance of the micro-reservoir surface, other physical properties of the material should be considered in the design of antibacterial surfaces. [Benz][Doc] and [Lid][Doc] are both transparent with a hint of ivory and produce no odor so their incorporation onto surfaces should not be unsightly or off-putting. Their thermal stability, too, is worth noting. As determined by thermogravimetric analysis, the temperature onset ($T_{5\%onset}$) of decomposition for [Benz][Doc] and [Lid][Doc] is 262 °C and 222 °C, respectively [13]. Most hospital and dental equipment that are designed for re-use are sterilized by steam autoclave, which normally operates at 121 °C exactly. Biohazardous waste disposal, on the other hand, is achieved by incineration facilities that reach a minimum of 900 °C [25]. In essence, both [Benz][Doc] and

[Lid][Doc] are thermally unaffected when sterilized, suggesting reusability, but decompose as desired if they were to be incinerated as waste.

A micro-reservoir surface prepared with HAILS potentially reduces the unintended leaching of antibacterial agents in two ways. First, HAILS are physically contained within micro-reservoirs, and second, even if they were to be released, their insoluble nature minimizes their dissemination and dispersal in aquatic ecosystems. Since the antibacterial agents are designed to stay inside the PDMS surface, it will be interesting to challenge the surface to long-term and reusability studies. Finally, the micro-reservoir design can be scaled down to the nanoscale, which would generate yet another way to reduce leaching as it would require orders of magnitude less volumes to fill nano-reservoirs and ILs would be better entrapped in nano-reservoirs by capillary action.

4.5 Conclusions and future Work

Filling [Benz][Doc] and [Lid][Doc] into a surface patterned with micro-reservoirs has the potential to yield numerous advantages over conventional techniques used to prepare an antibacterial surface. While a PDMS micro-reservoir surface prepared with HAILS delivered antibacterial properties as promised, it is the result of a thin residual layer of HAIL on top of the surface, and not the HAIL inside the wells that deliver the antibacterial action. Ongoing work is focused on effectively filling and removing the excess residue, possibly by wiping with cotton swab or through the use of spin coating. Next, the micro-reservoir features are to be scaled down to nano-reservoir features, which would reduce the amount of HAILS required to fill the surface. The search for HAILS that are acutely antibacterial to both Gram-positive and Gram-negative bacteria is also underway.

4.6 References

- [1] Tuson HH, Weibel DB, *Soft matter*, 2013;9:4368-80.
- [2] Hall-Stoodley L, Costerton JW, Stoodley P, *Nature Reviews Microbiology*, 2004;2:95-108.
- [3] Flemming H-C, Wingender J, *Nature Reviews Microbiology*, 2010;8:623-33.
- [4] Banerjee I, Pangule RC, Kane RS, *Adv Mater*, 2011;23:690-718.
- [5] Cloutier M, Mantovani D, Rosei F, *Trends in biotechnology*, 2015;33:637-52.
- [6] Hasan J, Crawford RJ, Ivanova EP, *Trends Biotechnol*, 2013;31:295-304.
- [7] Andersson DI, Hughes D, *Nat Rev Micro*, 2014;12:465-78.
- [8] Wolcott RD, Rhoads DD, Bennett ME, Wolcott BM, Gogokhia L, Costerton JW, Dowd SE, *J Wound Care*, 2010;19:45-53.
- [9] Barthlott W, Neinhuis C, *Planta*, 1997;202:1-8.
- [10] Bixler GD, Bhushan B, *Critical Reviews in Solid State and Materials Sciences*, 2015;40:1-37.
- [11] Ivanova EP, Hasan J, Webb HK, Truong VK, Watson GS, Watson JA, Baulin VA, Pogodin S, Wang JY, Tobin MJ, *Small*, 2012;8:2489-94.
- [12] Shamshina JL, Kelley SP, Gurau G, Rogers RD, *Nature*, 2015;528:188-9.
- [13] Hough WL, Smiglak M, Rodríguez H, Swatloski RP, Spear SK, Daly DT, Pernak J, Grisel JE, Carliss RD, Soutullo MD, *New Journal of Chemistry*, 2007;31:1429-36.
- [14] Bica K, Rodríguez H, Gurau G, Cojocarua OA, Riisager A, Fehrmann R, Rogers RD, *Chemical Communications*, 2012;48:5422-4.
- [15] Berton P, Di Bona KR, Yancey D, Rizvi SA, Gray M, Gurau G, Shamshina JL, Rasco JF, Rogers RD, *ACS Medicinal Chemistry Letters*, 2017;8:498-503.
- [16] Riisager A, Fehrmann R, Rodriguez H, Bica K, Rogers RD, Daly DT, Gurau G. US: Danmarks Tekniske Universitet, The Board of Trustees of The Univ. of Alabama for and on Behalf of the Univ. of Alabama, The Queens University of Belfast; 2011.
- [17] Pendleton JN, Gilmore BF, *International journal of antimicrobial agents*, 2015;46:131-9.
- [18] Kim J, Marshall MR, Wei C-i, *Journal of Agricultural and Food chemistry*, 1995;43:2839-45.
- [19] Teixeira B, Marques A, Ramos C, Neng NR, Nogueira JMF, Saraiva JA, Nunes ML, *Industrial Crops and Products*, 2013;43:587-95.
- [20] Gilbert P, Moore LE, *Journal of Applied Microbiology*, 2005;99:703-15.
- [21] Sedef Gocmen J, Buyukkocak U, Caglayan O, Aksoy A, *Journal of Dermatological Treatment*, 2008;19:351-3.
- [22] Taki Y, Seki K, Ikigai H, Nishihara S, Ueno H, Murota K, Masuda S, *Microbiology and immunology*, 1988;32:429-34.
- [23] Choi SY, Rodríguez H, Mirjafari A, Gilpin DF, McGrath S, Malcolm KR, Tunney MM, Rogers RD, McNally T, *Green Chemistry*, 2011;13:1527-35.
- [24] Choi SY, Rodríguez H, Gunaratne HN, Puga AV, Gilpin D, McGrath S, Vyle JS, Tunney MM, Rogers RD, McNally T, *RSC Advances*, 2014;4:8567-81.
- [25] Dempsey CR, Oppelt ET, *Air & Waste*, 1993;43:25-73.

Chapter 5: Conclusions and future work

Bacteria are ubiquitous in the environment. Rather than free-floating microorganisms, almost all bacteria prefer to form a community attached upon a surface. The presence of bacteria on a surface, or biofouling, is detrimental for many processes and can be threatening towards human health. Anti-biofouling strategies are required but conventional treatments to eliminate bacteria are becoming less effective because of antibacterial resistance – a looming crisis that humanity must tackle with innovative strategies. A prime example of human misuse which leads to resistance, the traditional design approach of antibacterial surfaces is to incorporate antibacterial compounds within the material and expect the release of said compound to deliver antibacterial effects. This practice leads to a sublethal background dose of the compound which is potentially ecotoxic and which promotes additional resistance mechanisms. Equally important from a product design perspective, these materials are short-lived due to quick burst-release kinetics, thus requiring replenishing. Future design strategies should aim for non-leaching antibacterial materials whose antibacterial properties can be sustained for extended periods to minimize the spread of antibacterial resistance and maximize efficacy.

Flora and fauna have co-existed for millions of years alongside bacterial pathogens. During that time, they have developed strategies to prevent biofouling of their natural surfaces. The wings of cicada and dragonfly, for example, consist of nanopillars and nanospikes respectively that inflict critical deformational stress upon attached bacteria. By preventing the accumulation and proliferation of bacteria, these insects can maintain the lightweight stature of their wings during flight. This bactericidal mechanism, which functions primarily through physical forces of nanostructures, is termed mechano-bactericidal and has attracted a great deal of attention in recent antibacterial research. By now, the mechano-bactericidal activity has been successfully duplicated

onto artificial substrates including gold, titanium, silicon, and polymethyl methacrylate. Plants too are well-known for their anti-biofouling abilities and do so both chemically and topographically. Chemically, plants produce antibacterial compounds in high concentrations meant to inhibit colonizing bacteria. Elevated levels of antibacterial compounds found in extracts and essential oils of herbs and spices are well-documented. In terms of topography, the leaves of lotus, rice, ryegrass, and reed canary grass plants are covered in waxy micro- and nanoscale cuticular structures such as nanobumps or nanowrinkles that result in highly hydrophobic leaves that shed water. This self-cleaning effect prevents the accumulation debris or microorganisms on their leaf surfaces where photosynthesis takes place.

A comprehensive understanding of the structure-function relationship of biological matter is necessary to harness nature's design to apply it towards biomimetic or bio-inspired research applications. Biomimetic efforts in antibacterial research aim to duplicate proven mechanisms of nature and transfer them onto artificial surfaces, whereas bio-inspired design leads to new functionalities or antibacterial applications. The aim of this thesis was to design anti-biofouling surface topographies taking inspiration from nature. This was achieved by initially reviewing mechano-bactericidal materials found on insects and animals (see Chapter 2) and assessing the hydrophobicity of the reed canary grass leaf topography (see Chapter 3) to gather inspiration. A novel antibacterial surface was designed featuring a topography patterned with micro-reservoirs. By filling the micro-reservoirs with antibacterial compounds in the form of HAILS, namely [Benz][Doc] and [Lid][Doc], the surface is expected to provide long-term antibacterial properties (see Chapter 4). HAILS are non-volatile and non-leaching and expected to be contained within the micro-reservoirs thereby reducing their unintended release while fully realizing their antibacterial properties. Future work will be addressed in a three-pronged approach.

Firstly, the design of micro-reservoirs detailed above should be improved by scaling down individual reservoirs from microscale to nanoscale dimensions. In this way, the quantity of antibacterial agents (in the form of ILs) required to fill the reservoirs is reduced by orders of magnitude. A nano-reservoir surface is therefore economically favorable (since designer ILs are expensive to synthesize); it will also improve sustainability as there are less antibacterial agents available to be released. Comprehensive solubility and leaching experiments should be conducted to definitively stake these claims. Furthermore, nano-reservoirs will provide better surface coverage, therefore enhancing antibacterial efficacy. Since the distance between two nano-reservoirs is smaller than the size of a single bacterium, any bacteria that come into contact with the nano-reservoir surface must be exposed to multiple reservoirs containing antibacterial agents. In comparison, a micro-reservoir design is prone to relatively large “dead” zones between two reservoirs where an attached bacterium may escape contact with contents in the reservoirs thereby remaining viable to proliferate. Reducing the volume required while simultaneously improving overall performance demonstrates the potential of nanotechnology. More specifically, it is the principle of enhanced surface area-to-volume ratio at the nanoscale in action. Unfortunately, scaling down is not a trivial process. At the microscale, filling reservoirs with ILs did not prove difficult. However, the same cannot be said for filling of nanoscale reservoirs. At these length scales, the surface tension of the IL as well as microscopic air pockets may overcome the effects of gravity. To effectively fill nano-reservoirs, a vacuum chamber is currently under construction. The nano-reservoir surface is to be placed within the vacuum chamber, after which the air in the chamber is purged. Next, ILs will be introduced into the chamber then mechanically pressed into the surface to ensure nano-reservoirs are filled.

Secondly, while countless applications require the complete eradication of bacteria, devices intended for biomedical applications are of high priority. Contamination of these devices could directly lead to infections that will be untreatable using traditional approaches. Biocompatibility is therefore a requirement for future antibacterial designs. Rather than painstakingly fabricating a material that may ultimately prove harmful to mammalian cells, one could use biopolymers as construction materials. Chapter 2 suggested that a mechano-bactericidal chitin substrate can be achieved. Chitin is not only compatible with the human body but offers accelerated cell regeneration capabilities as a scaffolding material. Chitin is commercially extracted from exoskeletons of crustaceans such as shrimp or crab. As an unused by-product of food sources, chitin is abundantly available, truly renewable and a low-cost material. The dissolution and subsequent repurposing of chitin is well-researched. In an ongoing project, a mold featuring nano-holes has been constructed by directly micro-replicating a wing of a cicada insect (*Tosena paviei*) with PDMS. Chitin extracted from shrimp shells using microwave-assisted dissolution with 1-ethyl-3-methylimidazolium acetate ([C₂mim][OAc]) was cast over the PDMS mold then air-dried to prepare a film. Ideally, once the chitin film is peeled from the mold it would feature mechano-bactericidal nanopillars structurally-inverse of the nano-holes. However, preliminary results indicate that the chitin film shrinks considerably during the drying process and nanoscale features are lost because of the shrinkage. Currently modifications to the casting and drying method are being explored.

Lastly, the combination of a surface exhibiting both mechano-bactericidal nanostructures alongside HAILs is of interest, as this would provide both chemical and physical antibacterial mechanisms that would be difficult for any bacteria to survive. This material would provide dual-action (chemical and mechanical) approaches to inactivate bacteria. Recall that mechano-

bactericidal nanostructures were most effective against Gram-negative bacteria but not as effective against Gram-positive species whereas the opposite trend was true for HAILS. Combining the two could create an unparalleled, wide-spectrum antibacterial material guaranteed to overcome any bacterial presence. Published techniques to construct mechano-bactericidal nanostructures are not applicable to achieve the combined surface. Almost all techniques to date employ top-down fabrication approaches such as acid-etching or thermal oxidation, conditions which would interfere with a surface pre-functionalized with an antibacterial agent. A survey of alternative techniques should be conducted. One potential approach is to blend HAILS into a biocompatible polymer matrix then embed mechano-bactericidal colloids partially into the polymer matrix before it is fully solidified. However, nanoscale manipulations of seemingly straightforward processes are confounding. Execution will give rise to further complications but its potential value is evident based on discussions in this thesis.

